



UNIVERSITÀ DEGLI STUDI DI SALERNO



UNIVERSITÀ DEGLI STUDI DI SALERNO  
Dipartimento di Farmacia

PhD Program  
in **Drug Discovery and Development**

XXXV Cycle — Academic Year 2022/2023

## *PhD Thesis in*

### *Proteomic investigation of the impact of Cannabidiolic acid on Eukaryotic Translation complex in glioblastoma*

Candidate

*Maria Laura Bellone*

Tutor

Prof. *Fabrizio Dal Piaz*

Co-Tutor

Prof. *Nunziatina De Tommasi*

PhD Program Coordinator: Prof. Dr. *Gianluca Sbardella*



# Index

<b>Abstract</b>	I
<b>Chapter 1- Introduction</b>	1
<b>1.1 Cannabis: an intriguing pharmacological plant</b>	3
<b>1.1.1 Chemical and biological space of cannabinoids</b>	5
<b>1.2 Cannabinoids and their role in nervous system diseases and in tumor pathologies</b>	11
<b>1.2.1 Anti-cancer effect of cannabinoids in glioma</b>	13
<b>1.3 Aim of the thesis project</b>	15
<b>1.4 Chemical proteomic approaches in drug discovery process</b>	16
<b>1.4.1 Drug Affinity Responsive Target Stability (DARTS)</b>	20
<b>1.4.2 Cellular Thermal Shift Assay (CETSA)</b>	22
<b>1.4.3 Mass Spectrometry-associated Limited-Proteolysis</b>	25
<b>1.4.4 SILAC: Stable Isotope Labelling by Amino acids in cell culture</b>	27
<b>1.4.4.1 Pulsed-SILAC: variant of classic SILAC to investigate nascent proteome</b>	29
<b>1.5 Two-dimensional and Three-dimensional cellular model</b>	31
<b>Chapter 2 –Study of the mechanism of action of CBDA in 2D cell model</b>	37
<b>Results</b>	39
<b>2.1 Eukaryotic translation complex identified as putative target of cannabinoids by DARTS assay</b>	39
<b>2.2 EIF2A-CBDA interaction validated by Cellular Thermal Shift Assay (CETSA)</b>	44
<b>2.3 CBDA-EIF2A interaction investigated by mass spectrometry-associated Limited Proteolysis</b>	46
<b>2.4 A close-up of EIF2A-CBDA interaction</b>	51
<b>2.4.1 Modeling of EIF2A</b>	51
<b>2.4.2 Modeling of CBDA-EIF2A complex</b>	54
<b>2.5 EIF2A: an overlooked alternative initiation factor</b>	59
<b>2.6 Interactome of EIF2A elucidate the mechanism of action of CBDA</b>	63
<b>2.7 CBDA remodels glioblastoma nascent proteome by targeting Eukaryotic Translation Complex</b>	69
<b>2.7.1 pulsed-SILAC reveals the impact of CBDA on nascent proteome in U87MG cells</b>	78
<b>2.7.2 Effect of CBDA on the expression of cancer hallmarks in U87MG cells</b>	80
<b>Discussion</b>	89
<b>Chapter 3 - Development of 3D glioblastoma cell model for the investigation of mechanism of action of novel drugs</b>	97
<b>Results</b>	99
<b>3.1 Different proteomic profile of 2D and 3D-U87MG cell model</b>	99

<b>3.2 U87MG-3D sandwich model: a glioblastoma cellular model for proteomic investigation of bioactivity of CBDA</b>	102
<b>3.3 CBDA-EIF2A binding suggests a different interactome of Eukaryotic translation complex between 2D- and 3D-cellular model</b>	107
<b>3.4 Interactome of EIF2A in 3D-U87MG cell model</b>	110
<b>Discussion</b>	111
<b>Chapter 4 – Conclusions</b>	117
<b>Conclusions</b>	119
<b>Chapter 5 - Material and Methods</b>	123
<b>Material and methods</b>	125
<b>5.1 Reagents and materials</b>	125
<b>5.2 Cell culture</b>	126
<b>5.3 Cellular Viability Assay</b>	126
<b>5.4 Drug Affinity Target Stability Assay (DARTS)</b>	127
<b>5.5 Cellular Thermal Shift Assay</b>	128
<b>5.6 EIF2A silencing siRNA treatment</b>	129
<b>5.7 Pulsed-Stable Isotope Labeling by amino acids in cell culture (pSILAC)</b>	129
<b>5.8 Limited Proteolysis</b>	130
<b>5.9 Computational Methods</b>	131
<b>5.10 Immunoprecipitation of EIF2A</b>	133
<b>5.11 3D cell model</b>	134
<b><i>5.11.1 Cell viability on 3D U87MG cells</i></b>	134
<b><i>5.11.2 Global proteome analysis on 2D and 3D U87MG cells</i></b>	135
<b><i>5.11.3 DARTS assay on 3D U87MG cells</i></b>	135
<b>References</b>	136



## Abstract

Phytocannabinoids, the major secondary metabolites of cannabis plants, exert a wide range of biological activities. The present work was focused on investigating the mechanism of action of cannabidiolic acid (CBDA) in U87MG glioblastoma cell line, exploiting the efficacy of chemical-proteomics based approaches in identifying target proteins of uncharacterized drugs. DARTS experiments showed Eukaryotic Initiation Translation Factor 2A (EIF2A) as a putative target of CBDA. This interaction was further validated by western blot and CETSA, thus showing a thermal stabilization of Eukaryotic Translation Complex conferred by CBDA. Moreover, Limited Proteolysis showed that the EIF2A C-terminal portion 460-480 could play a critical role in the molecular recognition of CBDA by the protein. This result was also confirmed by Molecular Dynamics (MD) calculations, which revealed that CBDA interacts with a stretch of residues in the 460-480 portion and in the adjacent C-terminal helix, acting as a bridge between these regions. Hence, since EIF2A is the initiator factor of translation process, the impact of CBDA-EIF2A interaction on proteins synthesis was investigated by p-SILAC and enrichment via click-chemistry. Comparing CBDA and EIF2A-silencing treatments, a similar remodeling of nascent proteome was detected in the two conditions in terms of protein expression reduction and biological effect. Particularly, CBDA appeared to induce an UPR response, triggering as a balancing effect between the ER-stress response and the attempt to restore cellular homeostasis. Moreover, EIF2A revealed to interact not only with eukaryotic translation proteins but also with the

proteins involved in triggering of UPR response and the CBDA-induced reorganization of eukaryotic translation machinery. Interestingly, these proteins seem to be involved in several pathways already highlighted by nascent proteome investigation.

In order to evaluate the protein-CBDA interaction in a cell model closer to the tumor *in vivo*, a 3D cell culture was set up using a classic-sandwich model. Based on the observation that in 2D- and 3D- cell model U87MG cells grow differently since in 3D they show a natural shape and more cellular interactions, a global proteome comparative analysis was firstly carried out. Interestingly, the obtained results highlighted a higher-amount of proteins involved in invasion cellular processes and cell-ECM interaction expressed by 3D-U87MG, compared to 2D-cultured cells. These findings prompted us to further study the effects of CBDA in 2D and 3D cellular models. In 3D cultured cells, CBDA showed a different cytotoxicity depending on the concentration of FBS in the upper and lower- gels and in the culture medium as well. DARTS assay performed in this cell system also suggested a direct correlation between the percentage of FBS used in cell culture conditions and the ability of CBDA to interact with EIF2A, thus confirming the critical role played by the molecule-FBS interaction on its availability. Furthermore, comparing the results of DARTS assays performed on 2D and 3D, a difference of the EIF2A interactome with respect to the entire translational complex was revealed in the two conditions. In contrast to 2D-cellular model, EIF2A was highly resistant to proteolysis in untreated 3D cultured cells, but was more digested after CBDA treatment. This result suggested that EIF2A in 3D-U87MG could be likely associated with the other protein partners more strongly than in the 2D model. In closing of this study, it is possible to state that the use of a multi-proteomic approach allowed us

to highlight the potential impact of CBDA on the eukaryotic translation machinery, also suggesting the importance of investigating the interactome differences that exist between innovative three-dimensional and conventional cellular models.

## **Chapter 1- Introduction**



# Introduction

## 1.1 Cannabis: an intriguing pharmacological plant

*Cannabis* is a plant genus of belonging to the *Cannabaceae* family, which includes three species, *Cannabis sativa*, *Cannabis indica* and *Cannabis ruderalis*, of which more than 700 strains have been defined (Pattnaik *et al.*, 2022). Currently, *Cannabis* species are classified into two different categories: drug-type and non-drug type. Specifically, drug-type Cannabis are the plants carrying a huge content of cannabinoids that have been accounted for several beneficial effects, whereas the non-drug ones are those that exhibit different profile in meroterpenoids and other small molecules and therefore can be used as a source of high-quality natural fiber (Pattnaik *et al.*, 2022). Botanically, Cannabis plants can be female, male or hermaphrodite (Figure 1).



**Figure 1** *Cannabis plant anatomy: representative image of male and female flowers – adopted from (Pattnaik et al., 2022)*

Unlike male flowers play a role in pollination process, female flowers and leaves are organs enriched of bioactive compounds, such as terpenes, alkaloids, flavonoids, lignans, quinones and anthocyanins. Particularly, the glandular trichomes of female flowers are characterized by a big amount of the main bioactive compounds, such as cannabinoids. Among them,  $\Delta^9$ -tetrahydrocannabinol ( $\Delta^9$ -THC) and cannabidiol (CBD) have been defined as the most abundant and characteristic compounds. In fact, cannabis-derived products (i.e. hemp and marijuana) can undergo a chemotype-based distinction based on the ratio THC:CBD, as the psychotropic effects only related to THC. Hence, these products are separated into three groups: herbal cannabis, hemp products and pharmaceutical-grade regulated cannabinoid-based medical products (CBMP) (Schilling, Melzer and McCabe, 2020; Vickery and Finch, 2020). Although herbal and hemp cannabis are respectively used

for recreational use and for manufacturing, the scientific community is focused in deepen the knowledge of cannabinoid-based products, also in order to set up a suitable clinical regulation. Currently, there are several products that have not obtained any regulatory approval, whereas few pharmaceutical preparations consisting of purified cannabinoids (THC, CBD or THC+CBD) have been properly approved by drug agencies. Indeed, depending on the different authorization in the various countries, THC is used for the treatment of chemotherapy-induced nausea and vomiting, CBD for the treatment of epilepsy, and their association in a 1:1 ratio is used for the treatment of spasticity in disease related to the central nervous system.

### **1.1.1 Chemical and biological space of cannabinoids**

*Cannabis sativa* is a rich source of a plethora of different molecules, such as terpenes, phenolic compounds and cannabinoids (Andre, Hausman and Guerriero, 2016). The latter are meroterpenoids of the resorcinylic type, bearing *p*-alkyl- and isoprenyl- substituents. Although  $\Delta^9$ -tetrahydrocannabinol ( $\Delta^9$ -THC) and cannabidiol (CBD) have been described as the main cannabinoid constituents, more than 100 cannabinoids have been identified (Hanuš *et al.*, 2016). Despite their chemical differences, they all derived from the same biosynthesis pathway. Cannabigerolic acid (CBGA), carboxylated form of CBG, plays a main role in cannabinoid biosynthesis. Hence, CBGA is synthesized starting from hexanoyl-CoA and malonyl-CoA, which react in presence of tetraketide synthase (TKS) and olivetolic acid cyclase (OAC) to constitute olivetolic acid. Finally, olivetolic acid is converted to cannabigerolic acid (CBGA) through a prenylation reaction catalyzed by aromatic prenyltransferase and geranyl pyrophosphate (Figure 2).

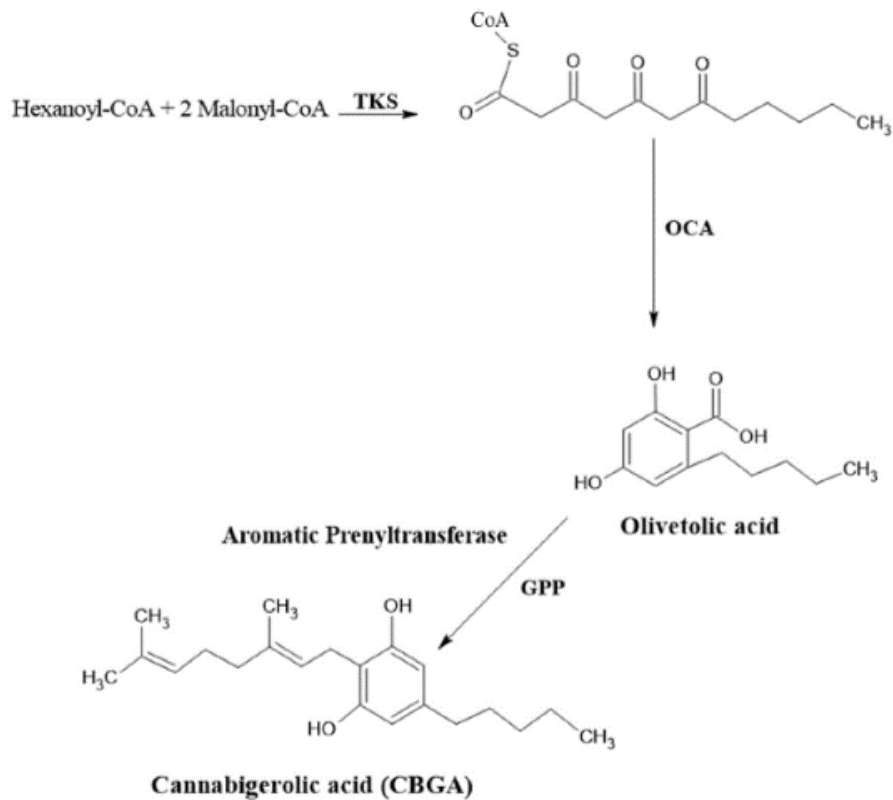


**Figure 2** Biosynthesis of cannabigerolic acid (CBGA) – adopted from (Pattnaik et al., 2022)

CBGA is the precursor cannabinoid and is converted into three main native cannabinoids: tetrahydrocannabinolic acid (THCA), cannabidiolic acid (CBDA) and cannabigerolic acid (CBCA), by specific synthase enzymes (Figure 3).

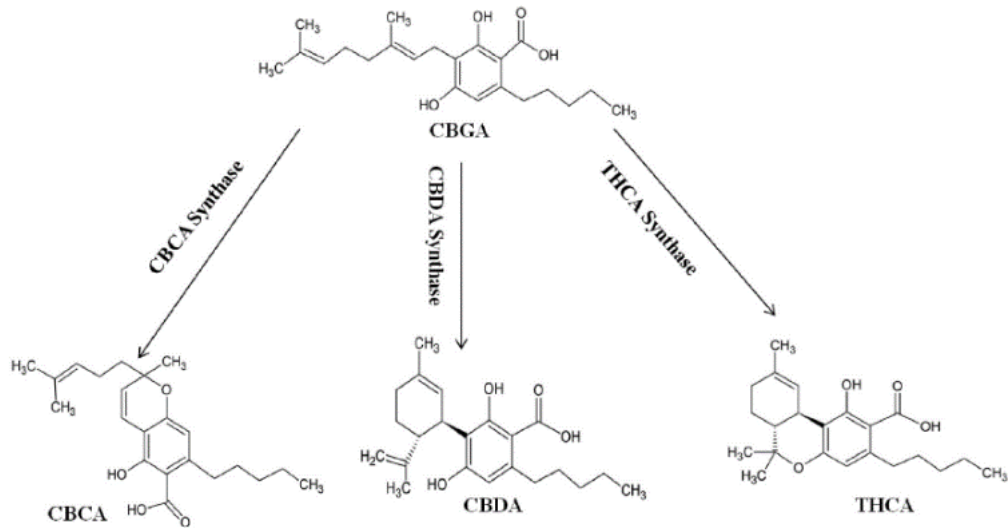


**Figure 3** Biosynthesis of cannabichromenic acid (CBCA), cannabidiolic acid (CBDA) and tetrahydrocannabinolic acid (THCA) from cannabigerolic acid – adopted from (Pattnaik *et al.*, 2022)

Among the most common cannabinoids, there are:  $\Delta^9$ -tetrahydrocannabinol ( $\Delta^9$ -THC),  $\Delta^8$ -tetrahydrocannabinol ( $\Delta^8$ -THC), cannabidiol (CBD), cannabigerol (CBG), cannabinol (CBN), cannabigerol (CBG), cannabidivarin (CBV), cannabichromene (CBC) and cannabidivarin (CBDV) (Morales, Hurst and Reggio, 2017)

Chemically, the wide variety of cannabinoids are due to differences in three moieties: isoprenyl residue, resorcinyl core and side-chain (Hanuš *et al.*, 2016).

- Isoprenyl residue: it can present different oligomerization, such as prenyl-terpenyl- sesquiterpenyl-. Its arrangement actually depends on carbon-carbon connectivity of their isoprenyl moiety (linear, monocyclic and bicyclic), the aromatization of p-menthyl moiety into a thymil moiety, the closure of further carbon-bonds and finally the closure of oxygen bridges between the isoprenyl and the resorcinyl moieties (Hanuš *et al.*, 2016);

- Resorcinylic moiety: it is carboxylated in native cannabinoids (acidic forms). In cannabinoids that have a single bond between isoprenyl and the aromatic moiety, the two unsubstituted aryl carbons are equivalent (Hanuš *et al.*, 2016);
- Resorcinylic side-chain: the substituent can be alkyl and aralkylic on the basis of the odd and even number of carbons, respectively (Hanuš *et al.*, 2016);

Phytocannabinoids can be grouped differently, based on their chemical features. Indeed, the main phytocannabinoids (Cannabigerol (CBG), Cannabidiol (CBD),  $\Delta^9$ -Tetrahydrocannabinol ( $\Delta^9$ -THC), Cannabichromene (CBC) and Cannabinol (CBN)) can be classified in neutral, acidic and varinic form (Figure 4).

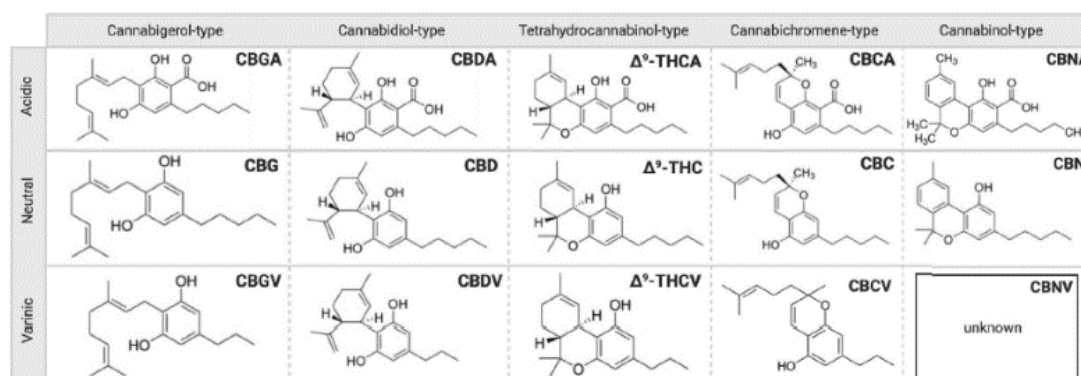


**Figure 4** Chemical structure of the main phytocannabinoids in their acidic, neutral and varinic form: Cannabigerol (CBG), Cannabidiol (CBD),  $\Delta^9$ -Tetrahydrocannabinol ( $\Delta^9$ -THC), Cannabichromene (CBC) and Cannabinol (CBN)-type – adopted from (Morales, Hurst and Reggio, 2017)

Besides, phytocannabinoids can also be classified into three big classes, based on their abundance and their original form: “aralkyl”, “minor” and “native”. Aralkyl group

consists of cannabinoids not exclusively found in Cannabis plant; the minor one includes the less abundant cannabinoids; finally, in the native class are classified all the non-enzymatically decarboxylated forms, whose bioactivity is not yet clear, as well as not adequately investigated as their neutral counterpart (Hanuš *et al.*, 2016; Schurman *et al.*, 2020).

The bioactivity of most cannabinoids is mediated by the interaction with two receptors belonging to the G-protein coupled receptor family CB<sub>1</sub> and CB<sub>2</sub>, which are mainly found, respectively, on presynaptic neurons and immune cells, including microglia, astrocytes, oligodendrocytes. Depending on the type of cannabinoid receptor to which they bind, the biological effect of cannabinoids is clearly different, as CB<sub>1</sub> activity is related to pain and anxiety whereas CB<sub>2</sub> modulation provides an anti-inflammatory effect (Zou and Kumar, 2018). Δ<sup>9</sup>-THC showed partial agonism towards both the receptors, while for CBD, whose affinity with the cannabinoid receptors is rather controversial, a weak antagonism has been detected in *in vitro* studies. However, the question of partial mixed agonism-antagonism activity of the cannabinoid towards these receptors is still unclear, as it might depend on cell types, receptor expression and other conditions (Mangal *et al.*, 2021). Despite these preliminary findings, other investigations focused on defining other possible biological endpoints underlying the broad bioactivity of these compounds were carried out. The putative further end-points were supposed to be serotonin receptor, additional G-protein coupled receptor (GPR) and opioid receptor as well. Δ<sup>9</sup>-THC has an antagonistic activity on 5-HT<sub>3A</sub> receptor, and an agonistic activity towards PPAR-γ and transient receptor potential channels TRPV<sub>2</sub>, TRPV<sub>3</sub> and TRPV<sub>4</sub>. Conversely, it showed no activity on the vanilloid type 1 receptor (TRPV<sub>1</sub>). Moreover, full and partial agonism have been detected respectively to 5-HT<sub>1A</sub> and

5-HT2A, whereas a non-competitive antagonism was revealed on 5-HT3A, GPR55 and GPR18 (Morales, Hurst and Reggio, 2017). The biological effects, derived from the potential affinity of cannabinoids with several receptors, could be reflected from the broad-spectrum of bioactivity of these natural compounds. Indeed, these interactions need to be contextualized into a complex and large biological system, better known as Endogenous Cannabinoids System (ECS). ECS was firstly investigated regarding the two endogenous endocannabinoids anandamide (AEA) and 2-arachidonoylglycerol (2-AG). Starting from the knowledge of their bioactivity, it was hypothesized that phytocannabinoids could potentially be able to interact with different receptors, thus triggering a crosstalk between different signaling pathways (Mangal *et al.*, 2021). This could be considered as the basis of various bioactivity of these compounds, whether endogenous or exogenous (Figure 5).

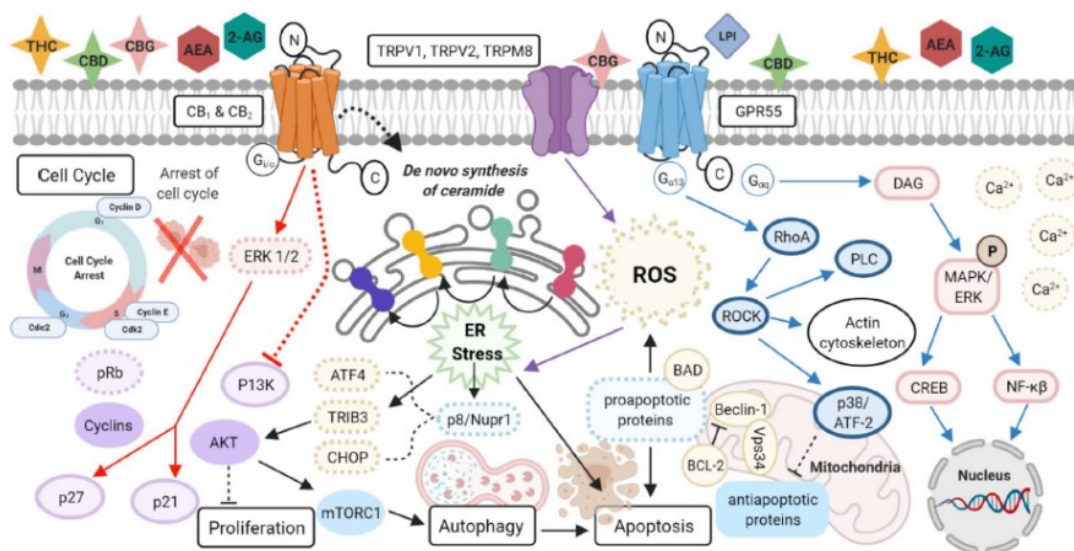


**Figure 5** Overview of crosstalk of signaling pathways of CB, TRPV and GPR receptor- adopted from (Mangal *et al.*, 2021)

Indeed, the activation of cannabinoid receptors triggers ERK1/2 signaling by activating p21 and p27 proteins, leading to the arrest of cell cycle through the inhibition of P13K signaling. CB signaling also induces mTORC1 downregulation, affecting the autophagy process. Additionally, GPR55 receptor activation triggers the activation of MAPK/ERK signaling, by inducing the release of  $\text{Ca}^{2+}$  and DAG from the PLC, and that of RhoA/ROCK pathway, which induces the release of ROS and subsequently the stimulation of the intrinsic apoptotic pathway.

## **1.2 Cannabinoids and their role in nervous system diseases and in tumor pathologies**

Based on knowledge of the mechanism of action underlying the ECS, the bioactivity of phytocannabinoids has been investigated more thoroughly. Considering their affinity for the CB and 5-HT<sub>1A</sub> receptors, the investigation of cannabinoids was focused primarily on central nervous system. In fact, they have been widely used for pathological pain and anxiety-related disorders for years. As already summarized (Ortiz, McMahon and Wilkerson, 2022), 5-HT<sub>1A</sub> receptor agonism has shown to be critical to inhibit nociception and provide beneficial effects, such as neuroprotective effects. In line with this evidence, cannabinoids are widely used for the treatment of Huntington, Parkinson, multiple sclerosis diseases, although the underlying pathogenesis of each is different.

Cannabinoids biological activities have also been revealed with regard to their palliative effect in cancer patients. Recently, some new therapies based on the use of these compounds have been widely employed: Marinol (THC) (AbbVie, North Chicago, IL, U.S.A.) and Cesamet (Nabilone, synthetic analogue of THC) (Meda Pharmaceuticals, Somerset, NJ, U.S.A.), used for chemotherapy-induced nausea

and vomiting, or Sativex (cannabis extract) (GW Pharmaceuticals, Salisbury, U.K.) prescribed to reduce cancer-associated pain.

However, the bioactivity of cannabinoids has not been limited only to the cancer-associated clinical signs, as the potential antitumor effect of these compounds was widely investigated (Velasco, Sánchez and Guzmán, 2016). Indeed, it is important to point out that in the context of ECS system, CB receptors and their ligands play a critical role. Accordingly, further investigation showed that loss or inhibition of CB<sub>1</sub> receptor triggers an increase in the aggressiveness of intestinal adenoma (Wang *et al.*, 2008). In contrast, CB<sub>1</sub> appears to have an ambiguous effect as its overexpression induces HER2 signaling in breast cancer with a pro-oncogenic role (Pérez-Gómez *et al.*, 2015). However, preclinical studies have shown interesting antitumor activity played by cannabinoids at various levels. First, a prevalent effect on the apoptotic or anti-proliferative effect was demonstrated, and an anti-metastatic effect was also detected in *in vivo* conditions. The mechanism underlying the pro-apoptotic role of cannabinoids concerns the endoplasmic reticular (ER) stimulation and the triggering of autophagy, which is indeed considered upstream of the apoptotic process (Velasco, Sánchez and Guzmán, 2016). A preliminary study was carried out on cannabidiol (CBD), which was shown to reduce a mitochondrial oxidative metabolism, thus inducing an anti-proliferative effect. Moreover, CBD induces an inhibition of the cell proliferation and invasion processes. Particularly, CBD was able to downregulate ERK and AKT signaling as well as hypoxia-inducible factor (HIF-1 $\alpha$ ) expression (Mangal *et al.*, 2021). In glioma cell lines, CBD caused mitochondrial dysfunction and mitophagy, by determining influx of calcium ions via Transient Receptor Potential Cation Channel Subfamily V Member 4 (TRPV4). Furthermore, growth inhibitory effect of CBD was evaluated in most representative

glioma cell lines thus obtaining an half inhibitory concentration ( $IC_{50}$ ) in the range 20-30  $\mu$ M (Huang *et al.*, 2021). The most accepted hypothesis is that CBD could induce stress of endoplasmic reticulum (ER) acting on ATF4-DDIT3-TRIB3-AKT-MTOR axis (Huang *et al.*, 2021). These findings suggested to set up innovative therapeutic protocols based on the use of CBD in combination with temozolomide (TMZ), a traditional chemotherapeutic drug currently used in glioblastoma treatment. In fact, recent investigations conducted on neurosphere cultures and mouse models have revealed the intriguing potential of the synergic effect of the aforementioned compounds (Torres *et al.*, 2011).

Also the most abundant phytocannabinoids,  $\Delta^9$ -THC, has shown a clear antitumor property. In pancreatic cancer cell lines, it was revealed to induce ER stress by significantly increasing p8 and ATF-4 as well as TRIB-3. *In vitro* effects were further confirmed on xenograft models of pancreatic cancer, thus suggesting a reduction in tumor burden after treatment with  $\Delta^9$ -THC (Carracedo *et al.*, 2006). Other less abundant cannabinoids revealed a potential anticancer effect that, for most of them, have been related to their interaction with CB<sub>1</sub> and CB<sub>2</sub> receptors. Recently their ability to modulate the channels GPR55, TRPM8 as well as TRPA1 and TRPV was suggested as possible mechanism of action (Mangal *et al.*, 2021).

### **1.2.1 Anti-cancer effect of cannabinoids in glioma**

The affinity of cannabinoids for the cannabinoids receptors has prompted the researchers to investigate their anti-tumor properties in brain tumors, such as glioblastoma. This is a tumor, whose aggressiveness is conferred by a heterogeneous microenvironment. Indeed, the presence in addition to the astrocytic

population, of leukocytes, protumor macrophages and endothelial cells leads to an increase in tumor invasion and progression. Although several chemotherapeutic drugs have given good results in *in vitro* studies, a therapy aimed at interfering with multiple pathways is strongly needed to obtain an efficacy therapy. Therefore, cannabinoids - inherently multi-target bioactive compounds - have been suggested as putative hits for developing new anti-glioblastoma drugs. Indeed, CBD has proven to be a very promising compound for the treatment of glioma in rat C6 glioma cells (Ligresti *et al.*, 2006). On other similar brain cell lines, CBD showed to inhibit cell proliferation, induce apoptosis and decrease the invasion processes (Qamri *et al.*, 2009; Solinas *et al.*, 2013). Although the psychotropic effect of THC, the first investigations were approximately carried out on CBD-THC mixtures, to take advantage on a possible synergic effect. In fact, both compounds were able to reduce tumor growth in nude mice and in U87MG cell line of human glioblastoma (López-Valero *et al.*, 2018). However, as the psychotropic effect of THC suggested to limit its use, the subsequent investigations were conducted only with CBD. Hence, the anticancer activity of CBD treatment for glioblastoma was revealed. In particular, CBD induced a significant reduction in tumor growth in xenograft human U87MG tumor (Massi *et al.*, 2004). Moreover, CBD was able to act on derived glioma stem cells (GSCs), a characteristic cellular population that confers greater resistance to the tumors against therapies. Indeed, when CBD were tested in GSC xenograft, an increase in the survival rate of mice was detected (Singer *et al.*, 2015).

Despite such interesting results obtained in the use of CBD as an anticancer agent, there is still a significant lack of data. Firstly, not all of the activities described for CBD may be ascribed to its interaction with the cannabinoid receptors. Secondly, there are many other cannabinoids whose activity and mechanism of action have

been poorly studied. For instance, native carboxylate cannabinoids, as previously discussed, represent a well-populated class of compounds almost completely orphan of bioactivity and receptors in human cells.

### 1.3 Aim of the thesis project

Phytocannabinoids, a class of more than 200 meroterpenoids, show a wide variety of cellular targets. Recent discoveries have shed light on the anti-inflammatory and anti-tumor properties of these molecules, thus qualifying them as privileged structures for biomedical research. The diversity of reported targets for some cannabinoids prompted us to investigate the vast dark area of the phytocannabinoids chemical space, neglected in terms of biological study. Indeed, although various phytocannabinoids have been studied for their mechanism of action, the bioactivity profile of native carboxylate species is still poorly understood. Therefore, the present research project is focused on the characterization of the molecular mechanism of action of the main abundant compound: cannabidiolic acid (CBDA) (Figure 6).

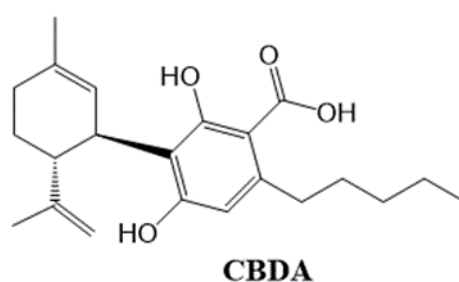


**Figure 6** Chemical structure of cannabidiolic acid (CBDA)

Based on the biological activity of the most studied cannabinoids (CBD and THC) on glioma tumor, the bioactivity of CBDA has been investigated in the context of glioblastoma, aiming to the identification of new target(s). To characterize its putative biological effect and elucidate the mechanism of action at a molecular level, a combination of proteomic-based biochemical and bioinformatic approaches have been used. The study has been carried out starting from the identification of protein target(s) of this compound, followed by an appropriate validation and by the investigation of the functional effect of CBDA interaction with its target in glioblastoma cells.

#### **1.4 Chemical proteomic approaches in drug discovery process**

Drug discovery is a process by which new molecules are identified as potential therapeutic candidates. It consists in the identification, characterization and, optionally, optimization of bioactive compounds, followed by the evaluation of their therapeutic efficacy (Henrich and Beutler, 2013). Drug discovery has always been focused on the investigation of conventional synthetic molecules and natural products. Comparing to the former, natural products have attracted the attention of the scientific community since they have a higher molecular mass, more sp<sup>3</sup> carbon atoms and oxygen atoms, fewer nitrogen and halogen atoms, higher numbers of H-bond acceptors and donors, lower calculated octanol–water partition coefficients and a great molecular rigidity (Henrich and Beutler, 2013). Therefore, some of these significant differences make them interesting and useful for drug screening. Despite these advantages, pharmaceutical companies have shown no significant interest in many of these compounds as they cannot be tested through the classical target-

based assays (Henrich and Beutler, 2013). However, there is still considerable interest in identifying molecular targets of natural products active against cancer and infectious disease. Indeed, although the use of such compounds is limited because of the complexity of the isolation and characterization processes, they are widely used as starting points for the design and chemical synthesis of new drugs. In fact, a functionalization or modification of the native structure of the molecule can improve its effect and also guarantee greater safety (Atanasov *et al.*, 2021). However, several drawbacks have been defined. One of them concerns the difficult functionalization due to small chemical structure. Moreover, these compounds can be present in small quantities in the natural sources restricting their isolation.

Drug discovery can be considered as a three-element equation, as bioactive compounds can interact with a molecular target that influences the phenotype of the disease. Considering that most molecular targets are proteins, chemical proteomic approaches are emerging as increasingly advanced techniques suitable to identify all the possible interactors of an investigated compound proteins in a biological system (Meissner *et al.*, 2022). Over the past few years, many types of proteomic strategies have been defined to that aim. Based on the possible protein stability conferred by the interaction with small molecule, a combination of approaches has been interpreted so that they complement each other.

Proteomic approaches are classified into two classes: bottom-up and top-down approaches. The first refers to the characterization of proteins starting from the analysis of peptides derived from proteolytic digestion. When bottom-up is performed on a protein mixture, it is called “shotgun proteomics”. Differently, top-down characterizes intact proteins directly from complex biological systems (Zhang

*et al.*, 2013). Both approaches have advantages and disadvantages. Therefore, a hybrid of bottom-up and top-down approaches has been defined as middle-down proteomics that analyzes larger peptide fragments than bottom-up proteomics (Wu *et al.*, 2012). The top-down approach has potential advantages for post-translation modifications (PTM) and protein isoform determination. However, it does not allow adequate protein fractionation, protein ionization and fragmentation in the gas phase. Therefore, since top-down is still facing many technical challenges, it is not yet considered a robust approach to the study of proteomics. On the contrary, bottom-up proteomics takes advantages that peptides are more easily separated by reversed-phase liquid chromatography, ionize and fragment well. These features make this approach able to perform high-throughput analysis, allowing the identification and quantification of thousands of proteins from complex lysates (Zhang *et al.*, 2013). Hence, bottom-up proteomics is currently considered as the most cost-effective approach for large-scale quantification of proteomes. It consists of several steps, as shown in workflow represented in (Figure 7).

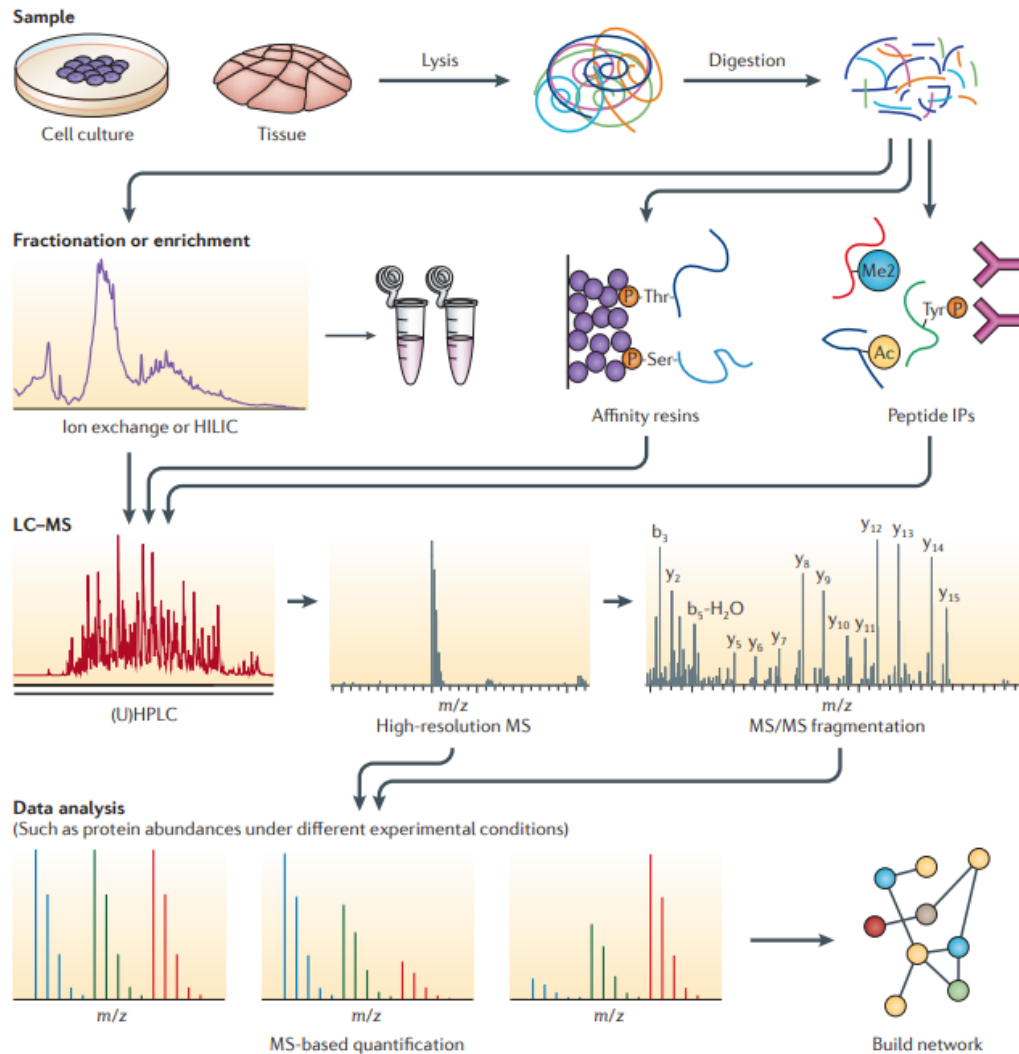


**Figure 7** Mass-spectrometry-based proteomics workflow – adopted from (Altelaar, Munoz and Heck, 2013)

Biological samples, even from different sources, are lysed, the obtained proteins are digested and the resulting peptides fractionated. Finally, these are analyzed by mass spectrometry (MS) and, after ionization, spectra of peptides and peptide fragments are acquired. These are subjected to a database search for peptide identification and the data are further processed and analyzed, by performing statistical tests to evaluate significant differences between samples (Altelaar, Munoz and Heck, 2013). The widely used proteomics and cell-based approaches for the

investigation of protein-molecule interaction are presented below. These are defined as conventional bottom-up proteomics strategies for peptide sequencing and consequently protein identification.

#### **1.4.1 Drug Affinity Responsive Target Stability (DARTS)**

For the target investigation, Drug Affinity Responsive Target Stability (DARTS) is one of the most innovative approaches introduced by (Lomenick *et al.*, 2009). The principle on which DARTS is based is the idea that structural changes in target molecules induced by unmodified small molecules could alter its sensitivity to proteases. The interaction between a small molecule and its protein target is established by ionic and hydrogen bonds, van der Waals and other intermolecular forces (Ren *et al.*, 2021). Compound binding may mask proteolytic sites yielding a different proteolytic pattern between free-protein and compound-bound protein.

Technically, DARTS can be performed on intact cells or on cell lysates. As a first step, the cells are treated with the molecule or vehicle alone. Then they undergo limited enzymatic digestion by a non-specific protease, followed by sodium dodecyl sulfate–polyacrylamide gel electrophoresis (SDS-PAGE). The peptides mixture is obtained by tryptic in-gel digestion and separated by liquid chromatograph mass spectrometry. The bottom-up proteomics data generated are finally analyzed by suitable bioinformatic tools, thus providing qualitative information on proteins potentially resistant to protease digestion (Figure 8).

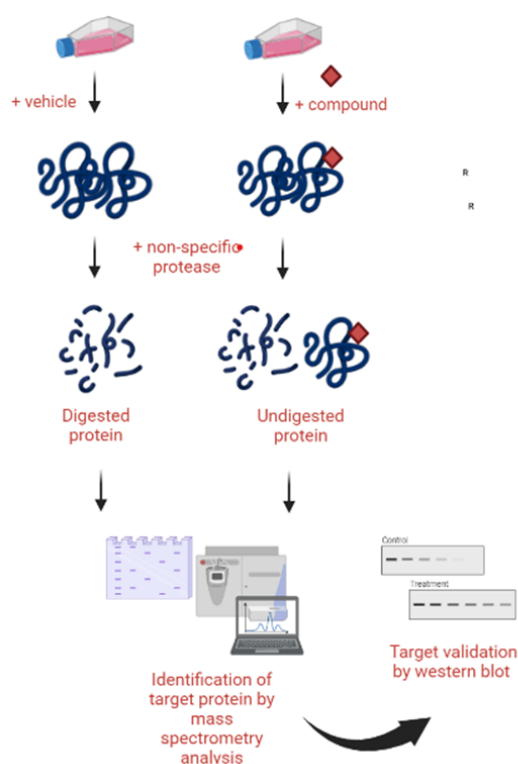


**Figure 8** *Experimental workflow of DARTS assay*

Due to the combination of DARTS with the development of the MS technique, in a context of using of orphan molecules, DARTS assay is used for untargeted analysis. However, DARTS can also be used to confirm and validate a protein-molecule binding already suggested by other means, and to estimate the strength of the interaction. In this case, western blot and secondary assays can be utilized to validate previously obtained data. Like other chemical proteomics approaches, DARTS technique presents advantages and disadvantages. First, it does not require labeled ligands, thus allowing to use small molecules. Moreover, it is independent of drug-induced biological effects, so it allows to analyze any compound of interest. In addition, it can be performed on any cell and tissue type. However, DARTS has potential limitations. Many proteins appear to be resistant to protease digestion as

the susceptibility strongly depends on protein conformational energy. Moreover, target identification may be limited as the protein is present in low abundance and therefore not easily recognized by mass spectrometry analysis (Huang, Wang and Zhang, 2021). Nevertheless, as shown by (Lomenick *et al.*, 2009), DARTS assay can be performed using inhibitory concentrations of the molecule, up to high micromolar concentration. Since DARTS assay aims to identify a molecular interaction, it is crucial to avoid cell death or any biological response. Therefore, the treatment is generally carried out using sub-toxic concentrations of the molecule for a very short incubation time. Finally, the translation of DARTS from *in vitro* to *in vivo* systems is quite critical, due to the different cell-membrane permeability and physiological environment. However, despite these technical and experimental disadvantages, DARTS appeared to be one of the most effective approaches for targeted and untargeted analyses of bioactive compounds.

#### **1.4.2 Cellular Thermal Shift Assay (CETSA)**

In a context of target engagement confirmation, Cellular Thermal Shift Assay (CETSA) is a technique based on the traditional Thermal Shift Assay (TSA). While TSA relies on use of purified recombinant protein or isolated protein domains, CETSA can be performed in cells (Henderson *et al.*, 2020). CETSA is based on the principle of thermodynamic stabilization inferred to a protein by the ligand-protein interaction. It detects a change in protein thermal stability induced by ligand binding thus evaluating drug target engagement as an implementation of thermal shift assays in a cellular model. Like DARTS assay, CETSA could be performed on cell lysate and intact cells, albeit the comparison of both techniques may provide

information on the availability of the drug for the protein target. Technically, CETSA consists primarily of cellular treatment with the molecule of interest, or vehicle as control. After incubation, the cells are exposed to a temperature range that can allow evaluating a potential thermal stabilization, lysed through a freeze-thaw cycle and centrifuged to remove cell debris and aggregates. The putative stabilization of the protein is detected by western blot. Hence, the apparent aggregation temperatures ( $T_{agg}$ ) measured with and without compound are compared and the occurrence of substantial shifts demonstrate the molecular interaction (Figure 9).

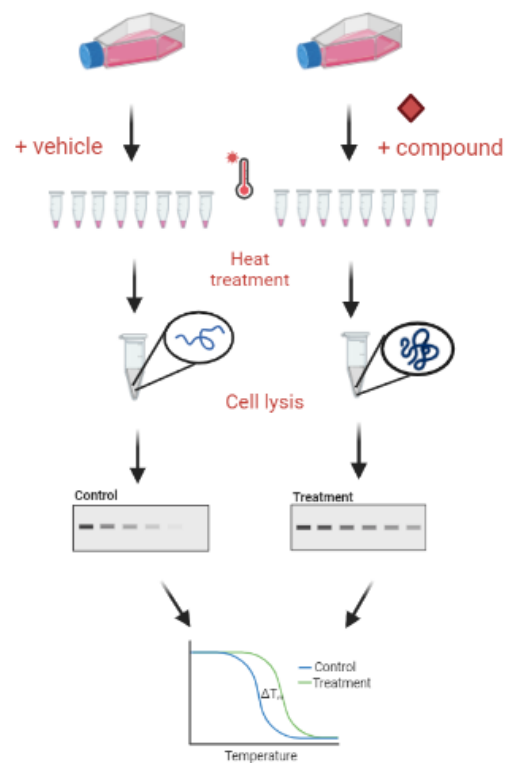


**Figure 9** *Experimental workflow of CETSA assay*

Binding confirmation can therefore be obtained by detecting the thermal stability shift in a treated sample where the amount of soluble protein will be more abundant than the negative control (Figure 10).

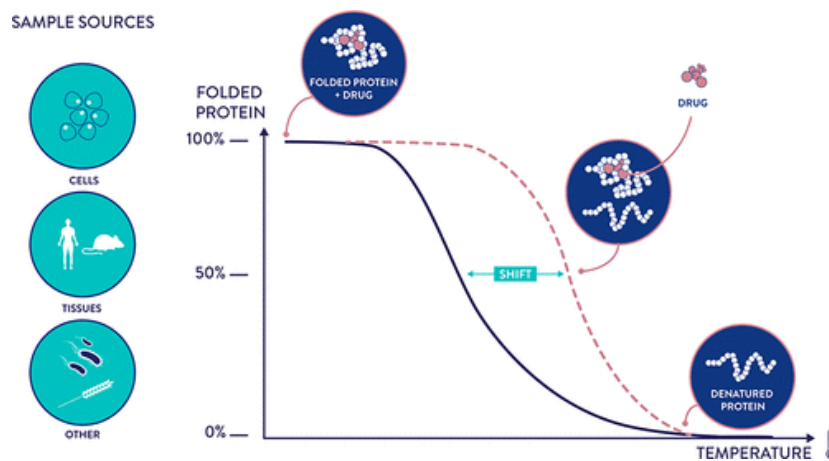


**Figure 10** Example of shift melting curve of protein without and with drug – adopted from (Lundgren, 2019)

One of the important advantages of this approach is that the small molecule can be analyzed unmodified. Additionally, as a cell-based assay, the entire cellular environment is involved. Some limitations have been identified, such as the detection system by western blot that limits the number of samples that can be analyzed (Jafari *et al.*, 2014). An improved CETSA approach is the Isothermal Dose-Response Fingerprints - CETSA (ITDRF-CETSA). In this technique, after the identification of the temperature at which the protein denatures and precipitates, protein stabilization can be evaluated as a function of increasing ligand concentration.

### **1.4.3 Mass Spectrometry-associated Limited-Proteolysis**

In a process of validation of molecular interaction ligand-protein, the aforementioned approaches could be complementary to each other. Additionally, secondary proteomic approaches could be used to obtain information on the specific binding site. Hence, since the mass spectrometry (MS) is currently used to study structural alteration and protein-protein interaction, the MS-associated limited-proteolysis (MS-LiP) has been identified as a novel proteomic approach for studying the binding site of small molecules (Feng *et al.*, 2014). LiP is a biochemical approach that provides information on protein structures and conformational changes. In brief, like DARTS technique, LiP is based on the principle that ligand binding causes changes in protein conformation (Schopper *et al.*, 2017). Therefore, proteases cannot access the same cleavage sites on the proteins without ligand with respect to them on the ligand-bound protein. Like most proteomic approaches, LiP can be applied to cell lysates and intact cell. Particularly, the main advantage of performing LiP in a cellular context concerns the analysis of protein structural alterations on a proteome-wide scale. These differently spliced peptides from the treated and untreated samples are then detected with MS. Technically, the protein-derived treatment or samples are subjected to one or double-pulse proteolysis. In the case of double-pulse proteolysis, a non-specific protease (e.g. proteinase K, thermolysis, subtilisin, etc.) is used in the first step. After a denaturation phase, that allows to linearize all the peptides derived from first-step digestion, these are subjected to an extensive trypsin digestion. In this way, peptides amenable to bottom-up proteomics are generated. Finally, a peptide mixture including both fully tryptic peptides and half-tryptic peptides deriving from the LiP step is produced. The mass spectrometry analysis and the use of software for qualitative and quantitative analysis thus

provide the characterization of peptides in control and treated samples and the protein abundance changes calculation (Schopper *et al.*, 2017) ( Figure 11).

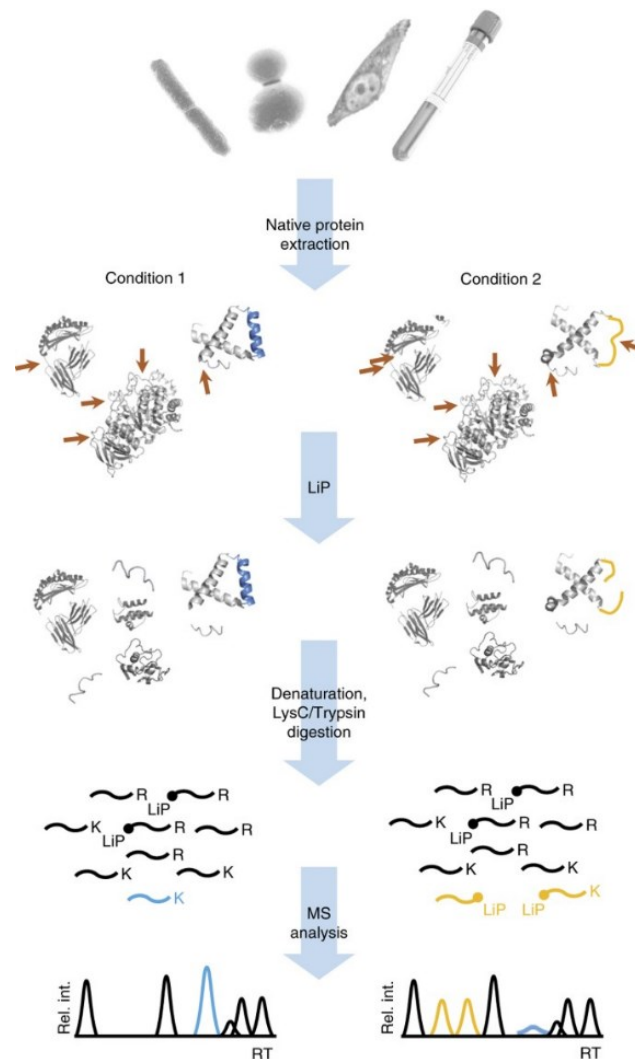


**Figure 11** General workflow of Limited Proteolysis- adopted from (Schopper *et al.*, 2017)

LiP has many types of applications as LiP-MS can detect protein structural rearrangements induced by specific perturbations (Feng *et al.*, 2014; Stauffer *et al.*, 2014). Additionally, this technique is also used for the investigation of protein aggregation and small-molecule-protein interaction (Pepelnjak, de Souza and Picotti, 2020). In the context of the use of orthogonal tools for the study of molecular

interaction, LiP technique supports data coming from or provides more information derived from other approaches.

#### **1.4.4 SILAC: Stable Isotope Labelling by Amino acids in cell culture**

For quantitative bottom-up proteomics, SILAC has emerged as an innovative and powerful approach. It is a mass spectrometry-based approach that aims to perform a quantitative proteomic analysis by monitoring metabolically labeled-proteins (Mann, 2006). It is based on the use of amino acids labeled with stable (non-radioactive) light-, medium- or heavy- isotopes that are metabolically incorporated into all of proteins in living cells. Hence, proteomes derived from different treatment can be distinguished according to the molecular weight of the light- or heavy- amino acids. Since both of the resulting populations are chemically identical but have different masses, the ratio between the intensities of the respective signals corresponds to the ratio of the same proteins in the two samples from the differently treated cells (Ong *et al.*, 2002; Chen *et al.*, 2015). SILAC is performed on growing cells in culture media containing amino acids labeled with different stable isotopes. Once the cell confluence is reached, the proteins are extracted, mixed, digested and subjected to LC-MS/MS and finally the resulting data are analyzed by proteomic software (Figure 12).

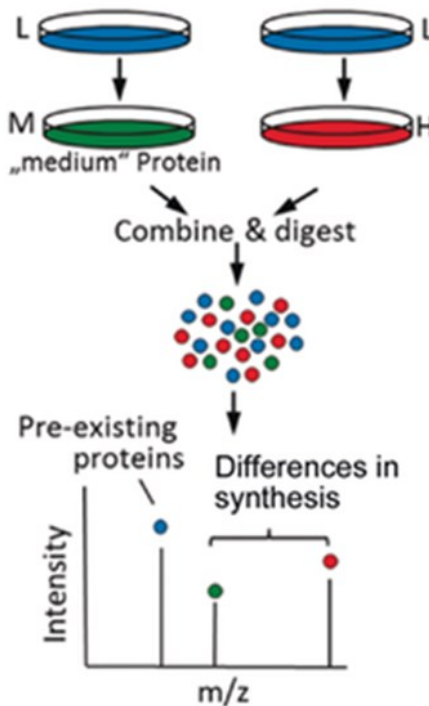


**Figure 12** General workflow of SILAC technique. Cells are cultured in the presence of stable-isotope labelled amino acids: light- (L) (blue), medium- (M) (green) or heavy- (H) (red). The different labelled proteins are subjected to the proteolytic digestion and analyzed by mass spectrometry -adopted from (Atzrodt *et al.*, 2018)

Mass spectrometry analysis is an unbiased method that provides characterization of all proteins present in samples for protein identification and quantification. Trypsin is a common proteolytic enzyme in proteomic approaches, it cleaves at the carboxyl-end of lysine and arginine residues of proteins. Therefore, in SILAC, the use of arginine and lysine as labeling amino acids in combination with trypsin digestion allows the quantification of all labeled peptides (Ibarrola *et al.*, 2003). SILAC approach enables to compare different conditions in a single, multiplexed experiment. Therefore, using three or two isotopically distinct forms of amino acids

(e.g. arginine and lysine), triple encoding SILAC allows comparison of three cellular populations in one single experiment (Ong and Mann, 2006).

Obviously, SILAC has advantages and several potential limitations. Firstly, it has been defined as an accurate qualitative and quantitative proteomic method. Additionally, it can be applied on a wide variety of dividing cell lines while also providing proteome and secretome analysis. At the same time, it suffers for the time-consuming cultural process and it cannot be used on nondividing cells and human samples (Mann, 2006). Other critical aspects need to be mentioned. Firstly, although SILAC medium is almost identical to the classic medium currently used in common cell culture systems, a critical choice concerns the use of serum; in fact, being a source of amino acid, it is preferable to use dialyzed serum (Ong and Mann, 2006). However, SILAC has been identified as a powerful and versatile approach as it can provide information on the whole proteome, analysis of changes in post-translational modification and phosphorylation, and finally for the definition of proteomic profiles at different time-frame as shown in a SILAC variant, known as pulsed-SILAC approach (Fierro-Monti *et al.*, 2013).

#### *1.4.4.1 Pulsed-SILAC: variant of classic SILAC to investigate nascent proteome*

SILAC can be applied to investigate the nascent proteome. Hence, pulsed-SILAC (p-SILAC) has been defined as a variant of a classic approach. This technique allows to perform the analysis of newly synthesized proteins since the labelling occurs only for a short time period. p-SILAC differs from SILAC primarily in two aspects. The first concerns the incorporation of azidohomoalanine (AHA), an azide-

bearing analogue of methionine, into newly synthesized proteins replacing methionine. The second concerns the use of the click chemistry reaction for the enrichment of newly synthesized proteins. In this approach, cells are treated with stable isotope labeled amino acids in the presence of AHA that is incorporated into newly synthesized proteins. Therefore, these azide-containing proteins are covalently coupled to an alkyne-activated resin via click-chemistry, in order to produce an adequate enrichment of only neo-synthesized proteins from a cell lysate, thus facilitating the MS-based detection of the relative peptides. Particularly, newly synthesized proteins are coupled to alkyne-functionalized agarose resin by 1,3-cycloaddition (click reaction) after 18h of reaction at room temperature (Figure 13).

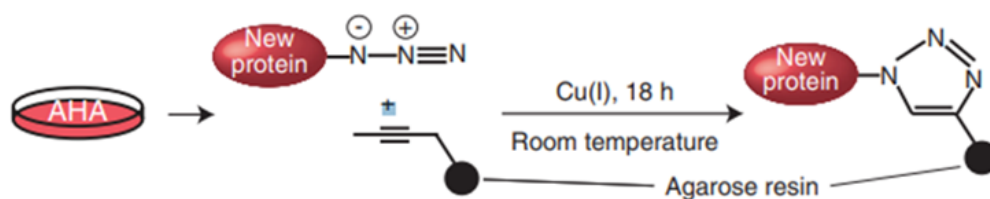


**Figure 13** Representation of the enrichment of newly synthesized proteins – adopted from (Eichelbaum et al., 2012)

Summarizing (Figure 14), cells are treated in the same way as the classic SILAC using light-, medium- or heavy-isotopes labelled medium and AHA as well. After a short period of treatment, the cells are lysed, mixed and subjected to click chemistry reaction. Then, resin-bound proteins undergo canonical reduction and alkylation phase, washed and digested by the trypsin enzyme. The peptides are separated, analyzed by LC-MS/MS and characterized by a suitable bioinformatic software.

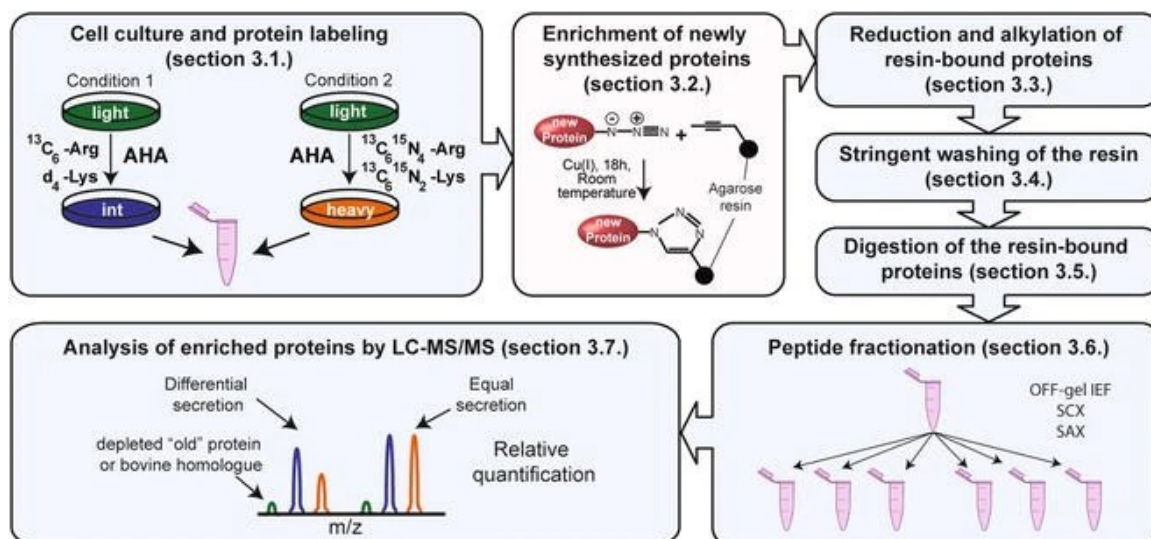


**Figure 14** Workflow of pulsed-SILAC technique – adopted from (Eichelbaum and Krijgsveld, 2014)

Pulsed SILAC coupled with advanced MS-based proteomic technologies thus enables the analytical coverage needed to assess the nascent proteome.

### 1.5 Two-dimensional and Three-dimensional cellular model

Currently, one of the major challenges concerns the development of biologically relevant models for drug testing and development. This difficulty stems from the complex architecture of tumors *in vivo*. Generally, despite the liquid ones, a solid tumor is characterized by a complex tumor microenvironment (TME), as a continuously evolving entity. The tumor cancer cells interact dynamically with cellular and non-cellular components, creating a heterogeneous microenvironment (Figure 15).

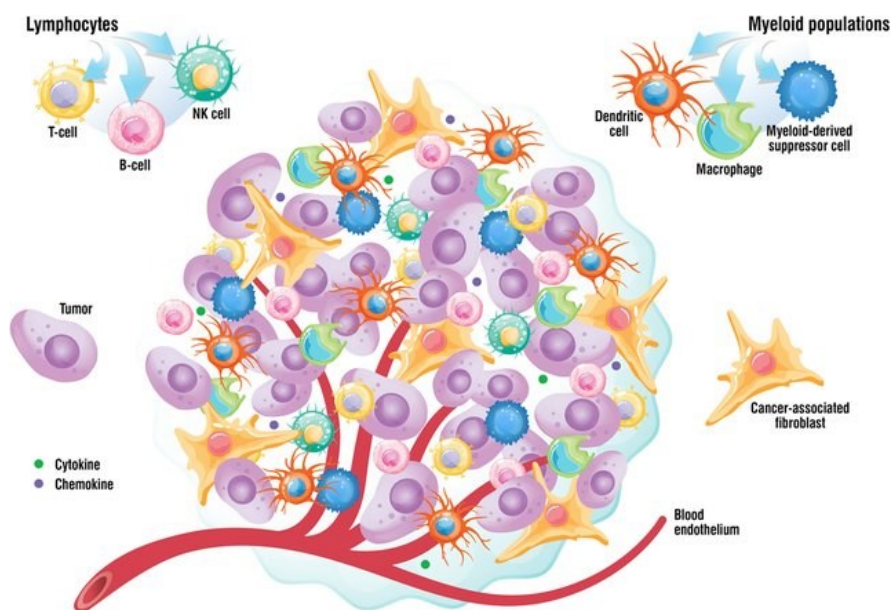


**Figure 15** Representation of tumor microenvironment- adopted from (Zhang and Veeramachaneni, 2022)

In fact, cellular component consists of stromal, fibroblast, endothelial cells as well as pro- and anti-tumor macrophage component. The non-cellular component concerns the extracellular matrix (ECM) which is important to promote tumor invasion (Baghban *et al.*, 2020). The ECM plays a critical role during invasion processes as it interacts with the basement membrane by cancer cells. Particularly, cancer cells secrete matrix metalloproteinase (MMP), proteolytic enzymes that facilitate invasion process and metastasis formation. The currently used cellular models grow as monolayer in flat surfaces. Hence, the resulting cellular morphology is influenced by the cultural conditions thus appearing flattered and stretched. This altered morphology affects cell-cell and cell-ECM interactions compared to *in vivo* tumor. Based on these evidences, the attention of scientific community is currently focused on the development of innovative cellular model capable of reproducing a tumor or pathology closer to *in vivo* conditions. Therefore, three-dimensional models

are replacing two-dimensional ones. Based on the technique used to generate them, these have been categorized in scaffold-based and non-scaffold-based models. Scaffold-based models, natural and synthetic materials are used to mimic the natural environment using fibrin, collagen and hyaluronic acid with the addition of synthetic materials. The cells are implanted in the matrix by adopting their natural shape and interacting with the environment. The scaffold-based 3D culture is divided into hydrogels and solid-state scaffold. Hydrogels are the most used scaffold because of their soft and rubbery consistence. Differently, solid state scaffolds create a solid 3D space, thus positioning the cells in a precise and natural 3D-tissue like structures. Differently, scaffold-free 3D cultures generate a flexible and adapting environment for cellular growth. Hence, the cells are able to spontaneously create multi-cellular aggregates that mimic solid tissue by establishing interaction with the extracellular environment. This system generates spheroids, that may include one- or more cellular lines, and organoids. The latter are 3D cellular aggregates derived from stem cells or primary tissue. Based on their distinctive biological provenience, they are able to generate *in vitro* real organs such as liver, pancreas, intestine, kidney and thyroid. Although the organoids seem to be the most appropriate cellular model, they have different disadvantages. In fact, the lack of vasculature and the limited replication rates make this system complicated to develop and to analyze (Joseph, Malindisa and Ntwasa, 2018; Jensen and Teng, 2020).

Three-dimensional cell models are widely used for drug discovery investigation. Specifically, their application is used for diseases modeling, target identification and validation, toxicity test as well as potency profiling. However, many limitations are still underlined. First, a standard 3D culture setting protocol for the official industry has not yet been defined. However, for canonical research investigation, 3D cell

model are currently used to reproduce tumor diseases. Based on the different cellular morphology compared to 2D cell model, 3D multi-aggregates cells reproduce the typical tumoral zones including oxygenation and nutrition availability. In fact, they represent the three tumor regions: necrotic zone, quiescent viable and proliferating zone (Figure16).

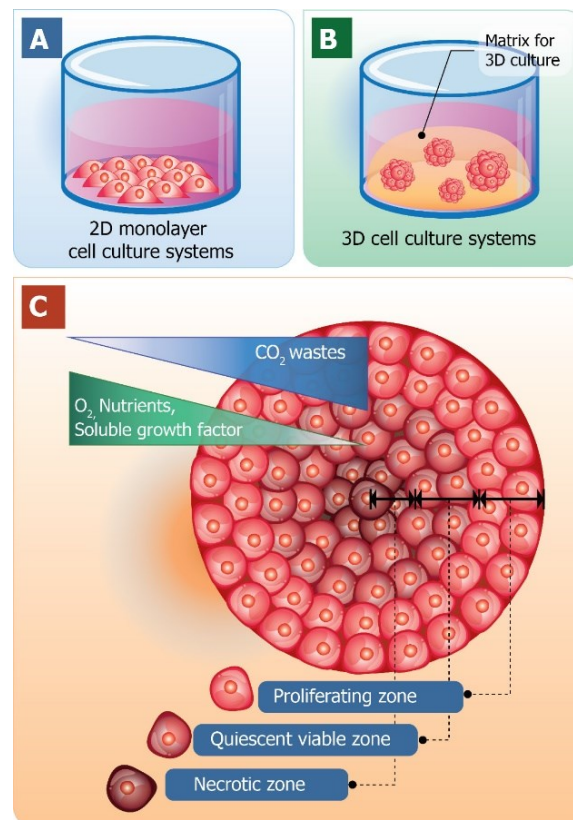


**Figure 16** Comparison of 2D and 3D cell models. A) 2D cellular model; B) 3D cellular model; C) The structural zones in a tumor 3D cell model- adopted from (Chaicharoenaudomrung, Kunhorm and Noisa, 2019)

Although the cost of reproduction and maintenance of 3D models is still high, they provide many technical advantages. Firstly, the possibility to extend the cell culturing up to 3 weeks, whereas 2D can be cultured until they are confluent. 3D reproduces

a natural cellular shape and accurate polarization. Additionally, in the context of drug testing, 3D shows a drug resistance quite similar to *in vivo* conditions. This finding suggests their potential application for drug investigation and high-throughput screening (Figure 17).

Characteristics	2D cell culture	3D cell culture
Morphology	Cells grow on a flat surface and have flat or stretched shape	Cells grow naturally into 3D aggregates/ spheroids in a 3D environment and natural shape retained
Cell shape	Single layer	Multiple layers
Cell to cell contact	Limited cell to cell contact, only on edges	Physiologic cell to cell contact similar to <i>in vivo</i>
Distribution of medium	Cells receive an equal amount of nutrients and growth factors from the medium during growth.	Cells do not receive an equal medium during growth. The core cell receive less growth factors and nutrients from the medium and tend to be in a hypoxic state, which is very similar to <i>in vivo</i> tissues, especially in tumors
Cell proliferation	Generally, cells proliferate at a fast rate than <i>in vivo</i>	Cells proliferate faster or slower depending on the type of cell or 3D system used
Protein/gene expression	Protein and gene expression profiles differ compared with <i>in vivo</i> models	Protein and gene expression profiles more similar to <i>in vivo</i> models
Cell differentiation	Moderately differentiated	Properly differentiated
Response to stimuli	Poor response to mechanical stimuli of cells	Good response to mechanical stimuli of cells
Viability	Sensitive to cytotoxin	Greater viability and less susceptible to external factors
Drug sensitivity	Cells are more sensitive to drugs and drug show high efficacy	Cells are more resistant to drugs and drug show low potency
Cell Stiffness	High stiffness	Low stiffness
Sub-culturing time	Allows cell to be grown in culture for up to 1 week	Allows cells to be grown in culture for almost 4 weeks

**Figure 17** Characteristics of 2D and 3D cell cultures-adopted from (Joseph, Malindisa and Ntwasa, 2018)



**Chapter 2 –Study of the mechanism of action of CBDA in  
2D cell model**



## Results

### **2.1 Eukaryotic translation complex identified as putative target of cannabinoids by DARTS assay**

Minor cannabinoids exhibit a wide plethora of biological effects, although their mechanism of action is still poorly understood. To shed light on the biological effect of CBDA in tumor cells, a chemical proteomics study was implemented. To this end, U87MG with epithelial morphology was chosen as a representative cell line of glioblastoma tumor. Preliminarily, the cytotoxicity of this compound against glioblastoma cells was evaluated. As previously demonstrated (Jacobsson *et al.*, 2000), CBDA shows a potential affinity to fetal bovine serum (FBS) proteins, which could result in a reduction in its bioavailability. Therefore, the cytotoxic effect of CBDA was studied in the presence of different amounts of FBS, using MTT reduction as an end-point. As expected, the cytotoxic effect of this molecule after 48 hours of treatment was inversely proportional to the concentration of FBS (Figure 18).

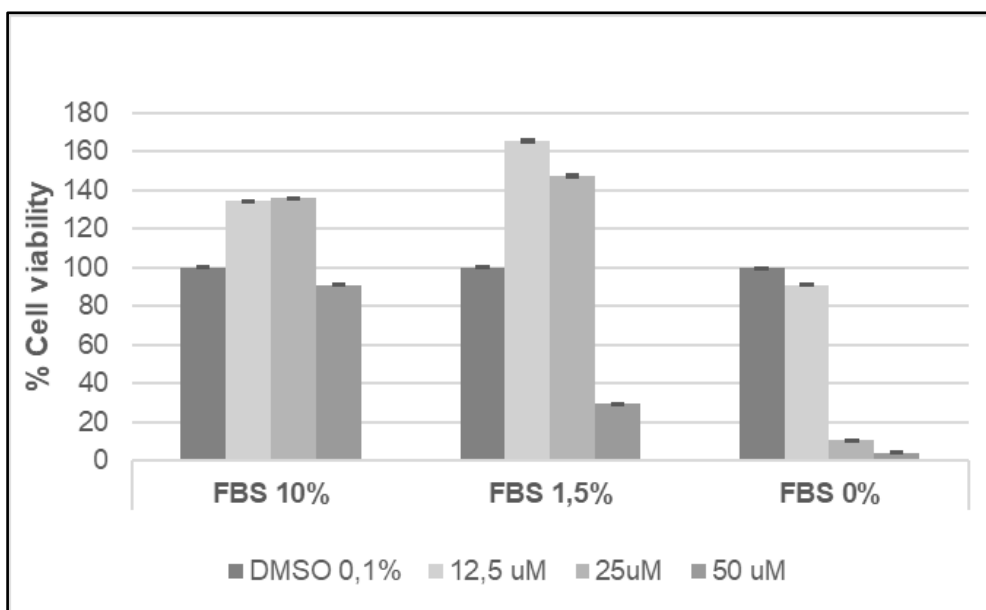


**Figure 18** *Percentage of cell viability after treatment with CBDA for 48 h, in the presence of different concentrations of FBS. This experiment is representative of two biological replicates*

In order to verify that this molecule was not toxic to the normal cell lines, MTT assay was also performed on Normal Human Astrocytes (NHA), and no significant cytotoxic effect has been revealed. Based on these preliminary experiments, cell treatments were carried out by incubating the cells with 50  $\mu$ M of CBDA in the presence of 10% FBS-DMEM, as under these conditions negligible cytotoxic effects were observed. The Drug Affinity Responsive Target Stability (DARTS) assay was chosen as the most effective approach to identify bioactive compounds protein targets. It was performed on both U87MG cell lysates and intact cells, to obtain complementary results. In fact, experiments conducted on cell lysates provide information on the potential interactivity of a bioactive compound, independently of its ability to efficiently cross the cell membrane and reach specific organelles inside the cell. Therefore, the experimental conditions depend only on the solubility of the

compound and its presumed affinity for the targets. Conversely, when the DARTS assay is performed using intact (and live) cells, treatment conditions must be optimized to utilize the highest non-toxic concentration of the bioactive and incubation times long enough to allow significant uptake into cells but not to induce noticeable changes in cellular metabolism. However, using this procedure, the compound/target interaction can occur in an effectively pseudo-physiological environment.

By merging the results obtained in all the analyses conducted using different conditions, ten proteins emerged as putative intracellular interactors of CBDA (Table 1).

**Table 1** *Proteins identified as putative CBDA targets in U87MG cell lines by DARTS experiments*

<b>ACCESSION</b>	<b>DESCRIPTION</b>
EF1A1_HUMAN	Elongation factor 1-alpha 1
EF1G_HUMAN	Elongation factor 1-gamma
EF2_HUMAN	Elongation factor 2
EIF2A_HUMAN	Eukaryotic translation initiation factor 2A
EIF3B_HUMAN	Eukaryotic translation initiation factor 3 subunit B
EIF3C_HUMAN	Eukaryotic translation initiation factor 3 subunit C
EIF3L_HUMAN	Eukaryotic translation initiation factor 3 subunit L
EIFCL_HUMAN	Eukaryotic translation initiation factor 3 subunit C-like protein
IF2G_HUMAN	Eukaryotic translation initiation factor 2 subunit 3
IF4A1_HUMAN	Eukaryotic initiation factor 4A

Interestingly, all of them are part of the Eukaryotic Translation machinery. Based on the literature, CBD, decarboxylated form of CBDA, seems to induce endoplasmic reticulum stress thus activating integrated stress response (ISR). Hence, the close correlation between ER stress and eukaryotic alternative translation has strengthened the hypothesis that cannabinoids could target eukaryotic translation machinery complex. Since the initiation translation phase is widely defined as the limiting step of the entire translation process, we first evaluated the Eukaryotic Initiation Translation Factor 2A as putative target of CBDA (Sonenberg and Hinnebusch, 2009). Besides, (Starck *et al.*, 2016) showed that EIF2A seems to play a critical role in translating the upstream open reading frames (uORFs) present in mRNAs controlled by the ISR. Therefore, in order to strengthen this preliminary result, the DARTS mass spectrometry-based results were validated by western blot analyses. At this aim, CBDA ability to interact with EIF2A was compared to that of other native cannabinoids: cannabidivarinic acid (CBDVA), cannabigerolic acid (CBGA) and cannabichromenic acid (CBCA) (Figure 19).

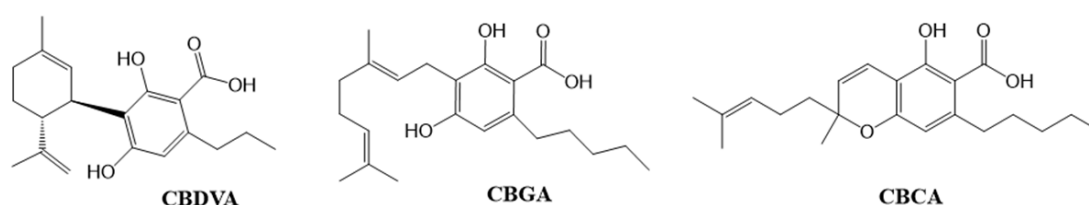


**Figure 19** Chemical structure of cannabidivarinic acid (CBDVA), cannabigerolic acid (CBGA) and cannabichromenic acid (CBCA)

U87MG cells were treated separately with CBDA, CBGA, CBDVA and CBCA, and DARTS detection of EIF2A was analyzed via immunoblotting (Figure 20).

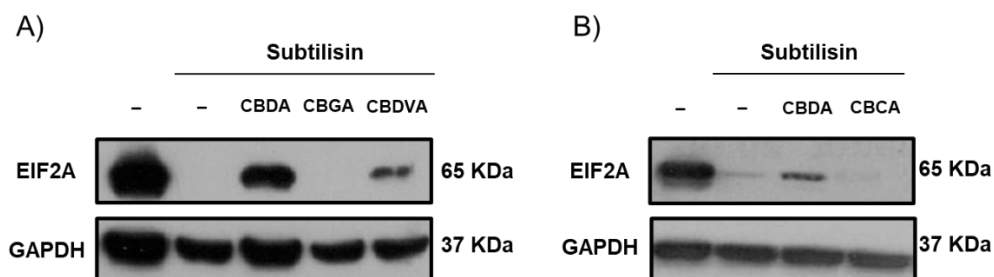


**Figure 20** Western blot analysis of EIF2A in DARTS experiment A) DARTS of CBDA, CBGA and CBDVA on U87MG cells B) DARTS of CBDA and CBCA on U87MG cells

CBDA turned out to be the most efficient compound in providing protection from proteolysis to EIF2A and can therefore be considered the one with an higher affinity for the protein. CBDVA too showed some ability to interact with EIF2A, while no potential affinity towards EIF2A was observed for CBGA and CBCA, as the protein digestion observed when the cells were treated with these compounds was superimposable to that of the controls. Interestingly, western blot revealed insight on the different interacting ability strongly correlated with the chemical structure of the compounds. The slightly less efficient interaction between CBDVA and EIF2A could be due to different side chain length of this compound compared to that of CBDA. Conversely, CBGA and CBCA structure significantly differ from that of CBDA, as the former carries one less ring, while in CBCA the presence of chromate ring makes whole structure much more rigid than that of the others.

Hence, these results prompted us to further validate the CBDA-EIF2A interaction by performing a more thorough investigation through proteomic approaches in which CBCA was considered as a negative control.

## **2.2 EIF2A-CBDA interaction validated by Cellular Thermal Shift Assay**

### **(CETSA)**

Cellular Thermal Shift Assay (CETSA) was used to validate the intracellular interaction between CBDA and EIF2A. This approach, as part of the Thermal Proteome Profiling, is based on the principle according to which the proteins subjected to heat undergo denaturation, thus becoming insoluble in the lysate solution. Since the binding of a protein with a small molecule produce a shift in its melting temperature (Mateus *et al.*, 2020), a supposed interaction can be confirmed by detecting a greater amount of a specific protein in a cellular sample subjected to incubation with the investigated compound, compared to the control one. According to these premises, CETSA experiment was carried out as follows.

U87MG cells were incubated with CBDA for 4 hours, then suspended in PBS and exposed to heat temperature. The same procedure was also carried out on untreated U87MG cells, which represented the negative control. Since EIF2A is part of a multiprotein complex, the effects of heating on the solubility of this protein were monitored over a wide range of temperatures (53-60 °C). The obtained results (Figure 21) demonstrated that CBDA induced a stabilization of EIF2A already at of 53°C, as inferred by higher amount of soluble protein detected in the treated

samples than in the negative control. This protective effect persisted also at higher temperature and only at 60 °C it became negligible.

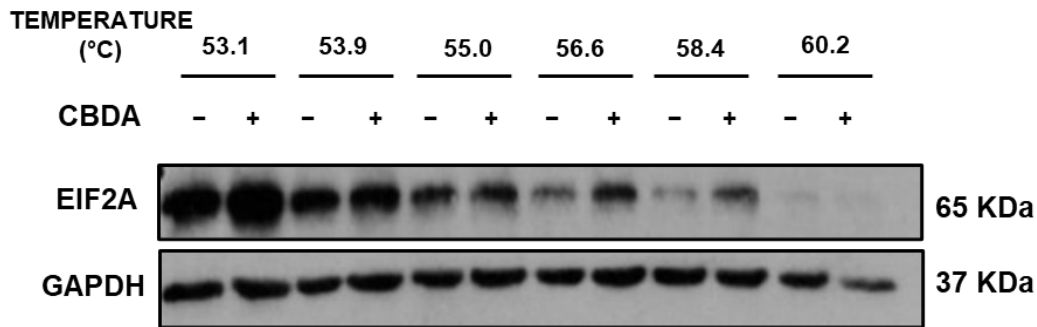


**Figure 21** Western blot analysis of EIF2A in CETSA experiment of CBDA on U87MG cells

In order to confirm that EIF2A stabilization was conferred specifically by CBDA, a CETSA analysis was also performed using CBCA as control. At this end, the level of soluble EIF2A was monitored at 59°C, which was chosen as the temperature more diagnostic to reveal even minimal differences in EIF2A stability following various treatments. Resulting WB (Figure 22) confirmed that only CBDA was able to confer resistance against the denaturation to the protein, whereas the amount of soluble protein revealed in the cells treated with CBCA was almost superimposable to that observed in the control.

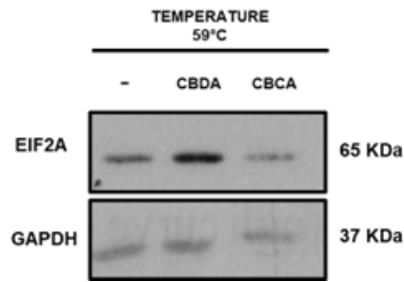


**Figure 22** Western blot analysis of EIF2A in CETSA experiment of CBDA and CBCA on U87MG cells

### 2.3 CBDA-EIF2A interaction investigated by mass spectrometry-associated Limited Proteolysis

A key point in the study of the interaction between a small molecule and its putative target is the definition of the protein region directly involved in the binding. Indeed, it on the one hand allows identifying the ligand structural features that can play a pivotal role to stabilize the interaction, on the other hand permits rationalize and/or forecast the effects of this binding on the protein activity.

The CBDA-EIF2A complex was therefore subjected to mass spectrometry-associated Limited Proteolysis experiments. This is an advanced technique that provides information on protein conformational changes following intermolecular binding, on a proteome-wide scale and in a complex biological environment (Schopper *et al.*, 2017). These experiments were performed adopting two different protocols involving a single- or a double digestion step, differing from each other according to the digestion phase performed and consequently to the specific results provided (Figure 23).

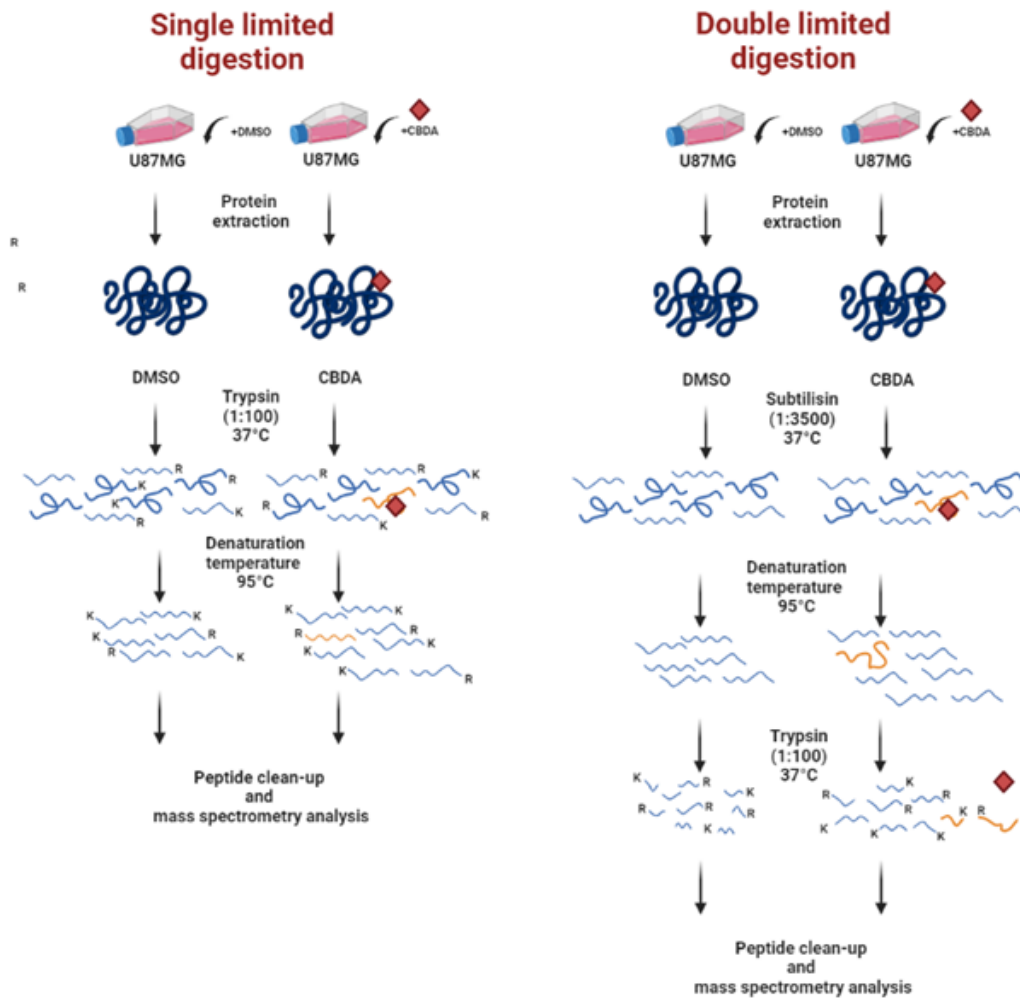


**Figure 23** Schematic workflow of single- and double-limited proteolysis performed on U87MG cells

In both the approaches, U87MG cells were treated with CBDA or vehicle alone (control) for 4 h, and then subjected to a non-denaturing lysis. The resulting lysates underwent limited enzymatic digestion and the obtained peptide mixture was cleaned-up and analyzed by mass spectrometry. The raw-data emerging from this process were processed by MaxQuant software, for qualitative and quantitative characterization of the peptides produced.

In the single-limited digestion approach, the cell lysates underwent to a limited proteolytic hydrolysis catalyzed by trypsin (enzyme:protein ratio 1:1000 w/w) at 37°C for 1h. Since the protein region directly involved in a binding should be more resistant to digestion in the treated sample compared to the negative one, tryptic peptides falling in the EIF2A portion interacting with CBDA should only be detected in control samples. Actually, the results of MaxQuant processing (Table 2) showed that peptide 481-495 aa was abundant in control samples, but absent in the lysate of CBDA-treated cells. Therefore, the amino acid Leucine 480 was considered potentially part of the protein region involved in binding to CBDA, as it was not accessible to trypsin in the CBDA-treated sample

**Table 2** *EIF2A peptides generated by trypsin limited digestion of control (CTR) and CBDA-treated (CBDA) U87MG cells lysates. The ratio of the amounts of each peptide in the two samples, calculated by MaxQuant, is reported. The experiment was carried out in duplicate and the results in the two replicates were superimposable.*

<b>Peptide</b>	<b>CBDA/CTR</b>
<b>2-11</b>	2.0
<b>62-75</b>	1.1
<b>76-90</b>	1.6
<b>145-158</b>	1.9
<b>400-416</b>	1.6
<b>417-427</b>	1.3
<b>436-457</b>	1.5
<b>478-495</b>	1.2
<b>481-495</b>	0.0
<b>496-511</b>	1.2
<b>521-533</b>	3.3

To further define the protein region actually involved in binding to CBDA, a double-limited enzymatic digestion protocol was performed using two different enzymes: subtilisin, obtained from *Bacillus subtilis*, and trypsin. As already tested in DARTS, in contrast to trypsin that is highly specific, subtilisin can catalyze the hydrolysis of almost any peptide bond in a protein. Therefore, U87MG cell lysates were first subjected to subtilisin digestion under controlled conditions (enzyme:protein ratio 1:3500 w/w at 37°C for 1h), followed by a denaturation phase and an extensive tryptic digestion (enzyme:protein ratio 1:100 w/w). In this approach, the protein region interacting with CBDA was protected from the subtilisin-catalyzed digestion and therefore digested exclusively by trypsin; conversely, unprotected regions were susceptible to the first proteolysis steps and the canonical tryptic peptides covering these protein regions could not be detected following the second digestion step. Therefore, tryptic fragments of the protein region involved in CBDA binding should only be present in the treated sample and not in the control (Table 3).

**Table 3** *EIF2A* peptides generated by subtilisin limited digestion followed by trypsin-catalyzed proteolysis of control (CTR) and CBDA-treated (CBDA) U87MG cells lysates. The ratio of the amounts of each peptide in the two samples, calculated by MaxQuant, is reported. The experiment was carried out in duplicate and the results in the two replicates were superimposable.

<b>Peptide</b>	<b>CTR/CBDA</b>
<b>87-110</b>	4.0
<b>306-317</b>	5.7
<b>425-441</b>	0.0
<b>461-482</b>	0.0
<b>521-536</b>	0.0

As expected, the obtained results showed that more tryptic fragments were identified in samples treated with CBDA than in control, thus suggesting that the cannabinoid induced an overall protein stabilization, providing some resistance to protease activity. Interestingly, single- and double-limited digestion provided a different number of peptides as further confirmation of the binding to CBDA. In particular, since double-limiting digestion is more accurate to preserve molecule-protein interaction, it is evident that the number of CBDA-treated sample derived specific tryptic fragments is lower than that of the single digestion because the tryptic fragments detected at MS come from protein regions digested summarily or not digested by subtilisin. However, by combining the results of the two approaches, the following protease resistance map of EIF2A as an effect of CBDA binding was revealed (Figure 24).

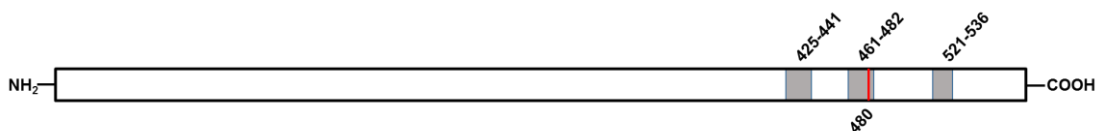


**Figure 24** *Protein regions (in grey) and specific peptide bond (in red) protected from proteolysis following EIF2A interaction with CBDA*

From these data, it was evident that the EIF2A region primarily affected by CBDA binding was the C-terminus, and in particular the segment 460-480. Indeed, the evidence that the peptide 461-482 was protected by the interaction of EIF2A with the cannabinoid was in agreement with the results of the previous experiment, thus suggesting that it was the protein region putatively involved in binding to CBDA.

## **2.4 A close-up of EIF2A-CBDA interaction**

### **2.4.1 Modeling of EIF2A**

To better elucidate the molecular interaction, a molecular docking-assisted investigation was carried out in collaboration with Dr. Rosa Maria Vitale of National Research Council (CNR) of Naples (Italy). Therefore, to get insight into the binding mode of CBDA toward EIF2A, a three-dimensional (3D) model of the full-length protein (1-585 aa) was obtained using AlphaFold program. EIF2A protein was predicted to consist in a N-terminal WD-repeat domain organized in a circularly-arranged nine-bladed  $\beta$ -propeller fold, formed by four-stranded antiparallel  $\beta$ -sheet motifs (1-415), followed by a poorly structured region which includes an  $\alpha$ -helix and a C-terminal coiled-coil (530-580). Since the x-ray structure of the human WD-repeat domain was released (PDB id: 8DYS) during the refinement of our theoretical model, this latter was compared to the experimental structure. The comparison showed that the 3D model is in full agreement with the experimental one, the best fit superposition at level of backbone atoms (Figure 25) resulting in a root mean square deviation (rmsd) value, 1.134 Å within the experimental resolution of the structure (1.80 Å).

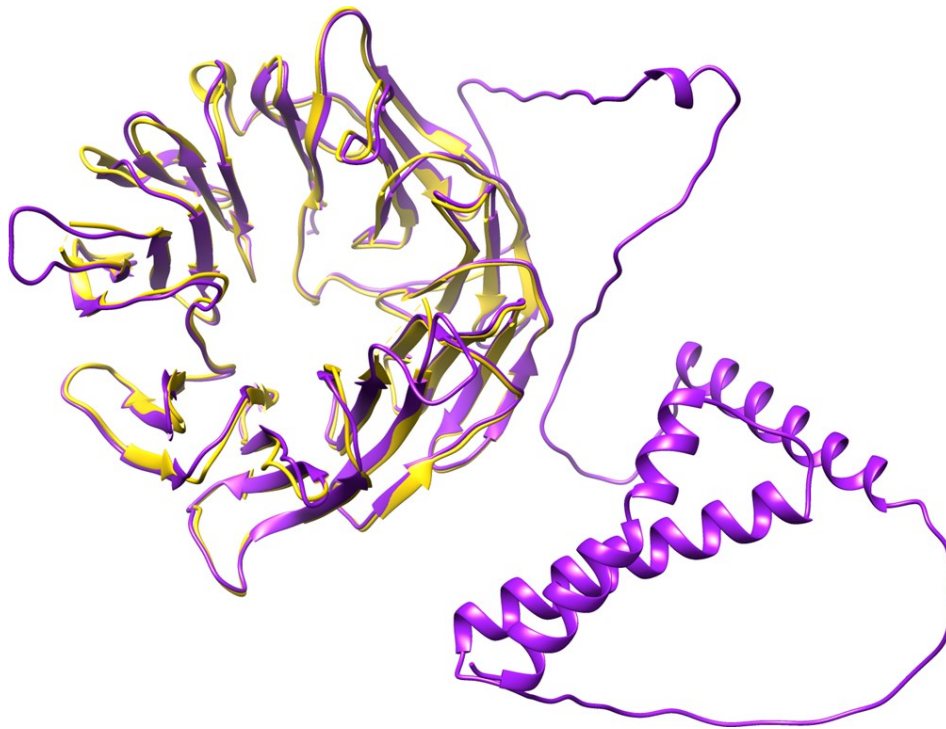


**Figure 25** Best fit at backbone level between the x-ray structure of WD-repeat domain (PDB id: 8DYS, yellow) and the correspondent domain of 3D model of the full-length EIF2A protein (purple).

However, the CBDA binding region identified by MS, encompassing residues 460-480, falls into the mostly unstructured region next to the N-terminal domain (1-415). Therefore, the starting 3D-model was subjected to a refinement using molecular dynamics (MD) simulations in explicit solvent on a time-scale of hundreds of nanoseconds (up to 400 ns) to allow possible rearrangements of the C-terminal region. Indeed, a MD trajectory analysis showed that a portion of residues (463-472) within the identified region stacks against a  $\beta$ -strand of the WD domain formed by residues 307-315 in an antiparallel manner to form an additional strand, stable over the whole simulated period (Figure 26). Indeed, some residues belonging to the 463-472 stretch engage stable H-bonds diagnostic of a  $\beta$ -strand with the flanking region

307-317: the backbone carbonyl and amide groups of Gln468 with the correspondent backbone groups of Asp311 (occurrence > 74%), the amide group of Glu465 with Thr314 carbonyl group (occurrence ~20%), the amide group of Met470 with the carbonyl group of Val309 (occurrence >40%) while the sidechains of Glu464 and Glu464 engage H-bonds with Thr314 sidechain and/or backbone. Moreover, during MD it was also observed a reorientation of the  $\alpha$ -helix 482-502 toward the stretch 463-472 (Figure 26), potentially contributing to the CBDA binding site.

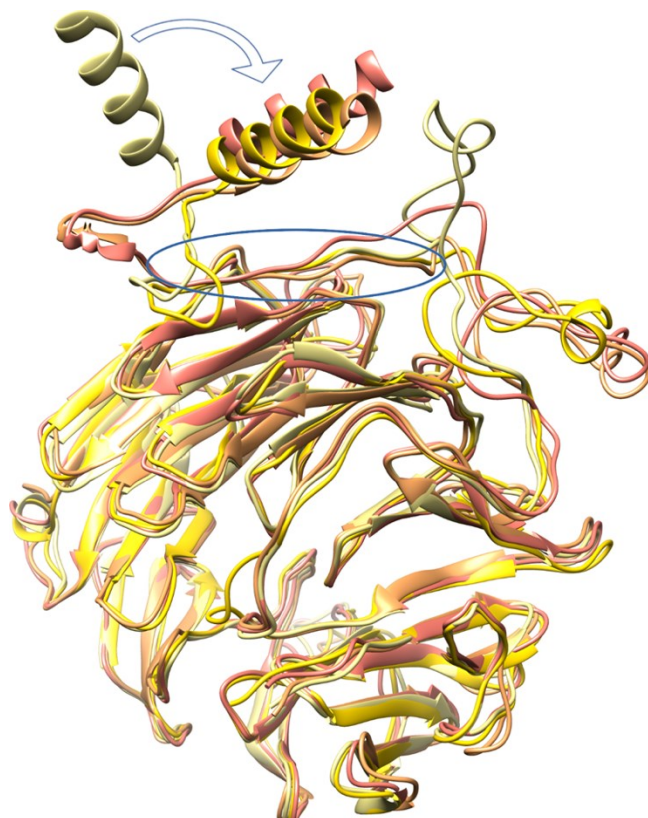


**Figure 26** Best fit at level of WD-domain of MD frames taken every 100 ns over the full simulated period (400ns). The MD frames are painted in a graded coloration from pale-yellow (100 ns) to salmon (400 ns). Arrow shows the movement of  $\alpha$ -helix observed during MD, while the 463-272 stretch flanking the WD-domain is highlighted by an ellipse. The C-terminal coiled coil has been omitted for clarity.

#### **2.4.2 Modeling of CBDA-EIF2A complex**

To find the putative binding mode of CBDA to EIF2A protein, a representative frame from the last 100 ns of MD trajectory was selected for docking studies, using a grid box centered on the 460-480 stretch of residues previously identified by MS. The docking complex, obtained by selecting the CBDA best pose in terms of binding

energy, underwent 100 ns of MD simulation to assess the stability of the binding pose and/or allow possible rearrangements of the ligand. Indeed, a rearrangement of the ligand is observed during the first part of MD (Figure 27).

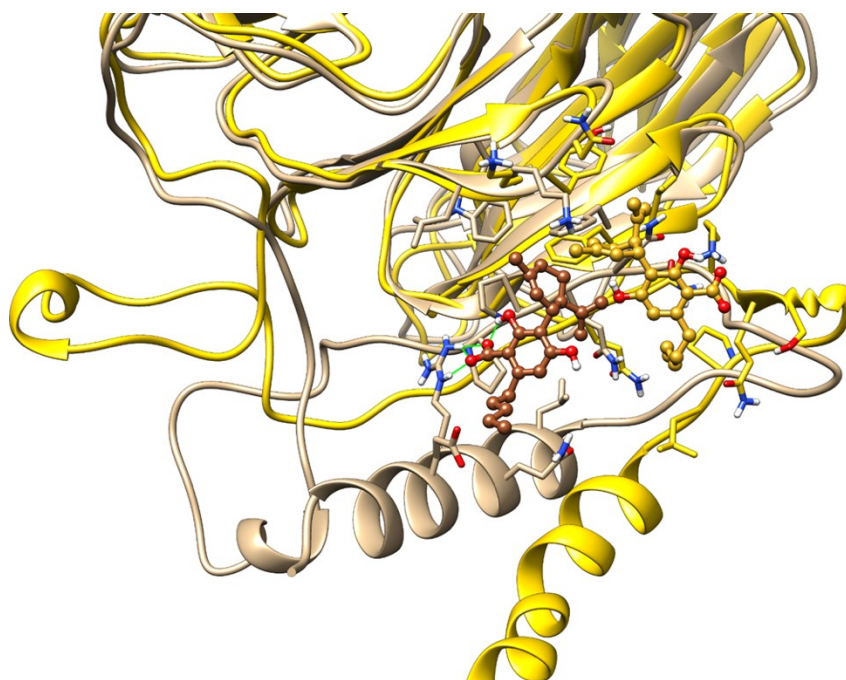


**Figure 27** *Best fit at level of backbone atoms of WD domain between the starting docking complex (yellow) and the representative MD frame (tan). CBDA is painted gold in the docking complex and brown in MD complex. H-bonds are shown as green lines. Residues within 4 Å from the ligand are shown in stick. Hydrogen, oxygen and nitrogen atoms are painted white, red and blue, respectively. The C-terminal coiled-coil has been omitted for clarity.*

The rearranged pose then remains stable during the simulated period, grafting together the stretch of residues 463-472, flanking the  $\beta$ -strand 307-315 of the WD domain, and the adjacent 482-502  $\alpha$ -helix, which becomes closer to the strand. In this new pose, the CBDA binding is stabilized by its ionic interaction with Arg489,

lying on the  $\alpha$ -helix, and by hydrophobic stacking interactions of CBDA aromatic and terpenoid rings with Pro466 and Pro467, respectively. The CBDA pentyl chain also contributes to the pattern of hydrophobic interactions with Leu 485 and Arg489 sidechains. The same computational protocol of docking plus molecular dynamics was applied to both CBCA enantiomers to evaluate if also this phytocannabinoid was able to recapitulate the same binding mode of CBDA. Albeit the starting docking poses of the CBCA enantiomers were similar to that of CBDA (Figure 28), during MD both complexes underwent dissociation, revealing an unstable interaction of CBCA with EIF2A.

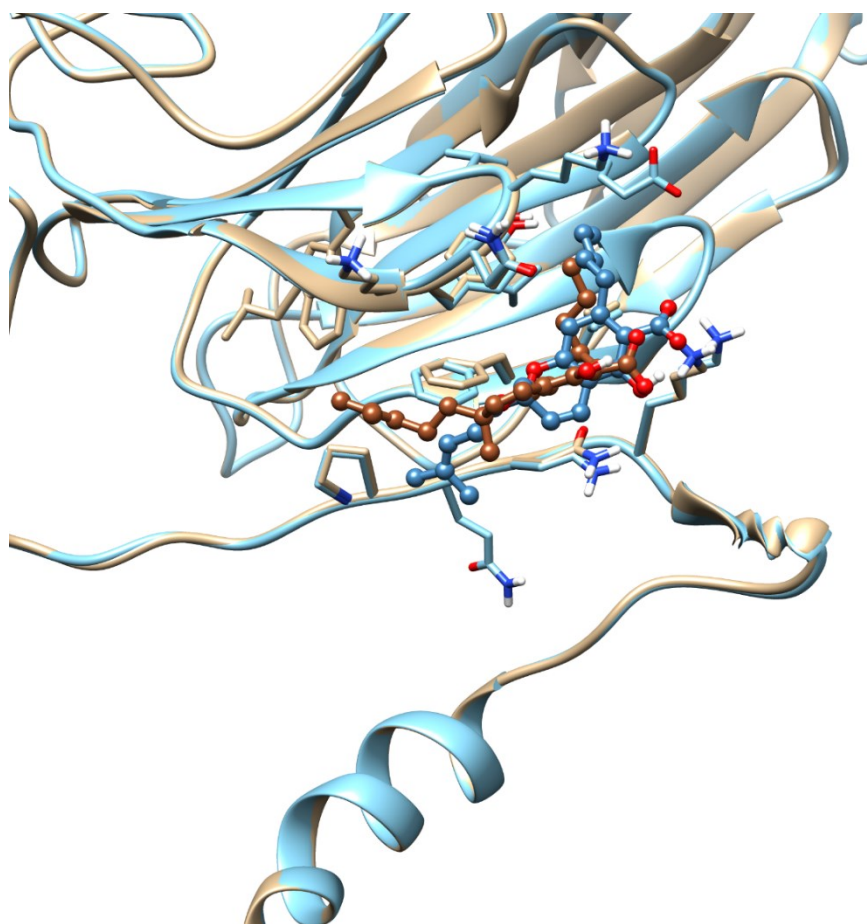


**Figure 28** Docking complexes of both CBCA enantiomers (protein painted sky blue and ligand steel blue for R enantiomer, protein tan and ligand brown for S enantiomer). Residues within 4 Å from the ligands are shown in stick. Hydrogen, oxygen and nitrogen atoms are painted in white, red and blue, respectively. The C-terminal coiled-coil has been omitted for clarity

To further assess the binding region identified for CBDA, a new MD simulation was carried out using as starting coordinates the dissociated complex with the compound placed at 40 Å from the binding site. Time-dependent NOE restraints between the ligand carbon atom bound to the terpenoid ring and the region 460-480 were applied during the first 100 ns of MD, followed by 100 ns of unrestrained MD. The choice of applying the restraints in the first part of MD was driven by the need of maximizing the exploration of the conformational space around the whole region of interest.

Again, the binding of CBDA occurred at the same site identified by the previous approach, confirming the region between the proline residue 466-467 and the nearby  $\alpha$ -helix as the putative binding site for CBDA (Figure 29). In this pose, CBDA engaged a  $\pi$ -cationic interaction with Arg489, an H-bond with Lys460 sidechain involving its carboxylate group and an H-bond with Gln488. The same approach was also adopted for both enantiomers of CBCA and again the ligand was unable to recapitulate the binding of CBDA. In view of these results, the effect of CBDA on the protein function could be explained by the ability of CBDA to stabilize the flexible  $\alpha$ -helix against the WD domain, ability due to the peculiar tilted structure of CBDA, and thus not observed for the more planar CBCA.

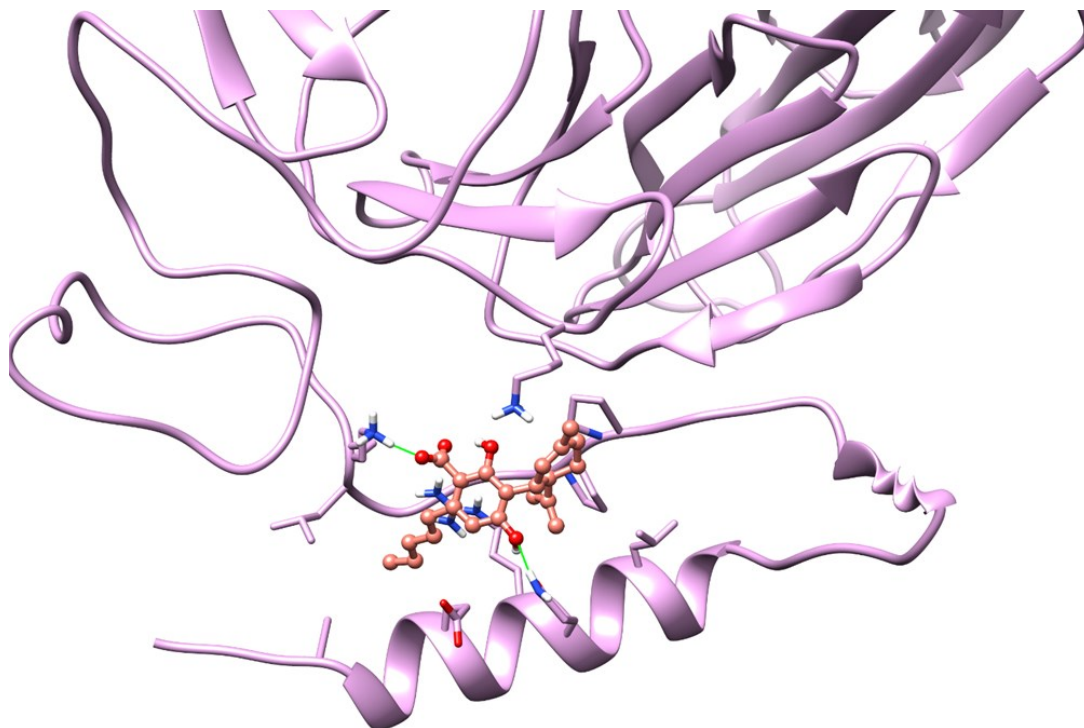


**Figure 29** *Representative frame from unrestrained MD of CBDA-EIF2A complex following the application of NOE restraints (protein pink, CBDA salmon ball & stick). Residues within 4 Å from the ligand are shown in stick. Hydrogen, oxygen and nitrogen atoms are painted white, red and blue, respectively. H-bonds are shown as green lines. The C-terminal coiled-coil has been omitted for clarity*

## **2.5 EIF2A: an overlooked alternative initiation factor**

The results achieved with the described experiments confirmed EIF2A as an interactor of CBDA in the glioblastoma cells. Its involvement in many stress-related cellular processes makes this protein an interesting target, also because its role in pathologies and its druggability were still poorly investigated.

The translation process is a core biological process occurring in all living cells that is performed by several initiation factors, better known as EIF. Translation is composed by four phases: initiation, elongation, termination and ribosome recycling

(Komar and Merrick, 2020). Initiation phase starts with the recognition of the AUG start codon in mRNA and initiator transfer RNA (tRNA) aminoacylated with methionine, thus establishing the reading frame. The elongation step provides to increase the polypeptide chains, and is followed by termination step in which the stop codon defines the translation arrest thus releasing the completed polypeptide chain. Finally, ribosome recycling serves to dissociate the ribosome into its subunits thus making them available to the next translation cycle (Figure 30).

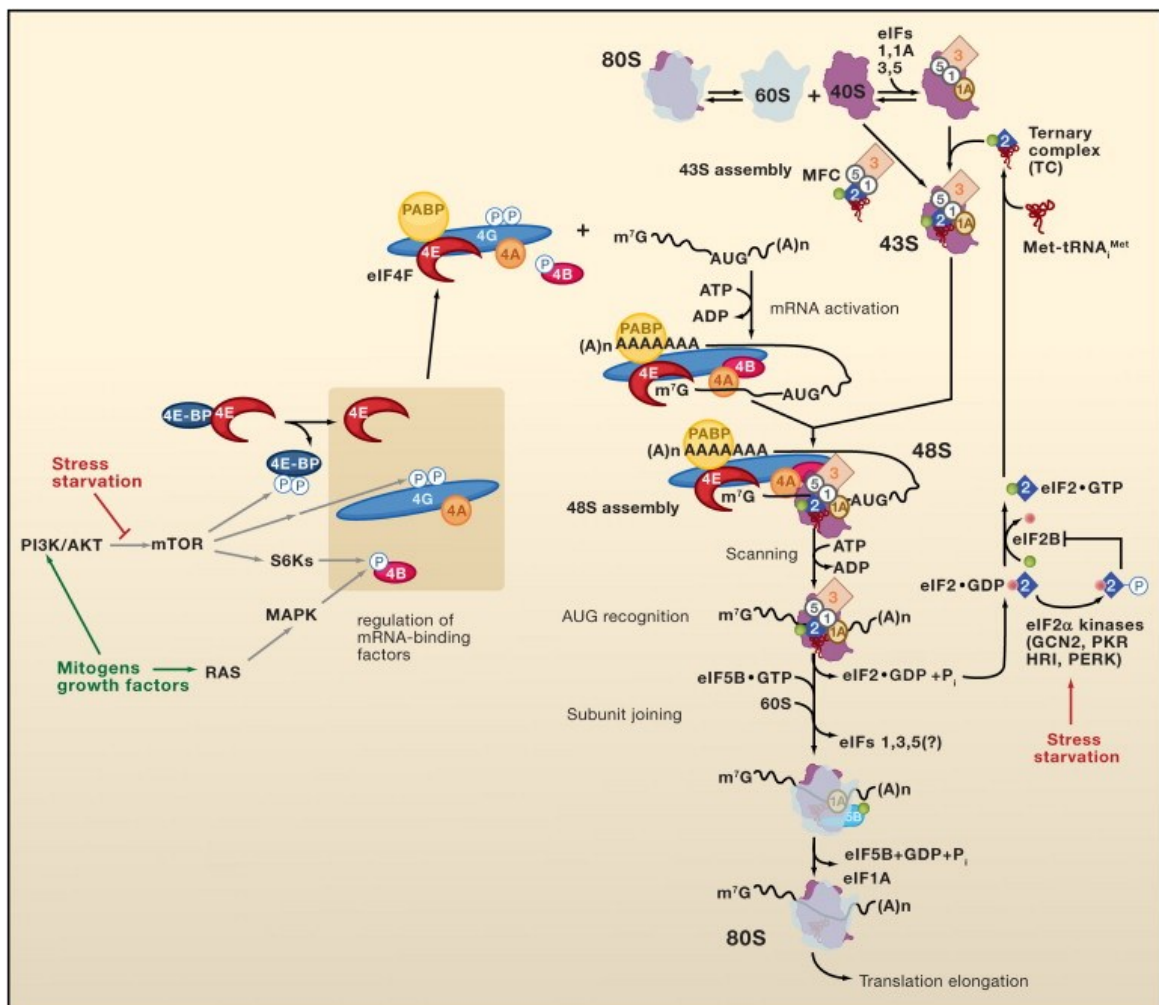


**Figure 30** *Eukaryotic Translation process- adopted from (Sonenberg and Hinnebusch, 2009)*

To allow this system to function properly, more than 12 EIF start the assembly of the pre-initiation complex. Among them, EIF2 plays a critical role as it recruits the initiator Met-tRNA to the 40S small ribosome subunit forming a ternary complex with GTP. Following the binding with the start codon, the hydrolysis of the EIF2-GTP bond is obtained by means of the GTPase action of EIF5. According to some studies, the initiation factor EIF2 plays a crucial role in the eukaryotic translation process. Specifically, EIF2 is composed of three subunits:  $\alpha$  subunit, having a phosphorylatable residue, which mainly serves for the regulation of the process;  $\beta$  subunit is responsible for binding the factors EIF2B and EIF5; finally,  $\gamma$  subunit is crucial for binding with the other components of ternary complex. The primary role of EIF2s is to mediate the interaction between Met-tRNA and the minor subunit of the eukaryotic ribosome; taking part in the ternary complex that involves EIF2 itself, a GTP molecule and Met-tRNA as well (Komar and Merrick, 2020). Considering that EIF2 $\alpha$  is involved in the major pathway of translation, in stress conditions it is phosphorylated thus determining a global protein expression inhibition. The phosphorylation process is activated in response to stress stimulus, better known as Integrated Stress Response (ISR), consisting of: deprivation of amino acids or heme, viral infection and ER stress. When one of these conditions determines EIF2 $\alpha$  phosphorylation and inactivation, an alternative Eukaryotic Initiation Translation Factor 2A (EIF2A) is activated. The latter is an initiator tRNA carrier refractory to eIF2 $\alpha$  kinases and appears to participate in antigen presentation by MHC class 1 molecule, stress responses, and tumor initiation (Kim *et al.*, 2018) (Figure 31).

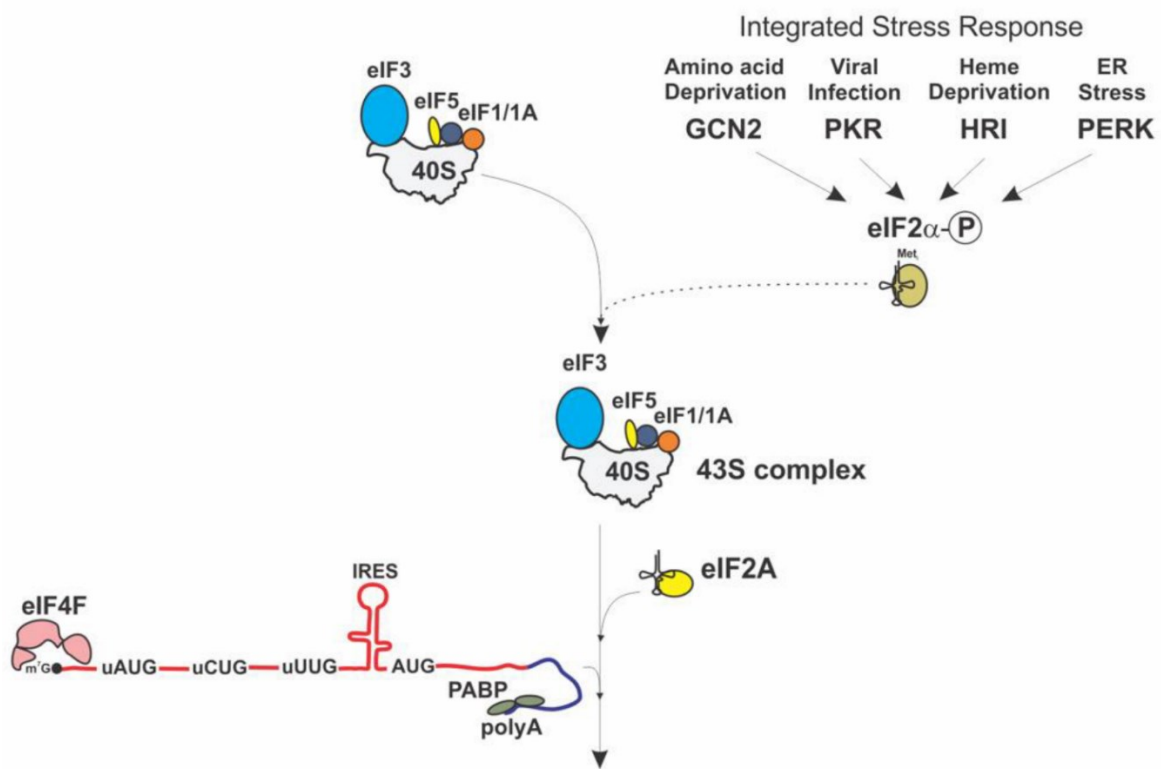


**Figure 31** *Integrated Stress Response (ISR) and EIF2A activation- adopted from (Komar and Merrick, 2020)*

Although the attention of the scientific community always concerned the major initiation factor EIF2 $\alpha$ , currently EIF2A has been identified as a protein having important roles in many pathological conditions. In fact, EIF2A starts to translate selected EIF2A-dependent cancer associated mRNA in an efficient way (Sendoel *et al.*, 2017). As previously shown (Sendoel *et al.*, 2017), in the early steps of tumorigenesis, mRNA translation is addressed to unconventional upstream initiation sites to express oncogenic proteins. The interest towards EIF2A should be quite important as it regulates the translation on upstream initiation sites thus having an important role in tumor progression.

Based on these findings, the scientific community has further shed light on the potential pathological role of EIF2A. In fact, it seems to be involved in resistant mechanism of paclitaxel treatment of triple-negative breast cancer cells, *in vitro* and *in vivo* as well (Chen *et al.*, 2019). Moreover, (Kwon *et al.*, 2017) showed that EIF2A is responsible for the translation of mRNA of c-Src, a non-receptor protein tyrosine kinase, whose overexpression is strongly correlated to the formation of solid tumors. High amount of c-Src was detected in cancer cells in which at the same time many mRNAs were repressed by the inactivation of EIF2. Although this, c-Src and other protein are translated because their translation is mediated by an internal ribosome entry site (IRES) element residing in 5' untranslated region (5'UTR) and in a part of the open reading frame (ORF).

## **2.6 Interactome of EIF2A elucidate the mechanism of action of CBDA**

The eukaryotic translation process is a central process that occurs in a cellular environment. As discussed above, EIF2A has been defined as an alternative starting factor of a long translation process that belongs to a larger multiprotein complex. The dynamic changes in the arrangement of this complex provides a still neglected idea about this intricate mechanism. Since our previous results showed that CBDA has a high affinity for the EIF2A, the changes of the interactome of this protein in the context of treatment with our compound of interest was studied. Indeed, given the significant changes occurring in the protein structure upon the cannabinoid binding, treatment of cells with CBDA was expected to affect the ability of EIF2A to participate in multiprotein complexes.

Therefore, U87MG cells were treated with CBDA and vehicle alone, as described for the previous approaches (Figure 32). EIF2A protein was immunoprecipitated by using a classical IP approach, based on cell lysate incubation first with a specific primary antibody against it and then followed by addition of Protein A/G support. The day after, proteins were eluted, run into 12% SDS-PAGE and in-gel digestion of each lane was performed.

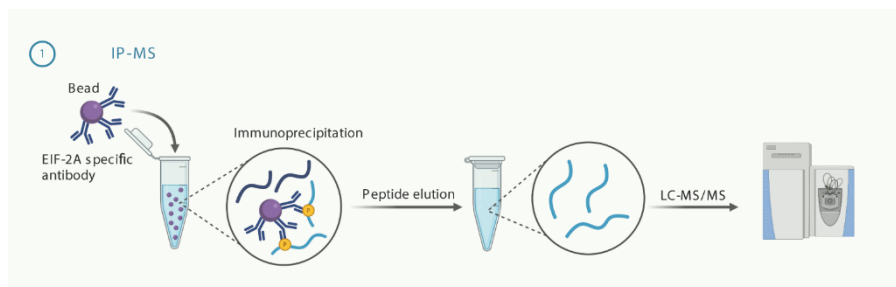


**Figure 32** *Immunoprecipitation of EIF2A and analysis by LC-MS/MS*

Finally, the peptides were analyzed by LC-MS/MS and characterized by Proteome Discoverer software (Table 4).

**Table 4** *Proteins whose abundance in the EIF2A IP increased following the treatment of U87MG cells treatment with CBDA*

<b>Description</b>	<b>Abundance Ratio (CBDA)/ (Control)</b>
HP47 protein (Fragment)	100
T-complex protein 1 subunit alpha	10.68
Beta globin (Fragment)	8.93
Hemoglobin subunit alpha	7.23
Elongation factor 1-gamma	6.82
60S ribosomal protein L7	6.80
Tumor protein D54	5.88
Calumenin	5.32
T-complex protein 1 subunit theta	4.54
F-actin-capping protein subunit beta	4.12
CD44 antigen	3.81
40S ribosomal protein S6	3.61
cDNA FLJ53009, highly similar to Calreticulin	3.32
Elongation factor 1-delta	3.07
Tubulin alpha-4A chain	2.96
40S ribosomal protein SA	2.84
L-lactate dehydrogenase	2.76
Lactotransferrin	2.30
cDNA FLJ58187, highly similar to Protein-glutamine gamma-glutamyltransferase 2	2.30
Proliferating cell nuclear antigen (Fragment)	2.30
Collagen alpha-1(I) chain	2.24
Protein Vpu OS=Human immunodeficiency virus 1	2.23
Epididymis secretory sperm binding protein Li 47e	2.21
HCG2039812, isoform CRA_b (Fragment)	2.03

Surprisingly, the abundance of many proteins co-precipitated with EIF2A increased following the cells treatment with CBDA, thus suggesting that the binding with the cannabinoid induced a stabilization of some protein-protein interactions involving EIF2A. Among the proteins resulted more abundant emerged EEF1G (EF1- $\gamma$ ), EEF1D and some ribosomal subunits. These data suggested that thanks to CBDA binding, EIF2A interacted more strongly with the elongation factor complex.

This hypothesis was further confirmed performing a new DARTS assay, aimed at monitoring the possible protection of EF1- $\gamma$  from proteolysis in the CBDA-treated U87MG cells (Figure 33).

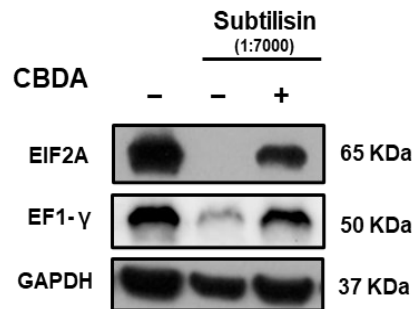


**Figure 33** Western blot analysis of EIF2A and EF1- $\gamma$  in DARTS experiment of CBDA on U87MG cells

Western blot showed that EF1- $\gamma$  appeared to be protected from proteolytic cleavage in CBDA treatment, although at a lower extent than EIF2A, thus suggesting that CBDA-EIF2A binding provides greater stabilization to the entire translation complex.

Additionally, EF1- $\gamma$  stabilization was also investigated by CETSA approach. Also in this case, the protein resistance to temperature increased after the treatment, although this effect was less evident than that observed for EIF2A (Figure 34).

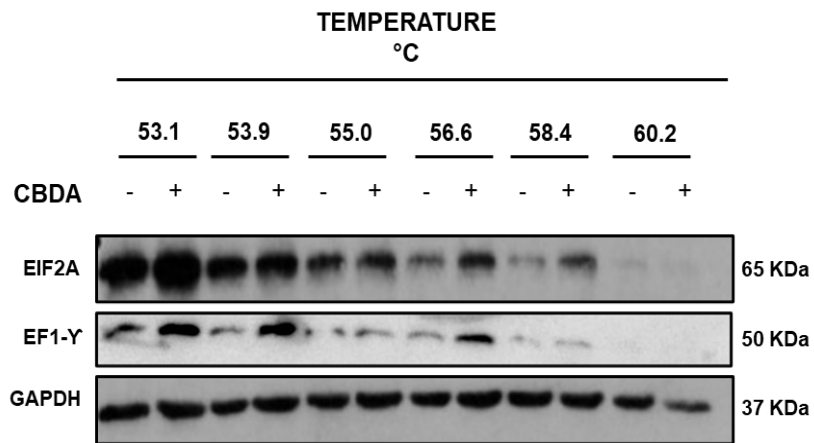


**Figure 34** Western blot analysis of EIF2A and EF1-Y in CETSA experiment of CBDA on U87MG cells

To obtain more insight in terms of biological function, a cytoscape investigation of the other proteins whose affinity for EIF2A was enhanced by CBDA treatment was carried out (Figure 35).

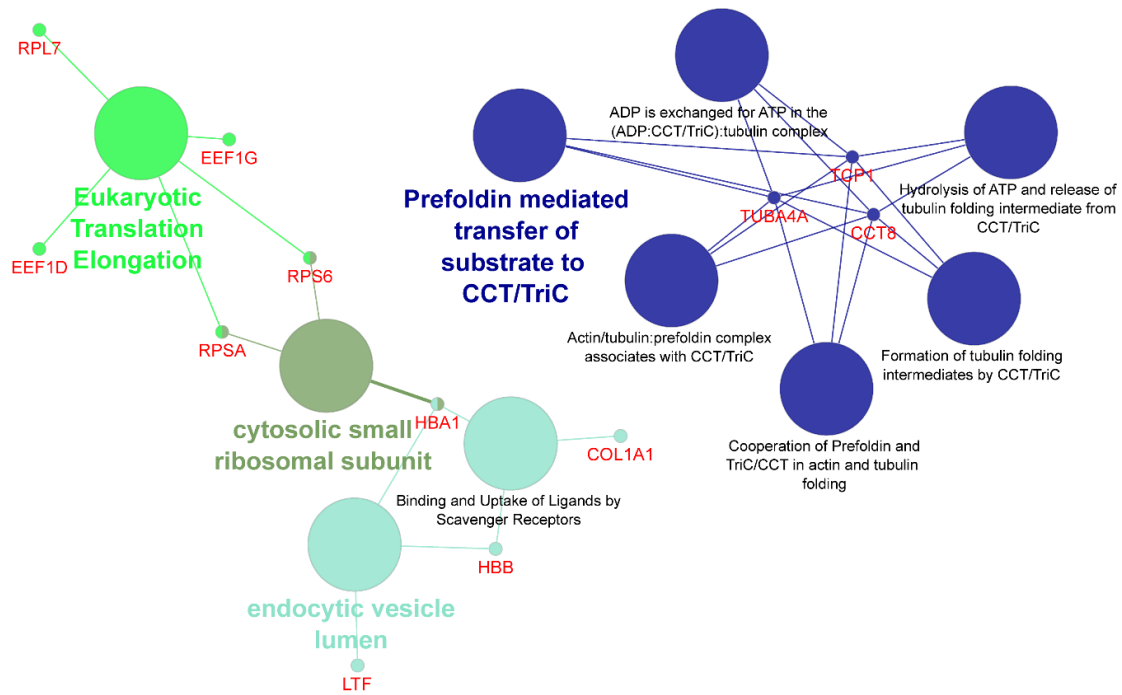


**Figure 35** Interactome of EIF2A in CBDA treatment with a focus on their biological functions

This analysis showed again that most of these proteins belonged to “Translation initiation complex formation”, but also those involved in the “Cytosolic small ribosomal subunit” emerged, thus confirming that CBDA-EIF2A interaction mainly affected the translation machinery complex. Interestingly, the occurrence of proteins belonging to the “Endocytic vesicle lumen” suggested that CBDA could have some impact on ER compartment. Hence, these findings strongly correlate with the ER-stress induced by CBD widely reported in literature (Heider *et al.*, 2022). Finally, it was noteworthy that in the CBDA-treated cells EIF2A interacted also with a eukaryotic molecular chaperone, better known as Chaperonin containing tailless complex polypeptide 1 (CCT) / tailless complex polypeptide 1 ring complex (TRiC). This complex is responsible of folding of cytoskeletal proteins, such as actin and tubulin, and some additional protein substrates (Grantham, 2020).

Summarily, these results suggested a biological effect of CBDA on eukaryotic translation machinery.

## **2.7 CBDA remodels glioblastoma nascent proteome by targeting Eukaryotic Translation Complex**

EIF2A is an initiation factor involved in the early stages of protein expression whose function is still overlooked (Komar and Merrick, 2020). Since CBDA binding to EIF2A to significantly affected the structure and interactome of this protein, the functional effect of this molecular interaction on global protein synthesis was investigated. To this aim, pulsed-SILAC approach was chosen as the elective method to assess the impact of CBDA-treatment on the nascent proteome of glioblastoma cells. p-SILAC is a variant of a classic SILAC, in which labelling only takes place for a short period of time. In this version of the approach, a pulse marking is carried out using L-Azidohomoalanine (AHA), a methionine analogue that allows rapid and sensitive enrichment of peptides by click-chemistry reaction, to isolate only newly synthesized proteins.

The main aim of this experiment was to confirm that the possible effects of CBDA on protein synthesis depends on EIF2A inhibition; therefore, EIF2A-silenced cells were chosen as a positive control. Furthermore, since our previous investigations have shown that CBCA, a cannabinoid acid that exhibits a clearly different chemical structure from CBDA, does not bind to EIF2A, we used CBCA-treated glioblastoma cells as negative control. The results obtained on these three systems were compared with those achieved on untreated wild-type glioblastoma cells (Figure 36).

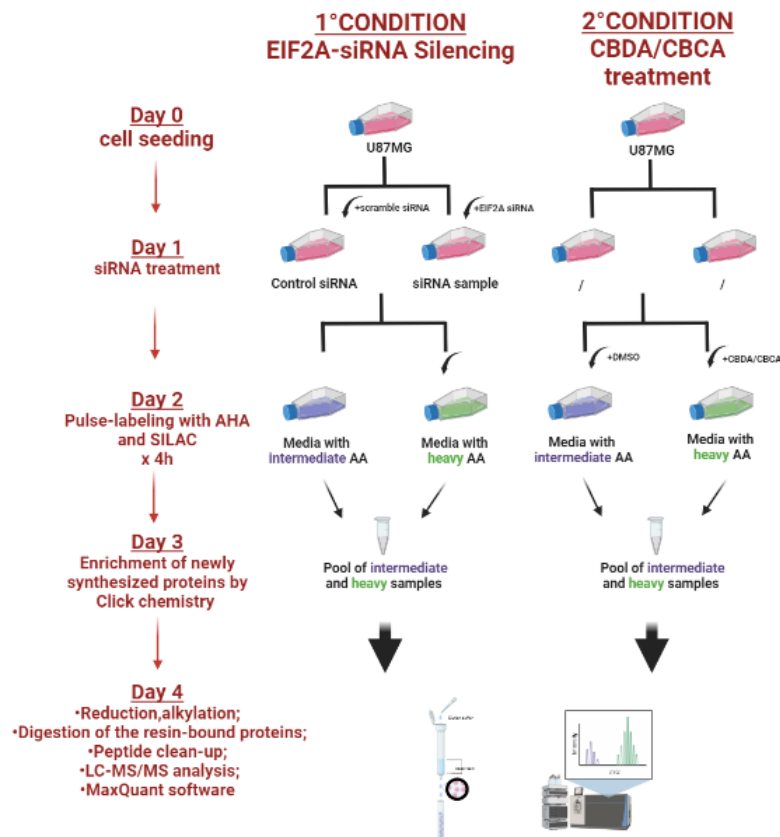


**Figure 36** Schematic workflow of pulsed-SILAC performed on EIF2A- siRNA silenced and CBDA-treated U87MG

EIF2A silencing was achieved using a specifically designed siRNA. Considering that silencing-treatment should precede p-SILAC technique, a classic approach of forward transfection by Lipofectamine was chosen as the most appropriate system, since it was less amenable to induce additional stresses to the cells. U87MG cells were therefore treated with 10 nM EIF2A-siRNA at two different time points of transfection (24h and 48h) and the effects of these treatments on EIF2A silencing were evaluated. To make a correct comparison between positive control and the cells incubated 4h with CBDA, the possible effects of 4 h wash-out on EIF2A silencing were also monitored. As shown in (Figure 37), the EIF2A protein was

silenced at both times of transfection, although a slightly higher efficiency was observed following 48 h of incubation.

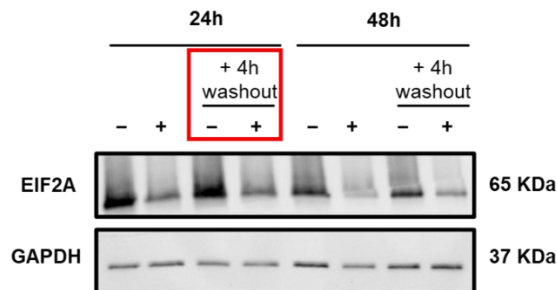


**Figure 37** Western blot analysis of EIF2A in EIF2A-silencing experiment on U87MG cells

However, to minimize the transfection-derived stress on the cells in order to affect negligibly cells before of the p-SILAC procedure, a 24h transfection procedure was adopted. Besides, 4h washout did not induce any significant alteration in EIF2A restoring expression, regardless of the incubation time.

Once U87MG cells were seeded at the same time for both experimental conditions, siRNA- silencing was induced for 24h. The day after, pulsed-SILAC assay was carried out using two experimental conditions. Firstly, U87MG were pre-treated with amino acids-depletion medium for 40 minutes to deplete intracellular stores of Lysine, Arginine and Methionine. Then, the cells of the silencing-condition were treated with intermediate and heavy medium in the control and siRNA samples, respectively. Instead, U87MG cells were treated with the vehicle and the molecule in the presence of intermediate and heavy medium, respectively. AHA was added in each sample and all of them were incubated at 37°C for 4 hours. Cell samples

derived from each experimental condition were mixed with the control, digested and analyzed by MS. The intensity ratio measured for the peptide pairs differing in mass for the different isotopes corresponded to the abundance ratio of the proteins to which these peptides belong. Bioinformatic analysis of these data thus provided detailed information on modulation of newly synthesized proteins by each different treatment.

The well-shaped volcano plots summarizing the differences observed between each sample and the untreated wild-type cells allowed assessing the good quality of p-SILAC results (Figure 38). In addition, the scatter plot similarly represented the good Pearson correlation, thus confirming the robustness of statistical analyses.

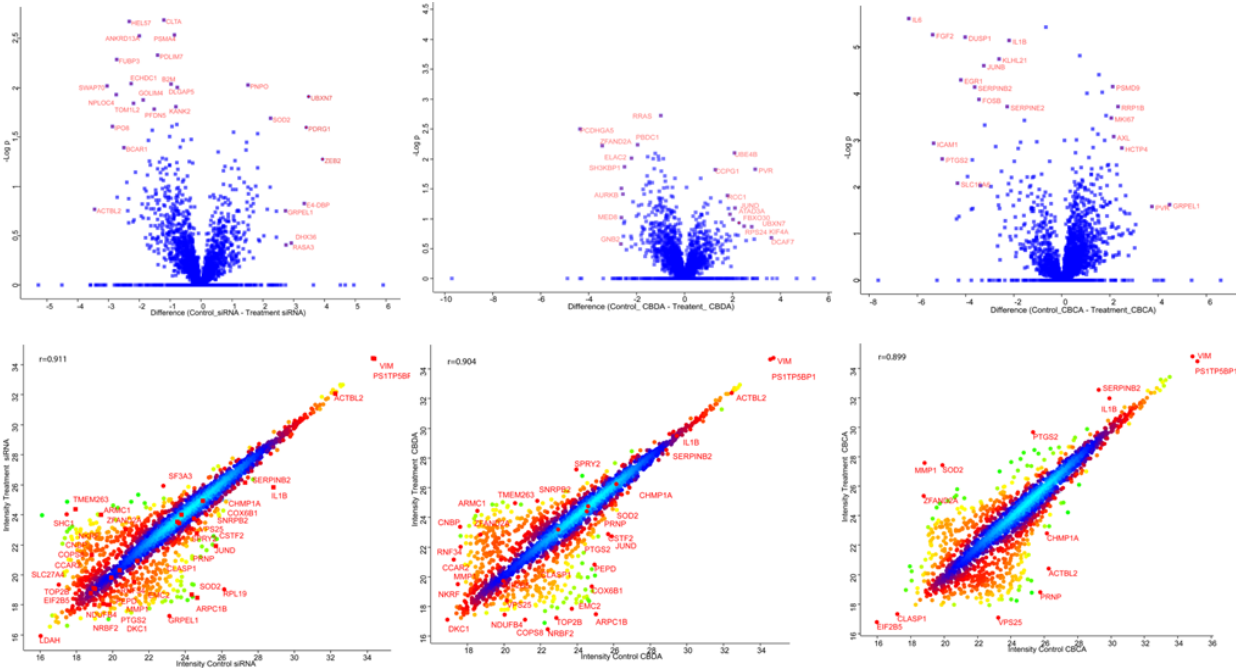


**Figure 38** Volcano plot and scatter plot of nascent proteome of siRNA-, CBDA- and CBCA-treated U87MG cells

The results of SILAC-based quantitative proteomics were initially summarized in a heat-map, reporting the variation in the abundance of all identified proteins that occurred between different samples and untreated cells (Figure 39).

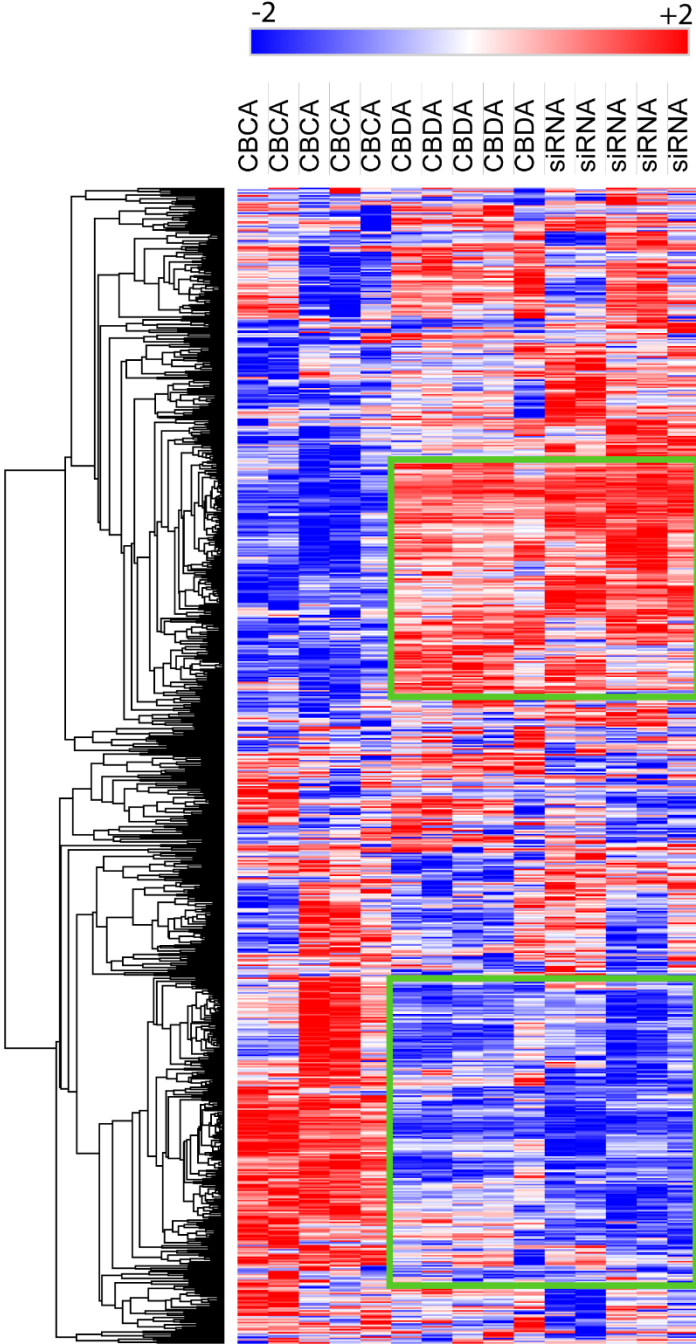


**Figure 39** Heat-map of down- and up-regulated protein clusters in CBDA-, CBCA- and siRNA-treated U87MG

The first important evidence emerging from this overview was that, in terms of both up-regulated and down-regulated newly synthesized proteins, CBDA treatment and EIF2A silencing produced comparable effects. Indeed, observing the heat-map it is possible to detect a number of proteins whose expression level change was very similar in these two samples. Conversely, following CBCA treatment a clearly different pattern than previous ones was observed. These data confirmed, also at a functional level, the interaction between CBDA and EIF2A, and demonstrated that the cannabinoid inhibits EIF2A activity similarly to the EIF2A-siRNA-mediated silencing.

To compare further the proteome expression data between the different investigated conditions, fuzzy-c means clustering was performed on all five experimental replicates. (Figure 40).

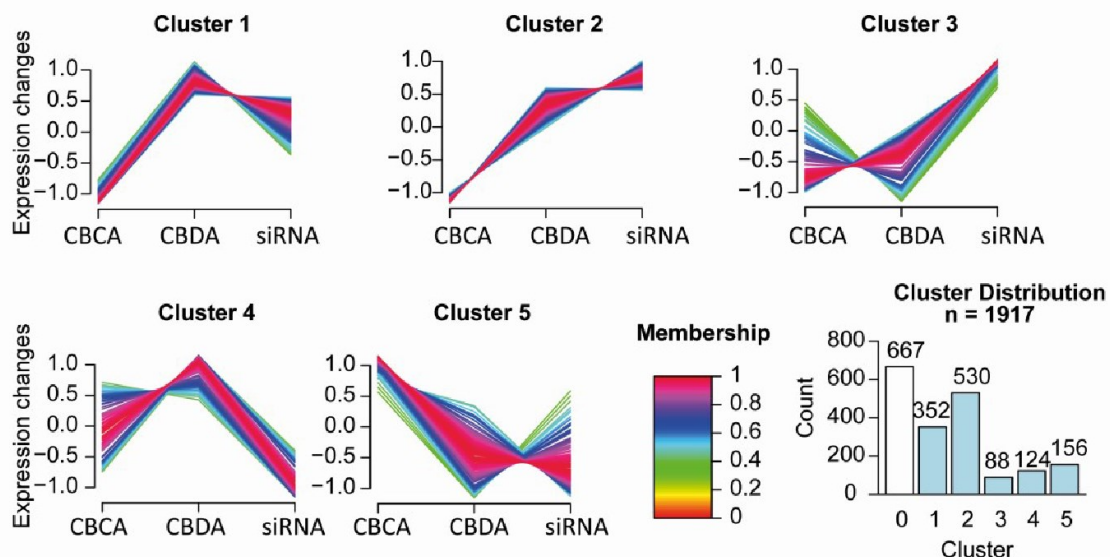


**Figure 40** Fuzzy-c means clustering of newly synthesized proteins in CBDA-, CBCA-, and siRNA-treated U87MG cells

The color legend shows the similarity in terms of color of the heat-map. Based on this analysis, it was evident that cluster 2 showed a very high similarity between the data obtained for CBDA and siRNA samples. In order to assess the impact of CBDA on the nascent proteome in line with EIF2A-silencing, we consider this cluster for further analysis. Reporting in details the proteins collected in cluster 2 in a heat map, a further confirm of the similarity between CBDA and the positive control was obtained, whereas CBCA-treated cells were definitively different (Figure 41).

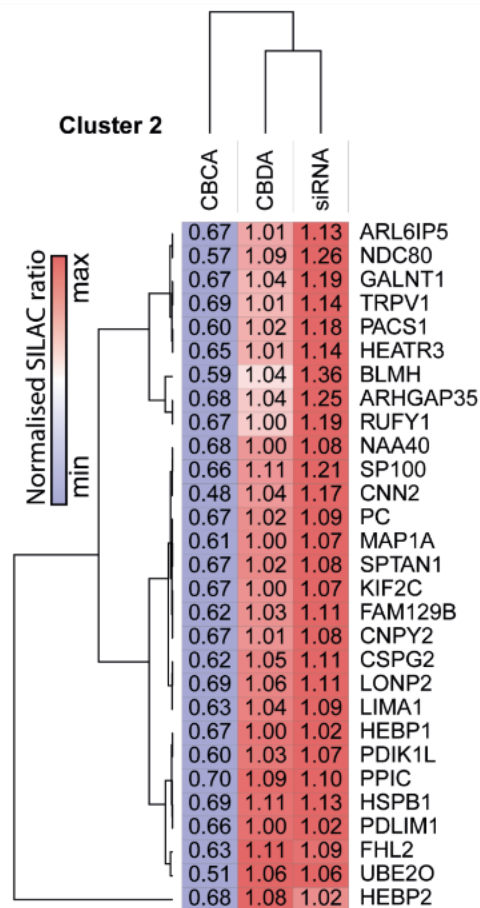


**Figure 41** Heat-map of cluster 2 related to newly synthesized proteins from CBDA-, CBCA- and siRNA-treated U87MG cells

As reported in (Figure 42), CBDA- and siRNA-treatment produced a very similar fold-change in respect of the control in the levels of protein grouped in cluster 2. These proteins were also analyzed in a co-expression plot, which describes the expression together and provides more information about their expression values.

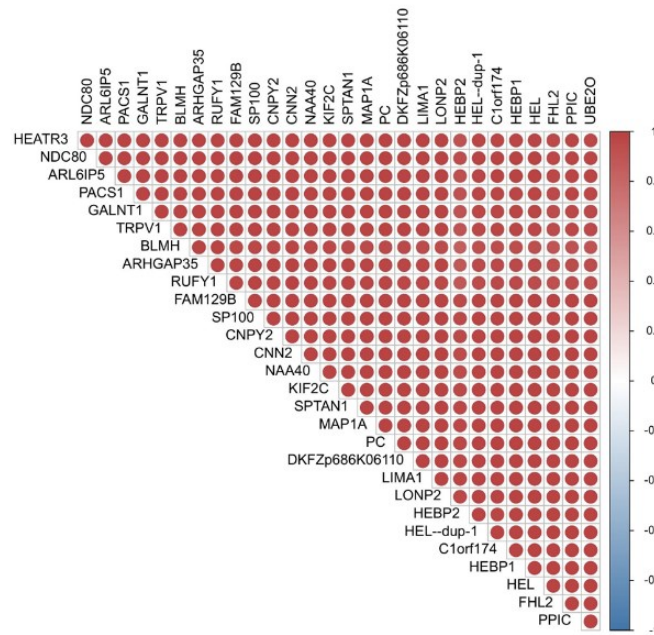
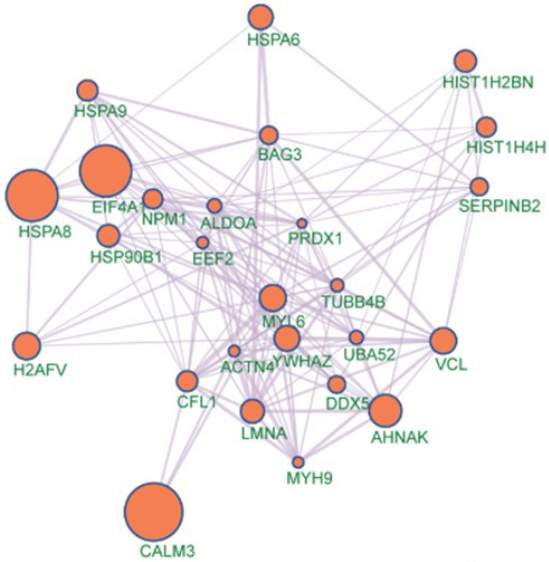


**Figure 42** Co-expression proteins of CBDA- and siRNA-treated U87MG

The resulting graph showed a high correlation between them and defines that they are somewhat dependent on each other for their functionality. However, although silencing mechanism cannot be compared to the molecular interaction of CBDA with EIF2A in terms of biological effect and time of impact on protein function, the result on the nascent proteome appeared almost comparable.

A particularly interesting result emerged from the Gene Set Enrichment Analysis (GSEA) performed on the top-20 overexpressed proteins in common in the two

samples (Figure 43), demonstrating that most of them were proteins related to endoplasmic reticulum stress.



Gene Set Name	Description	p-value	FDR q-value
<b><u>HALLMARK_UNFOLDED_PROTEIN_RESPONSE</u></b>	Genes up-regulated during unfolded protein response, a cellular stress response related to the endoplasmic reticulum.	6.53 e <sup>-13</sup>	1.56 e <sup>-10</sup>
<b><u>HALLMARK_MTORC1_SIGNALING</u></b>	Genes up-regulated through activation of mTORC1 complex.	7.71 e <sup>-6</sup>	9.21 e <sup>-4</sup>
<b><u>CAMP_UP.V1_DN</u></b>	Genes down-regulated in response to cAMP signaling pathway activation by thyrotropin (TSH).	2.74 e <sup>-4</sup>	1.11 e <sup>-2</sup>
<b><u>HALLMARK_MITOTIC_SPINDLE</u></b>	Genes important for mitotic spindle assembly.	2.74 e <sup>-4</sup>	1.11 e <sup>-2</sup>
<b><u>HALLMARK_APICAL_JUNCTION</u></b>	Genes encoding components of apical junction complex.	2.78 e <sup>-4</sup>	1.11 e <sup>-2</sup>

**Figure 43** Top-20 co-expression proteins in CBDA- and siRNA-treated U87MG cells with related GSEA analysis

### 2.7.1 pulsed-SILAC reveals the impact of CBDA on nascent proteome in U87MG cells

Once confirmed that the consequences of CBDA treatment on protein neo-synthesis in glioblastoma cells should depend on its ability to affect EIF2A activity, we moved to study in detail the p-SILAC results. Therefore, to better elucidate the biological effects of these molecules on glioblastoma cells, we selected the top 100-upregulated proteins of CBDA- and CBCA-treated samples, thus collecting the relevant reports with respect to the biological database (Figure 44).

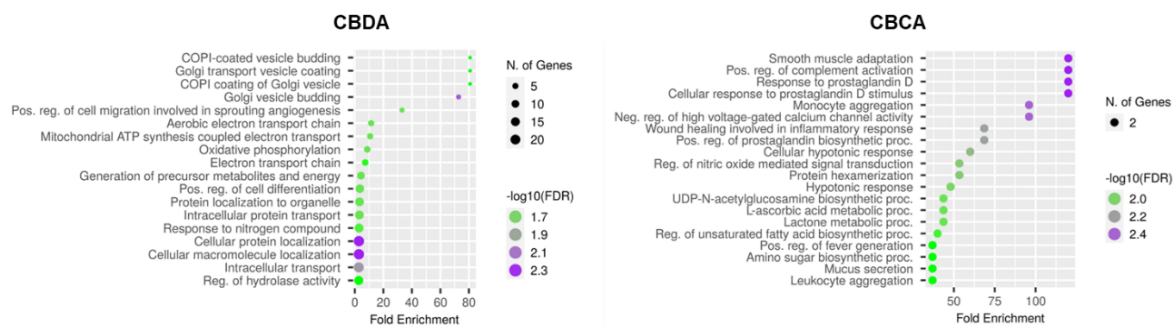


**Figure 44** Top-100 over-expressed proteins in CBDA- and CBCA-treated U87MG cells

As shown in (Figure 44), p-SILAC data showed that CBDA induced, above all, an increase in the expression of proteins involved in vesicle transport and in all processes concerning proteins localization, such as proteins involved in the budding and transport of COPI-coated vesicles, particularly with regard to the Golgi apparatus. In addition, the database of biological processes confirms the increase in the oxidative phosphorylation process with consequent effect on the overactivation of the electron transport chain and on the transport of electrons coupled to mitochondrial ATP synthesis. Differently, CBCA seems to be more

involved in immune regulatory processes by determining an overexpression of proteins involved in complement activation and cellular responses to inflammatory cytokines as already reported in the literature, in particular with regard to its decarboxylated form (Stone *et al.*, 2020).

Also, interesting information were deduced observing the proteins whose neo-synthesis was reduced following CBDA-treatment. Indeed, looking at the volcano plot summarizing the differences in the nascent proteome of CBDA-treated and control U87MG cells, the three proteins more down-regulated were RRAS, PCDHGA5 and PBDC1 (Figure 45).

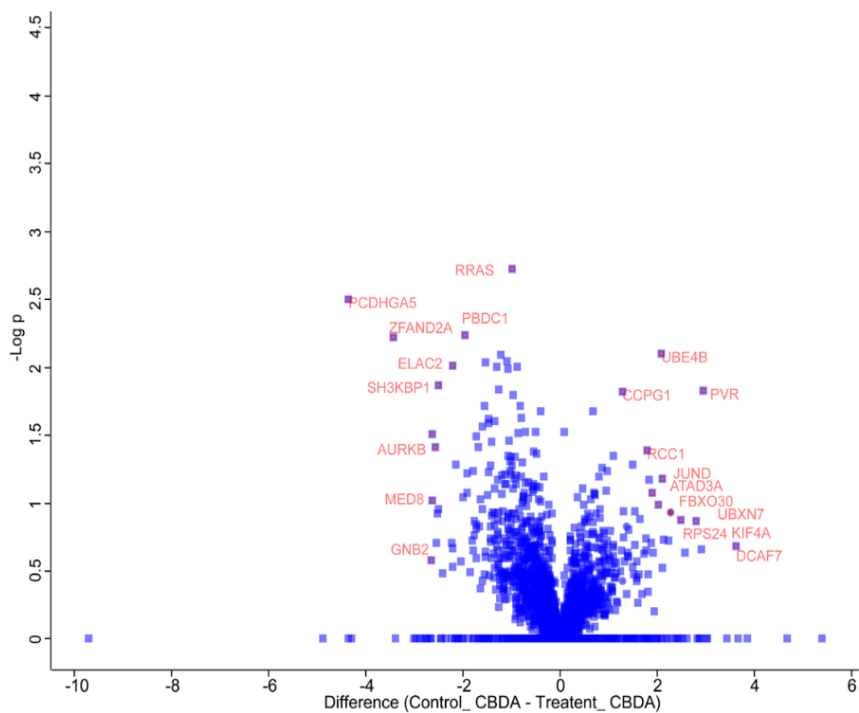


**Figure 45** *Volcano plot emerging from the comparison of nascent proteome in CBDA-treated and control U87MG cells*

Therefore, a survival analysis was performed using querying Cancer Genome Atlas (TCGA) datasets. The obtained results demonstrated that in the TCGA Glioblastoma multiforme (GBM) cohort, low levels of expression of RRAS, PCDHGA5 and PBDC1 correlate with an increased patient survival (Figure 46).

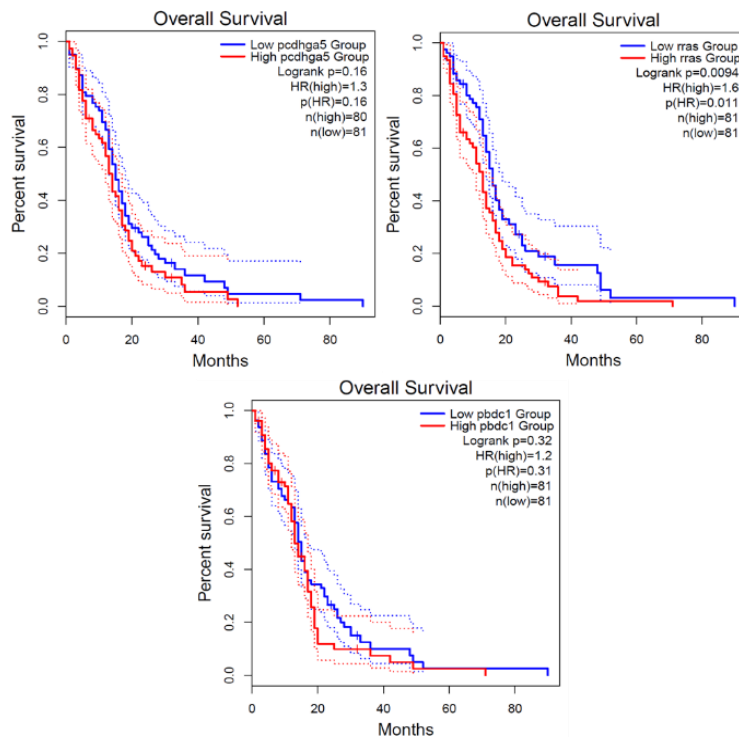


**Figure 46** Survival analysis based on the high p-value proteins which are down regulated upon treatment with CBDA and required to express low in Glioblastoma multiforme

### 2.7.2 Effect of CBDA on the expression of cancer hallmarks in U87MG cells

In order to investigate the possible antitumoral effect of CBDA, the up- and down-regulated proteins were analyzed respect to the hallmark database (Figure 47).

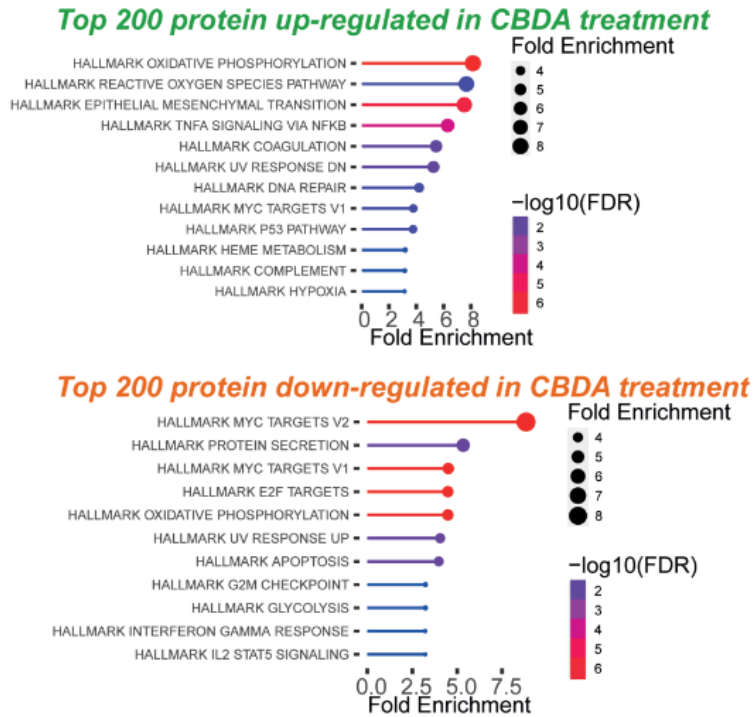


**Figure 47** Hallmark-based grouping of the Top-200 proteins up- and down-regulated in CBDA-treated U87MG cells

The most up-regulated proteins appeared to be involved in oxidative phosphorylation as well as in reactive oxygen species pathway. This result is in line with the potential effect of CBD reported in literature, as CBD seems to elicit an endoplasmic reticulum (ER) stress response (Lim, Devi and Rozenfeld, 2011; de la Harpe, Beukes and Frost, 2022). Specifically, ER stress can be induced by different stimuli thus activating the unfolded protein response (UPR). However, the latter is important for restoring homeostasis and cell survival (de la Harpe, Beukes and Frost, 2022). Current scientific literature suggests that cannabinoids can induce ER stress by increasing reactive oxidative phosphorylation and influencing the UPR response. Based on our finding, in the early stages of treatment, CBDA appears to

induce ER stress. In addition, our interest was also focused on the up-regulation of proteins involved in epithelial mesenchymal transition (EMT). The EMT transition is a highly dynamic process that occurs in advanced tumor conditions in which cancer cells lose their cell polarity and cell-to-cell adhesion, thus changing their epithelial characteristics into mesenchymal ones. This process provides a condition of greater aggressiveness where migratory and invasive properties prevail (Roche, 2018). In detail, the up-regulation of these proteins has widely been reported as response to ER stress in different cell lines. In fact, in tubular epithelial cell lines, EMT was probably induced by ER stress through autophagy response via activation of c-Src kinase (Liu, 2004; Yang *et al.*, 2005; Ulianich *et al.*, 2008; Tanjore *et al.*, 2011; Moon *et al.*, 2014).

Regarding down-regulated proteins, the expression levels of the MYC targets v1 and v2 appear to be affected significantly by CBDA treatment. MYC has been identified as one of the more studied oncogenes, with a critical and fundamental role in promoting the tumor condition. It is a transcription factor that regulates most human genes involved in cell cycle regulation. In this context, a subset of genes regulated by MYC have been classified as MYC targets v1 and MYC Targets v2. Both have been reported to be associated with cancer aggressiveness and poor survival prognosis in breast cancer patients (Schulze *et al.*, 2020). Also, some E2F targets were down-regulated. Since E2F is involved in the mechanistic survival/death switch under ER stress, this finding again suggested that CBDA treatment could reduce the capability of cancer cell to respond to stressing conditions (Pagliarini *et al.*, 2015). Moreover, it is noteworthy that oxidative phosphorylation proteins appear to be down- and up-regulated as well. In order to

evaluate more-in depth this double modulation of oxidative phosphorylation, we evaluated only the expression of those proteins (Figure 48).

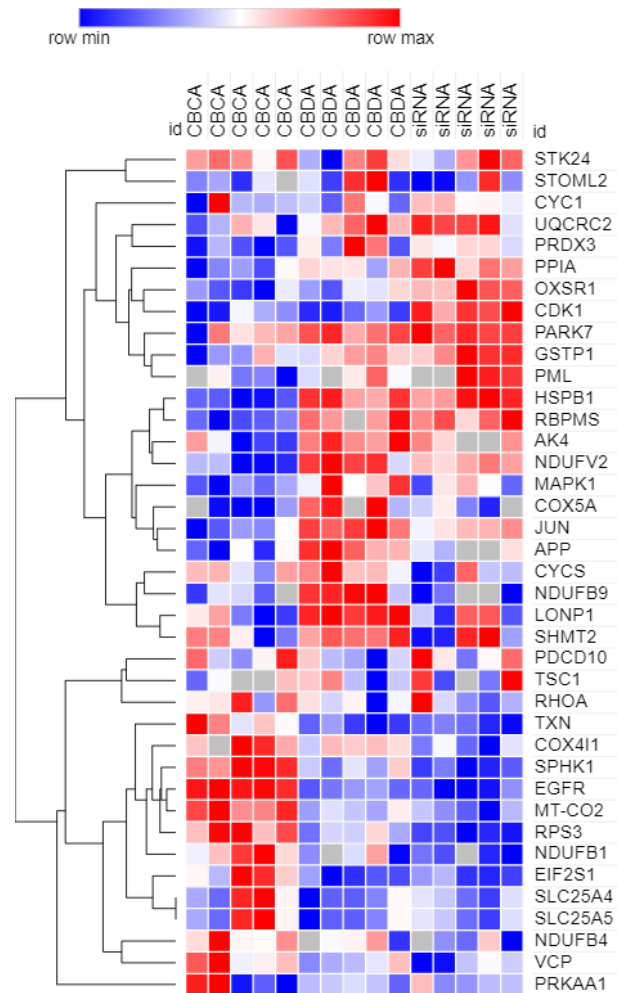


**Figure 48** Heat-map of oxidative phosphorylation- related newly synthesized proteins in siRNA-, CBDA- and CBCA-treated U87MG cells

Also focusing on these proteins, it is possible to highlight a similar effect between CBDA and siRNA treatments. Concerning the up-regulated proteins, those displaying the more evident changes appeared to be involved in oxidative stress-related responses, as inferred by the up-regulation of proteins as PARK7, OXSR1

and GSTP1, although the latter two are significantly up-regulated in three of five biological replicates. PARK7 (Parkinson disease protein 7) is a multifunctional protein that acts as an oxidative stress sensor, with antioxidant and transcription modulatory activity (Dolgacheva *et al.*, 2019). OXSR1 (Serine/threonine-protein kinase OSR1) regulates downstream kinases in response to environmental stress as well as GSTP1 (Glutathione S-transferase Pi) that is involved in detoxification process (Chen *et al.*, 2020; Cui *et al.*, 2020). Other proteins activated under stress conditions that were over-expressed after CBDA treatment were PML (promyelocytic leukemia), AK4 (Adenylate Kinase 4) and PRDX3 (Peroxiredoxin 3) (Liu *et al.*, 2009; Sahin Umut *et al.*, 2014; Rebelo *et al.*, 2021). As described above for OXSR1 and GSTP1, also PML and PRDX3 were differently up-regulated in each of biological replicates. Nevertheless, up-regulation of these proteins is almost significant because correlated to the other ones. In particular, AK4 maintains cell survival as a stress-responsive effect, whereas PRDX3 is a thioredoxin-dependent peroxide-dependent peroxide-reductase mitochondrial that plays a role in protecting cells against oxidative stress by detoxifying peroxides. Based on these data, it could be evinced that CBDA-treated cells, similarly to the EIF2A silenced ones, attempted to restoring of homeostatic response possibly produced by the treatments to avoid cell death. Apparently, this goal is achieved through the up-regulation of PPIA (Peptidyl-prolyl cis-trans isomerase A), which can induce a correct folding of synthesized proteins, and of HSPB1 (Heat shock protein beta-1), a small heat shock protein whose activation has been demonstrated to be fundamental in autophagy response to prevent the cell apoptosis and death (Matsumoto *et al.*, 2015).

Analogously, also some down-regulated proteins are related to the intracellular oxidative processes. TXN (Thioredoxin) emerged as one of the oxidative

phosphorylation pathway-related proteins, which are most significantly down-regulated. It participates in various redox reactions through the reversible oxidation of its active center dithiol to a disulfide and catalyzes dithiol-disulfide exchange reactions. It makes a reversible S-nitrosylation of cysteine residues in target proteins. In fact, a specific transmigration reaction between procaspase-3 and thioredoxin-1 prevents apoptotic process (Mitchell *et al.*, 2007). Summarily, these results suggests that CBDA appears to induce oxidative stress in 4 hours of treatment while restoring, at the same time, a compensatory mechanism of homeostasis.

Since EIF2A is an initiation translation factor, the CBDA effect on the nascent proteome has also been studied in terms of eukaryotic translation process (Figure 49).

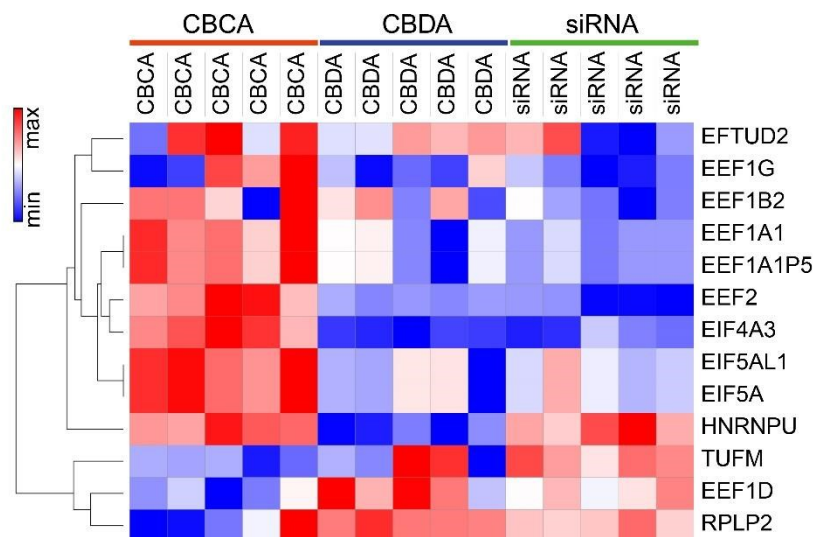


**Figure 49** Heat-map of Eukaryotic machinery complex-related newly synthesized proteins in siRNA-, CBDA- and CBCA-treated U87MG cells

As shown in oxidative phosphorylation, an inverse correlation between CBDA-siRNA and CBCA was detected. Specifically, all translation factors were down-regulated in CBDA- and siRNA-treated cells, in particular many initiation (EIF4A3, EIF5AL1, EIF5A) and elongation factors (EEF1G, EEF1A1, EEF2). The only exception consists of EEF1D (eukaryotic translation elongation factor 1 delta), which was up-regulated. It is a component of the EEF1B protein complex and in gliomas its down-regulation of EEF1D expression appears to inhibit the activation of the PI3K/AKT pathway, thus leading to cell proliferation arrest (Xu *et al.*, 2021). Additionally, down-regulation of RPLP2 (60S acidic ribosomal protein P2) has caught our attention. Indeed, (Artero-Castro *et al.*, 2015) showed that RPLP down-regulation leads to stress-induced autophagy. Therefore, down-regulation of both these proteins confirms the activation of autophagy effect as a stress-response following CBDA and siRNA treatment.

Another interesting result emerging by matching the results obtained by IP and p-SILAC experiments. Indeed, the analysis of EIF2A interactome revealed that, following CBDA treatment, the protein enhanced its affinity not only towards translation factors, but also for proteins involved in the cell response to ER stress. Interestingly, all these proteins belonged to those whose neo-synthesis was down-regulated after cells incubation with the cannabinoid (Figure 50).

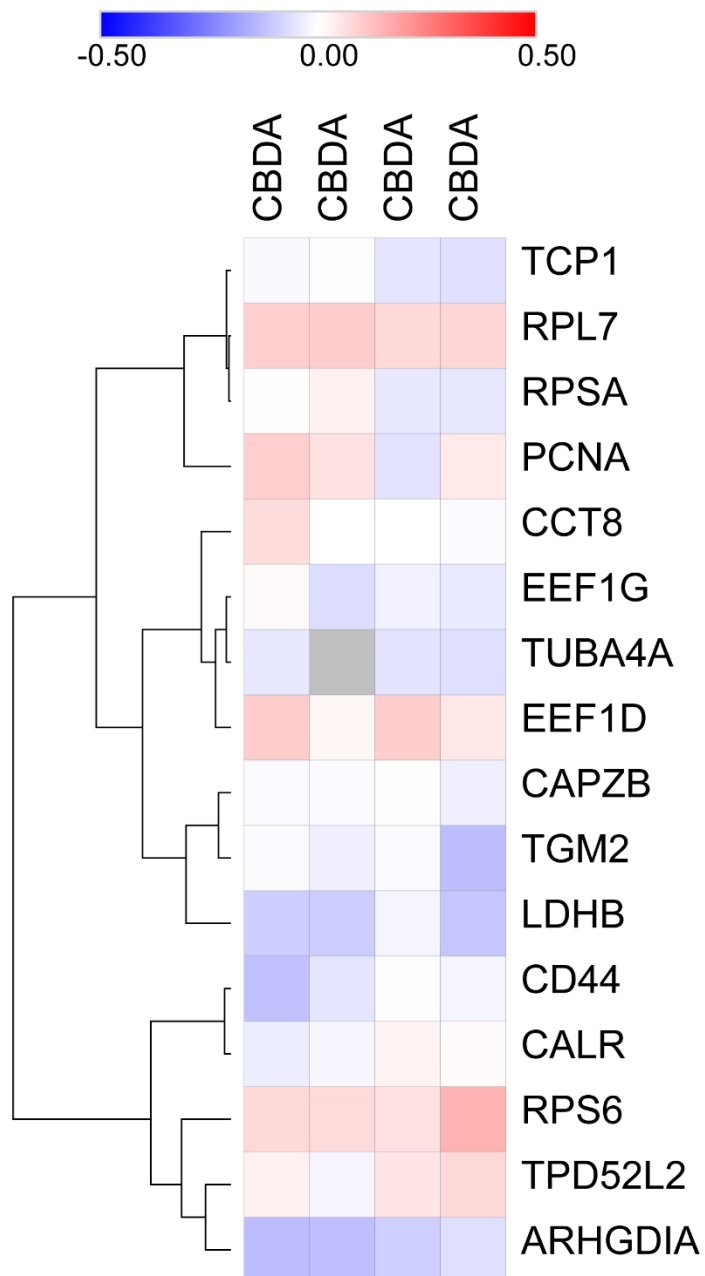


**Figure 50** Heat-map of newly synthesized proteins down-regulated in p-SILAC interacting with EIF2A

Summarily, some of them are correlated to the unfolded protein response (UPR) that is activated by endoplasmic reticulum (ER) stress, caused by accumulation of misfolded proteins into the ER or oxidative stress (Benedetti *et al.*, 2022). These evidences suggested that CBDA could reduce bioavailability of proteins responsible

for the protection of the cancer cells from ER stress acting with a double mechanism:  
at an interactome level by capturing them in macrocomplexes and at a  
transcriptional level by preventing their expression.

## Discussion

In recent decades, THC and CBD have been identified as the two most important cannabinoids. Although the bioactivity of phytocannabinoids has been extensively investigated, their mechanism of action is not fully understood. Based on the literature, CBDA, identified as the main native phytocannabinoid in fiber and seed oil varieties of hemp, has shown many beneficial effects: anticonvulsant, anticancer, antiemetic and anti-inflammatory effect, mediated by its putative affinity for enzyme (COX-2) and receptor (TRP type) proteins (Formato *et al.*, 2020; Navarro *et al.*, 2020). Nevertheless, its mechanism of action still has not been investigated in detail. As the chemical proteomics approach is proving to be a powerful strategy in the drug discovery processes, in the present research a thorough targeted investigation of CBDA in the glioblastoma was performed. Generally, drug discovery can be classified into two main strategies: target-based and phenotype-based drug discovery. The first strategy is based on the preliminary selection of a target molecule, followed by its validation and bioactivity screening. Conversely, phenotype-based drug discovery relies on cellular assays that monitor phenotypes, such as cell proliferation and differentiation (Terstappen *et al.*, 2007). Although this last approach allows the use of an intact biological system capable of mimicking the real clinical response, it leaves the molecular target unknown. The process of identifying the molecular target is defined as "target deconvolution", with respect to which different chemical proteomic strategies can be used based on the characteristics of the compound (Kubota, Funabashi and Ogura, 2019).

In the present study, the identification of EIF2A as a protein target of CBDA represents a clear demonstration of the potentiality of using target-based multi-complementary chemical proteomic approaches for a deep investigation of molecule-protein interaction. First, the DARTS coupled with MS-based proteomics allowed to perform an untargeted analysis, followed by a preliminary validation by western blot. Since the binding affinity strength should also be investigated with a complementary technique, CETSA experiments were performed. The achieved results demonstrated that cells treatment with CBDA increased the EIF2A stability to thermal denaturation, thus confirming the occurrence of the binding between the cannabinoid and the protein. Nevertheless, target identification is not limited to define an interactor of a bioactive compound, but it should also be aimed at defining the protein region required for the molecular binding. Therefore, protein sequence involved in the interaction with CBDA were identified by limited proteolysis experiments. In this context, a combination of single- and double-step limited digestion provided identification of the protein binding site; indeed, single-limited digestion has provided an approximate identification of the Leu480 site as putatively involved in binding, while, by double-limited digestion approach the region 461-480 was finally identified as the portion responsible of EIF2A interaction with CBDA. This result was confirmed by Molecular Dynamics, showing that CBDA rearranged from the initial docking pose, engaging stable interactions with a stretch of residues in the 460-480 portion and in the adjacent C-terminal helix, acting as a bridge between these regions. For proteins engaged in multi-protein complexes as EIF2A, the dynamic conformation changes conferred to by a small molecule could play a critical role in further molecular recognitions. Based on the literature, the sequence 461-480 appeared to fall in a region involved in the interaction with other fundamental

eukaryotic factor and critical for the protein function. First, the 460-500 portion in EIF2A appeared to be required for its interactions with eIF5B, Met-tRNA<sup>iMet</sup> and mRNA. Indeed, eIF5B is critical for increasing the activity of eIF2A in loading Met-tRNA<sup>iMet</sup> onto a 40S ribosome (Kim *et al.*, 2018). Furthermore, as reported by Reineke and collaborators, changes in this protein region could affect its activity, as demonstrated by the evidence that deletion in region 460-521 results in a loss of function of EIF2A in yeast (Reineke *et al.*, 2011).

Accordingly, the experiments performed on EIF2A immune-precipitates demonstrated that, in the presence of CBDA the protein affinity for several partners was clearly enhanced. Interestingly, EIF2A interacted with an higher efficacy not only with eukaryotic translation factors, as demonstrated by EEF1G increased resistance to protein denaturation following CBDA treatment, but also with proteins that mediate the biological effect of CBDA. In fact, the evaluation of the EIF2A interactome prompted us to consider it as the central protein able to regulate the biological effect of CBDA. In the aim of attempt to hypothesize a mechanism of action of CBDA, it is important to take into account the biological evidences reported for the major cannabinoids, which have been supposed to be related to the TRPV channel, although their function is still poorly understood. Indeed, TRPV1 and TRPV2 are present in the cytoplasmic membranes and on the endoplasmic reticulum membrane that regulate calcium concentration. A deregulation of this homeostatic process induces a production of reactive oxygen species (ROS) and an evident stress of the endoplasmic reticulum, which ultimately leads to cell death (Seltzer *et al.*, 2020). Interestingly, different TRPV cell localization was detected on different glioma cell lines. Precisely, (Amantini *et al.*, 2007) demonstrated by confocal microscopic analysis that TRPV1 localizes differently in the cytoplasmic

and astrocytic processes of NHA cells, in U87MG cells it is localized in discrete points in the cytoplasmic and perinuclear regions, while in U373 cells they are localized on the plasma membrane. This discovery sheds light on the role of the vanilloid receptor TRPV in mediating glioma cell apoptosis (Amantini *et al.*, 2007). Among various TRPV channels, in particular TRPV4 was found to co-localize with Stromal Interacting Molecule 1 (STIM1), a calcium-sensing protein that acts as key regulator of calcium pools in the ER (Pavez *et al.*, 2019; Haustrate, Prevarskaya and Lehen'kyi, 2020). However, although a significant correlation was found between the TRPV channel and ER stress, their interaction needs to be elucidated. Since the antitumor activity of CBDA is still substantially overlooked, we first investigated the possible relationship between the CBDA-EIF2A binding and ER stress, by the investigation of the effect of CBDA on glioblastoma nascent proteome. In this context, it was noteworthy that the comparison between CBDA treatment-EIF2A silencing validated the ability of the cannabinoid to inhibit EIF2A thus elucidating its mechanism of action. Indeed, their similar modulation of up- and down-regulated proteins confirms a similar effect on the nascent proteome, although EIF2A-siRNA and CBDA acted differently on the protein. Interestingly, up-regulated proteins were involved in oxidative phosphorylation as well as in reactive oxygen species pathway. Although with a lower fold enrichment value, oxidative phosphorylation also appears to be down-regulated. This dual effect could be representative of a condition of interaction between ER stress and the attempt to restore cellular homeostasis. Indeed, CBDA appears to induce ER stress likely induced by an accumulation of misfolded proteins, thus activating UPR response. Parallely, CBDA-treated cells, similarly to siRNA control, induce a reestablishment of homeostatic response thus avoiding cell death. As widely reported in the

literature, the accumulation of misfolded proteins in the ER lumen can trigger ER stress and subsequently a persistent ER stress can lead to cell damage. Therefore, to avoid cell death, autophagy process can be activated, thereby protecting cells from the excessive ER stress by restoring cellular homeostasis (Perner and Krüger, 2022). Indeed, the over-expression of newly synthesized proteins, PPIA and HSPB1, is representative of an attempt by glioblastoma cell to activate the autophagy process as PPIA is involved in the folding of newly synthesized proteins while HSPB1, as heat shock protein, plays a fundamental role in prevention of cell death. Besides, other oxidative stress-related proteins (PARK7, OXSR1, PRDX3, GSTP1, AK4, TXN) appeared to be similarly modulated in CBDA- as well as in siRNA-treatment. Interestingly, the modulated expression of most of them is perfectly correlated with their biological function of stress-sensors or in detoxification process.

Since EIF2A is a protein involved in the eukaryotic translation machinery, a focus on the eukaryotic translation factors was carried out. Indeed, although most of them appeared to be up-regulated, EEF1D and RPLP2 appeared as the only ones to be down-regulated in CBDA- as well as in siRNA-treatment thus confirming that the EIF2A-CBDA interaction have some impact also on the eukaryotic translation process. However, further confirmation of the triggering of the autophagic response concerns also RPLP2 whose down-regulation leads to stress-induced autophagy. Finally, the GSEA of the top-20 co-expression proteins in CBDA- and siRNA-treated U87MG cells, confirmed an activation of the hallmark UPR response. All together, these evidences indicated a significant effect of CBDA treatment on ER stress, which could be revealed by both the modulation of the expression of proteins involved in the cell protection from this insult and by the cellular response aimed at

restore the correct homeostasis. This partial effect of CBDA treatment could be due to the short-term treatment that putatively was not sufficient to induce cellular stress leading directly to cell death. However, it should not be underestimated that the effect of CBDA (and of many cannabinoids) on cell viability is strongly related to the amount of FBS used in the cell cultures. The potential affinity of cannabinoids for fetal bovine serum proteins was speculated, as these compounds provided some cytotoxicity only when administrated to cancer cells in the presence of low concentrations of FBS. This observation led to the conclusion that the serum proteins could interact with cannabinoids reducing their bioavailability. In fact, even in preliminary evaluation that we performed by MTT assay, the cytotoxic effect of CBDA was inversely proportional to the concentration of FBS in the culture medium. In the present work, since we were interested in prevent cell death following CBDA treatments, the experiments were performed in the culturing conditions assuring the higher cell viability, which coincided with those whose cells were grown (10% FBS). Indeed, as reported by (Sainz-Cort, Müller-Sánchez and Espel, 2020), the effect of a drug should be evaluated under the same experimental growth conditions. If growth and treatment conditions differ by one or more variables, cell death cannot be associated solely with treatment but with a combination of all variables. Moreover, as confirmed by (Eastman, 2017), this interesting evidence opens a fundamental question regarding the improper use of the cytotoxicity test. Indeed, the latter could provide false evidences on the cytotoxic effect. The associated risk could be to propose bioactive molecules as potential anticancer compounds due to their “potential” cytotoxic effect increased only by the simple reduction of growth factors essential for the cell growth. However, it is almost common to eliminate or reduce FBS concentration to perform cells treatments with the cannabinoids, as

already showed in many studies regarding CBD (Solinas *et al.*, 2013; Scott, Dalglish and Liu, 2017).

Therefore, based on our finding and on the previous considerations, a completely new relationship could be postulated between the concentration of FBS in the cell medium and the effects of the cannabinoid on cancer cells. Indeed, the evidence that CBDA affects the ability of the glioma cells in respond to stressors, prompted us to hypothesize that the deprivation of survival factors by the media could sensitize cells to subsequent treatment with the cannabinoid. Substantially, CBDA treatment could induce cancer cell death through the exacerbation of pre-existing ER stress depending on FBS deprivation.



**Chapter 3 - Development of 3D glioblastoma cell model  
for the investigation of mechanism of action of novel  
drugs**



# Results

## 3.1 Different proteomic profile of 2D and 3D-U87MG cell model

For over a century, bi-dimensional cell cultures have been used as almost the unique *in vitro* model for drug discovery and development, allowing shedding light on promising biological activity of natural and synthetic compounds. However, in most cases, *in vitro* findings have not been confirmed in subsequent clinical studies, often due to bi-dimensional cells that inaccurately represent cell biology *in vivo*. In recent decades, innovative cellular models able to mimic tumor macrostructure have been defined (Joseph, Malindisa and Ntwasa, 2018). Hence, these could serve as better choices to carry out high-content screening approaches and preclinical phase in drug discovery and development process. Based on these premises, a secondary aim of this project was to develop an innovative cellular model representative of glioblastoma tumor and then use it to perform target investigation on CBDA.

Depending on the selected cell line, different biomaterial can be used to create a three-dimensional cellular model: laminin, matrigel, hyaluronic acid and collagen. Since the matrigel has been defined as one of the most complete biomaterials, in this project it was used for the creation of a 3D sandwich cell model (Figure 51).

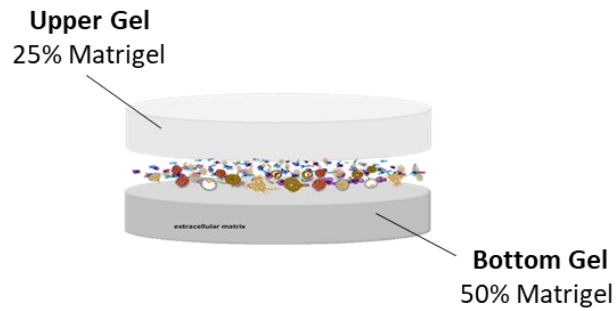


**Figure 51** *Representation of three-dimensional sandwich cell model*

It consists of two layers of gel: bottom- and upper-gel. The bottom-gel is composed of 50% of matrigel while the upper gel is 25%. This difference generates a different stiffness, allowing the growth of cells in the middle layer. In order to reach a proper cellular confluency, the endpoint of cell growth was set at 5 days.

A morphological comparison of 2D- and 3D-U87MG cells was carried out. As expected, in the 2D system U87MG cells grew as monolayer, whereas, in 3D model they adopted their natural shape, thus establishing interaction with other cells three-dimensionally (Figure 52).

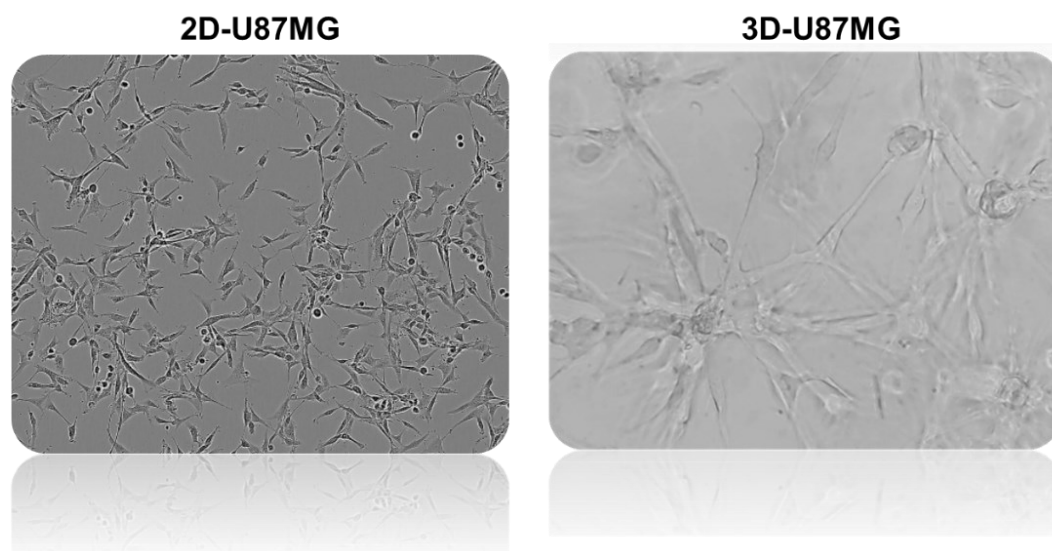


**Figure 52** Cellular morphology of 2D- and 3D-U87MG cells

These preliminary observations prompted us to study the 2D and 3D cell proteome. U87MG were cultured in 2D and in 3D-sandwich cellular model and then cell lysates were loaded onto 12% SDS-PAGE to perform gel-digestion. The peptides were analyzed by LC-MS and finally a characterization of the protein content was performed using the MaxQuant software. Significant and reproducible differences were observed. In more detail, as shown in the volcano plot (Figure 53), U87MG cells cultured in a three-dimensional cellular model express higher amounts of proteins involved in cellular invasion processes, such as the annexins family, than the 2D cultured ones. Moreover, Chondroitin Sulfate Proteoglycan (CSPG4) and Nidogen 1 (NID1) appear to be the two proteins more over-expressed in 3D cell model. CSPG4 is a type I transmembrane glycoprotein that binds one or more components of the ECM and NID1 is a sulfated glycoprotein widely present in basement membranes and associated with laminin. These results highlighted how cells that grow in three dimensions, having to establish bonds with other cells throughout the surrounding space, express higher levels of proteins involved in

intercellular interactions. Although this result was not surprising also in the light of the previously described morphological analysis, it demonstrated how the two cellular models (2D and 3D) carry differences at the proteomic level, which could significantly influence in vitro drug discovery and development studies.

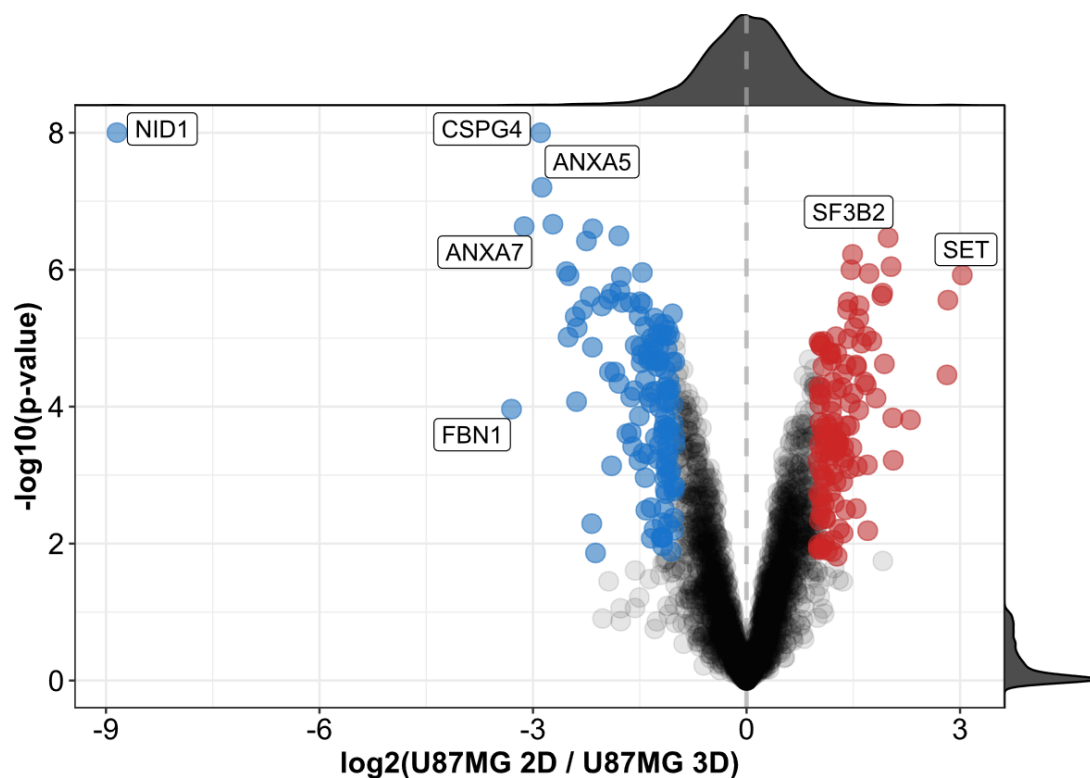


**Figure 53** *Volcano plot comparing proteomic profile of 2D- and 3D-U87MG cells*

### **3.2 U87MG-3D sandwich model: a glioblastoma cellular model for proteomic investigation of bioactivity of CBDA**

Based on the interesting proteomic profile of the 3D glioblastoma cell line, the molecular interaction between CBDA and protein target EIF2A was investigated also in 3D cellular model. Based on the strong impact observed for FBS concentration on the biological activity of cannabinoids, 3D cell models were obtained using

different concentrations of FBS. Therefore, the following experimental conditions were set up as follows:

1) Bottom/Upper Gel: 0%FBS. Culture medium for maintenance/molecule incubation: 1,5%FBS-DMEM

2) Bottom/Upper Gel: 1,5%FBS. Culture medium for maintenance/molecule incubation: 1,5%FBS

3) Bottom/Upper Gel: 0%FBS. Culture medium for maintenance/molecule incubation: 10%FBS

4) Bottom/Upper Gel: 10%FBS. Culture medium for maintenance/molecule incubation: 10%FBS

In the conditions 2 and 4 we observed the formation of cellular protrusions 3 hours after preparing the 3D cell model and before adding the culture medium, whereas the absence of FBS in the conditions 1 and 3 prevented the cells to acquire their classical morphology (Figure 54). This preliminary observation confirmed the critical importance of FBS concentration in promoting proper cell growth and morphology. Indeed, the addition of the 10% FBS-culture medium restored the proper cell growth and cellular protrusions after 24h (Figure 55).

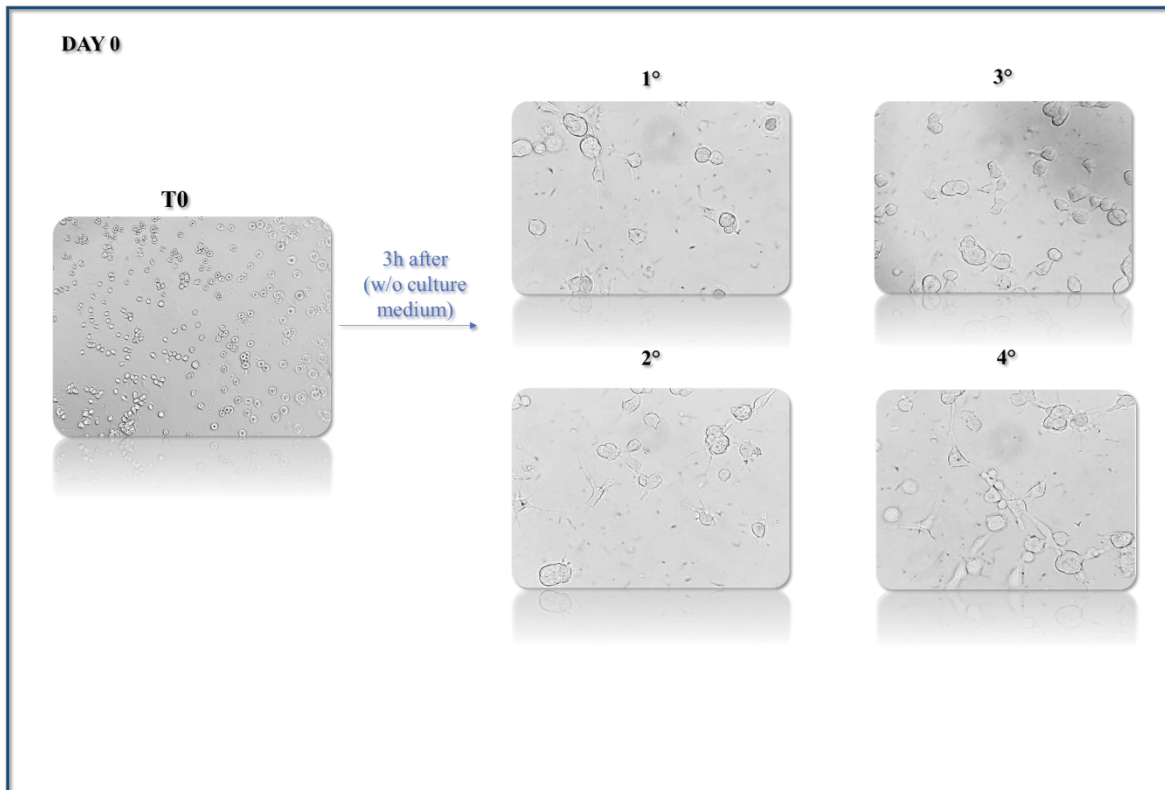


**Figure 54** U87MG 3D culture: 3 hours after preparation of “sandwich model”.  
Experimental points were the following: 1) Bottom/Upper Gel: 0%FBS; 2)  
Bottom/Upper Gel: 1,5%FBS; 3) Bottom/Upper Gel: 0%FBS; 4) Bottom/Upper Gel:  
10%FBS

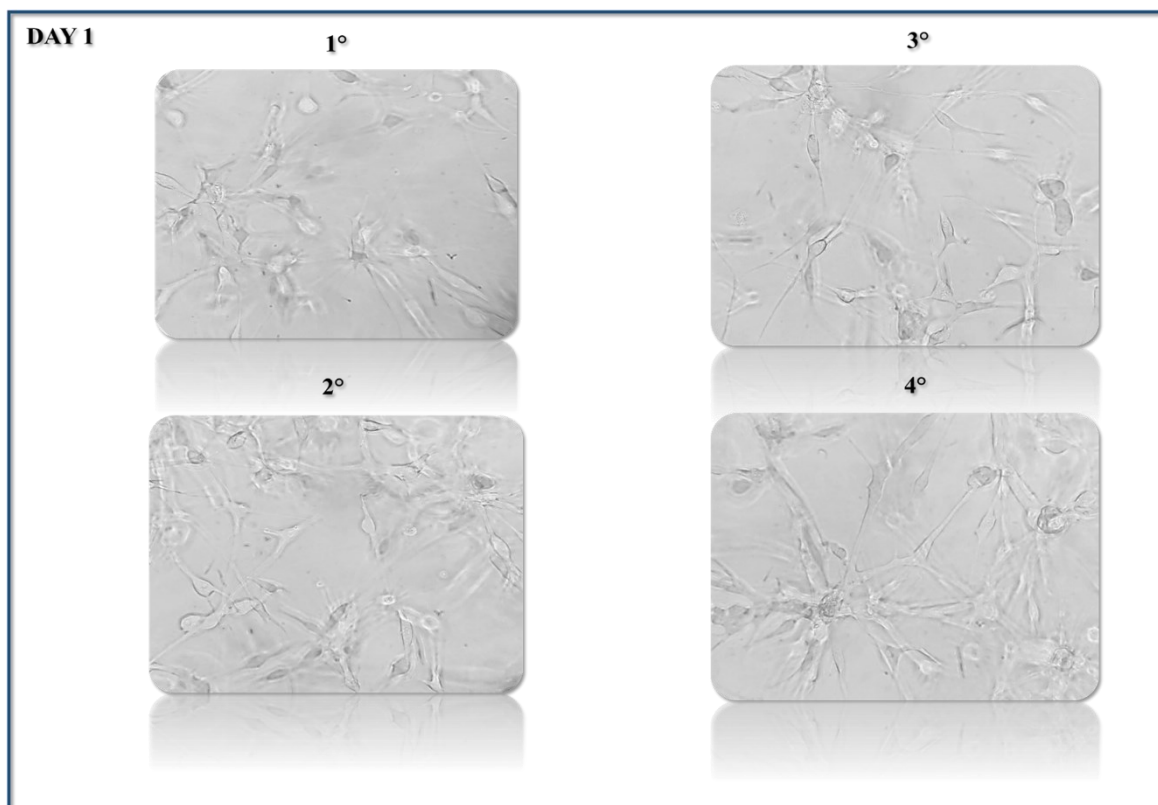


**Figure 55** U87MG 3D culture: 24 hours after preparation of “sandwich model”. 1) Bottom/Upper Gel: 0%FBS. Culture medium: 1,5%FBS-DMEM; 2) Bottom/Upper Gel: 1,5%FBS. Culture medium: 1,5%FBS; 3) Bottom/Upper Gel: 0%FBS. Culture medium: 10%FBS; 4) Bottom/Upper Gel: 10%FBS. Culture medium: 10%FBS

As already shown in bi-dimensional U87MG cultures, also in 3D-cell model CBDA showed a different cytotoxicity depending on the concentration of FBS in the gel and in the culture medium, CBDA was incubated for 72h with each of the three cellular models characterized by the lowest concentrations of FBS. As shown in (Figure 56), the CBDA toxicity was inversely proportional to FBS concentration. Indeed, the efficacy of CBDA in induce cell death was reduced by the presence of a 1.5% FBS in the gels and was almost completely abrogated by a 10% FBS in the culture medium.

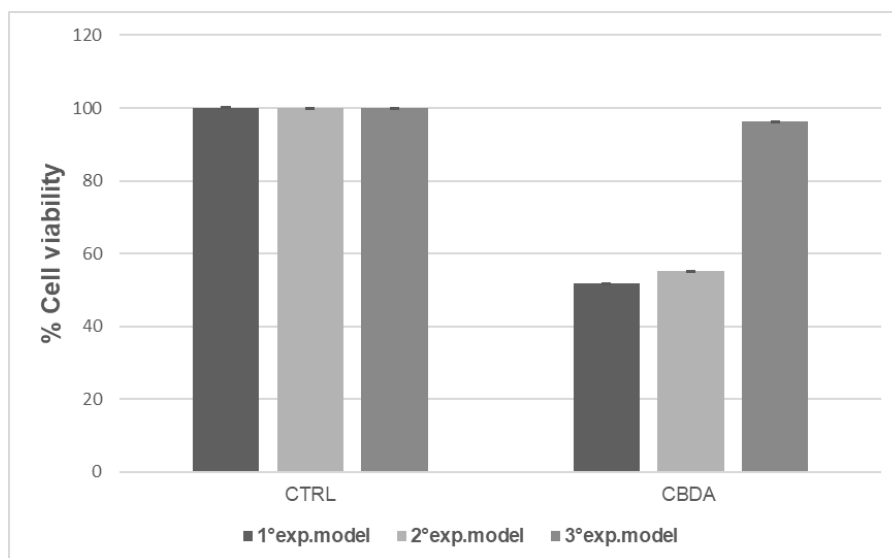


**Figure 56** MTT assay of CBDA (50  $\mu$ M) on 3D U87MG cells cultured in the three experimental cellular model 1°exp.model: Bottom/Upper Gel: 0%FBS. Culture medium: 1,5%FBS-DMEM; 2°exp.model: Bottom/Upper Gel: 1,5%FBS. Culture medium: 1,5%FBS; 3° exp.model: Bottom/Upper Gel: 0%FBS. Culture medium: 10%FBS. This experiment is representative of two biological replicates

These results prompted us to use the 2° and 3° experimental models for subsequent studies. The 2° experimental model was selected because the presence of an equal concentration of FBS in both matrigel and culture medium should allow a homogeneous delivery of CBDA. The 3° model was selected because it was closer to the conventional 2D U87MG cultures on which a target investigation was successfully conducted. Moreover, preliminary analyses were performed to select the CBDA incubation time with the 3D cultured cells. Given the peculiar constitution of the cell models, it was assumed that the time required to achieve adequate uptake of the compound into the cells could be longer than that taken for 2D cultures. However, it was mandatory to perform our analyses before significant changes

occurred in the cells. Therefore, a 24-hour incubation time was selected to perform further investigations.

### 3.3 CBDA-EIF2A binding suggests a different interactome of Eukaryotic translation complex between 2D- and 3D-cellular model

As discussed, we have demonstrated that in 2D-U87MG cells CBDA is able to bind EIF2A protein, significantly influencing its activity. Therefore, we studied CBDA-EIF2A interaction in a 3D cellular model by DARTS approach, using both the model 2 and 3 above described (Figure 57).

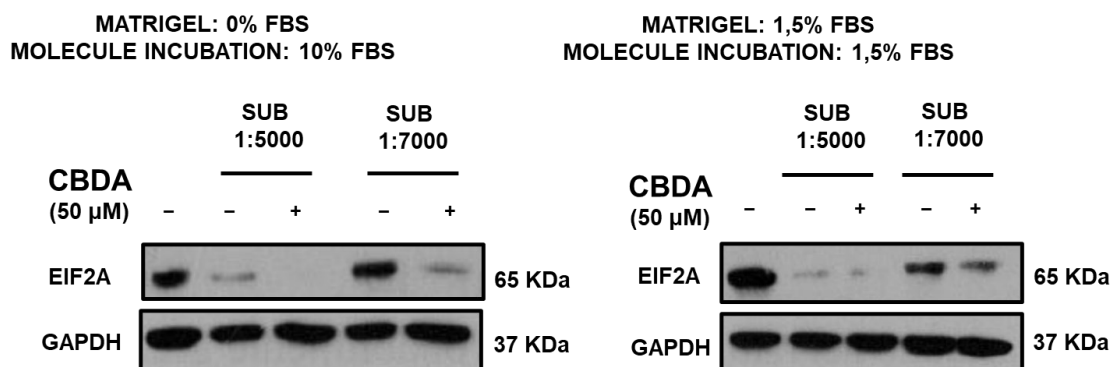


**Figure 57** DARTS assay of EIF2A performed on 3D U87MG cellular model A) Matrigel of bottom/upper gel at 0% FBS and cell culture medium at 10% FBS; B) Matrigel of bottom/upper gel at 1.5% FBS and cell culture medium at 1.5% FBS

The obtained results showed that a direct correlation between the percentage of FBS used in the cell culture and the ability of CBDA to interact with EIF2A occurred. Indeed, in the 1.5% FBS- Matrigel cultured 3D cells, compared to 0%FBS, EIF2A protein appeared to be less susceptible to proteolytic digestion in sample treatment

than in control. It could be due to the increased interaction of CBDA with fetal serum proteins in the gel which results in a lower bioavailability of the molecule. Nevertheless, in both cell models DARTS assay confirmed the EIF2A-CBDA interaction in a subtilisin-dose dependent manner, albeit with an apparent opposite effect. Therefore, a comparison between results in 2D and 3D-cell model was carried out (Figure 58).

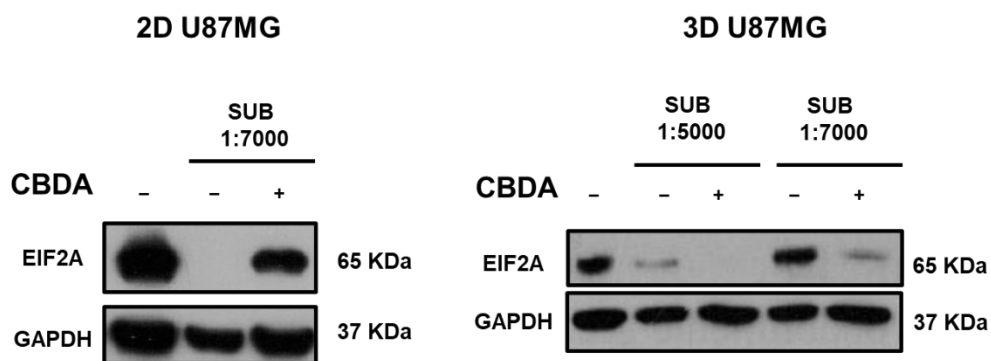


**Figure 58** Comparison of DARTS results between 2D and 3D cell cultures

As showed in the figure, in 2D U87MG cultures, EIF2A was completely digested by subtilisin in the untreated sample and became quite resistant to the proteolysis in the presence of CBDA-treated. Conversely, in the 3D-cultured cells EIF2A was almost undigested in control samples, but following CBDA treatment it susceptibility to subtilisin-catalyzed proteolysis sensibly increased. Although unexpected, this result confirmed the ability of CBDA to interfere with the stability of EIF2A, demonstrating that an interaction between the cannabinoid and the protein also occurred in this cellular model.

A possible explanation of this data was given based on what was observed in the 2D cellular model. In those conditions we demonstrated that the high protection

conferred to EIF2A by CBDA was mediated by the stabilization of the interaction of the protein with its protein partners. Therefore we hypothesized that exactly the opposite happened in cells cultured in 3D and that the binding of CBDA with EIF2A could interfere with the interactome that this protein establishes in these conditions. In 2D cell model DARTS and CETSA experiments allowed demonstrating that EEF1G was stabilized by CBDA binding to EIF2A, putatively as a consequence of the formation of a stabilized multiprotein complex. Therefore, to confirm our hypothesis we moved to evaluate EF1- $\gamma$ /EIF2A interaction in a context of a presumed different interactome in the 3D cellular model, performing a WB-based DARTS monitoring the digestion of EF1- $\gamma$  (Figure 59).

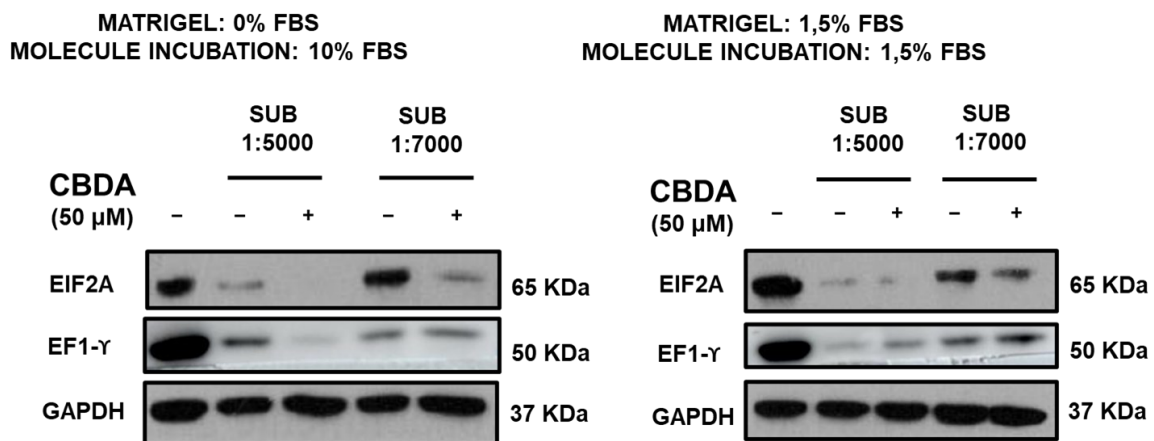


**Figure 59** DARTS assay of EF1- $\gamma$  in 3D U87MG cell model

Interestingly, in line with the 3D-DARTS results on EIF2A, EF1- $\gamma$  was more resistant to proteolytic digestion in the negative sample than in CBDA-treated cells resulting also more abundant in the control sample in a subtilisin dose dependent manner. Precisely, unlike EIF2A, at the lowest concentration of subtilisin (1:7000), EF1- $\gamma$

appeared to be equally present in DMSO- and CBDA-treated cells. In summary, these findings confirmed the specific binding between CBDA and EIF2A also providing more insights about the different interaction affinity between eukaryotic translation factors.

### **3.4 Interactome of EIF2A in 3D-U87MG cell model**

As shown above, DARTS analysis showed that CBDA-EIF2A interaction also occurred in 3D cellular model. Interestingly, CBDA appeared to induce a different proteolytic resistant digestion of EIF2A by comparing 2D and 3D cellular model. This finding suggested the occurrence of an intrinsic difference in the EIF2A interactome in the two cell models. Based on this hypothesis, we carried out an IP-based experiment in 3D cultured cells. The proteomic investigation of the EIF2A-immunoprecipitated proteins in this model incubated or not with CBDA showed that translation and ribosomal proteins were significantly more abundant in the untreated cells. Moreover, the EIF2A interactome involved a larger number of proteins when the cells were not subjected to CBDA treatment. Therefore, accordingly with DARTS results, CBDA appeared to affect the binding of EIF2A with several partners, thus making the protein more susceptible to proteolysis. However, the EIF2A interactome in 3D cells seems to be clearly different to that observed in 2D cell model. Indeed, a preliminary comparison of IP-related protein of the untreated 2D- and 3D-cellular models showed a greater abundance of translation machinery- related proteins in the three-dimensional cellular model compared to classical bidimensional cultures.

## Discussion

In recent decades, three-dimensional cellular models have replaced conventional cultures thus allowing the study of complex tumor or diseases in an increasingly realistic model. In *in vivo* conditions, tumors are characterized by the presence of the extracellular matrix, which provides adequate stiffness to cell growth due to its biochemical and mechanical properties. Particularly, in the brain the stiffness plays a fundamental role in regulating brain development and plasticity (Barnes, Przybyla and Weaver, 2017; Alcaraz *et al.*, 2018). Therefore, these findings give rise to the need of innovative cellular model that allows to produce more relevant results than conventional cultures. In this context, the suitable matrix plays a critical role. Interestingly, (Härmä *et al.*, 2010) showed that the matrix leads the cells into a more adaptable shape as different prostate cancer cell lines form spheroids differently. Notably, LAPC-4 show up with grape-like phenotype. RWPE-2/w99 and ALVA show a different morphology resembling a stellate “invasive” phenotype. Finally, LNCaP and PrEc form bulk and round phenotype, respectively. However, many cancer cell lines failed to form the spheroid in matrigel thus remaining as single cells. Currently, many types of three-dimensional cellular model have been defined depending on the biomaterial in order to support several processes such as cell-cell, cell-ECM interaction and cell line-base cell polarity. Indeed, (Härmä *et al.*, 2010) showed that Collagen and Matrigel induce cellular morphology differently. Although PC-3 cells form spheroids in Matrigel, when incorporated into pure collagen they form loose aggregates without establishing cell-cell interaction. Furthermore, they do not assume a definite morphology. Therefore, these findings demonstrate that the

choice of a suitable matrix plays a critical role in 3D cell culture. Matrigel is the first successful biomaterial composed of ECM proteins which allows to support the formation of cellular structures thus providing adequate stiffness where cell-cell and cell-ECM interactions are established differently.

Based on these considerations, the present work aimed to elucidate the mechanism of action of bioactive cannabinoids using chemical proteomic approaches in an innovative cellular model, such as the classic sandwich model that represent an *in vitro* model closer to *in vivo* conditions.

Global proteome analysis performed in 2D and 3D clearly indicated that the different conditions of cell culture produce significant differences in protein expression. Such difference is particularly dramatic for specific classes of protein, more than any other, proteins involved in recognition and intercellular interactions. A significant example is provided by the over-expression of Annexins family proteins in 3D. Annexins, a large family of calcium-dependent membrane-binding proteins, are associated with cytoskeleton proteins or matri-cellular proteins which are involved in the cell-extracellular matrix interaction (Mirzaei *et al.*, 2016). Particularly, Annexin A7 (ANXA7), shown as the most specific up-regulated proteins in 3D, correlates with all major stages of carcinogenesis phases, from the tumor occurrence to the metastasis process (Guo *et al.*, 2013). Furthermore, CSPG4 and NID1 also appeared to be more expressed in 3D model than in the 2D. CSPG4 is a type I transmembrane glycoprotein that binds one or more components of the ECM. (Pellegatta *et al.*, 2018) demonstrated that it can trigger the activation of oncogenic pathways related to the progression of different tumors such as glioma cancer. In addition, NID1 is significantly up-regulated in glioma tissue where it has been

identified as potential therapeutic target in glioma patients. In ovarian cancer it promotes epithelial-mesenchymal transition (EMT) and metastasis (Zhou *et al.*, 2017). Overall, these data are consistent with the difference in the biochemical environment that surrounds the cells that develop in a monolayer or in three dimensions. The latter, in fact, are surrounded by other cells and have less direct access to the substances present in the culture medium. These findings clearly demonstrate the potential features of the 3D sandwich model that is able of reproducing the *in vivo* tumor conditions. In particular, the expression of these proteins is representative of increased cell motility and invasiveness, compared to conventional monolayer cultures. On the other hand, the observed discrepancy between the proteome of 2D- and 3D-cultured cells raises doubts about the validity of the two-dimensional model for the study of the mechanism of action and the identification of the molecular target of drugs and bioactive compounds.

Therefore, since in the 2D cell model the Eukaryotic Translation complex has been identified as a target of CBDA, we aimed to investigate such interaction in the 3D sandwich model of glioblastoma. Interestingly, EIF2A emerged as a CBDA target also in this culture models, demonstrating that the affinity of this small molecule for its protein partner was negligibly affected by the growing conditions. However, comparing the DARTS results achieved using 2D- and 3D-cultured cells the most evident difference concerned the susceptibility of EIF2A to proteolysis in the untreated cells. Indeed, in both the conditions the protein appeared to be partially protected from subtilisin-catalyzed digestion in the presence of CBDA, but in the absence of the cannabinoid it was fully digested in the 2D-cultured cells and completely protected in the 3D-cultured ones. This result could be explained by assuming a difference in the EIF2A interactome in the two conditions. The

Eukaryotic translation machinery is a highly dynamic complex involving many different proteins in turns, which play specific roles at different stages of translation process. In addition, protein-protein interactions play a critical role in the biological context although the structure of many proteins and their ability to interact are still overlooked. Indeed, Klinge and collaborators showed that over time the eukaryotic translation complex has acquired a significant evolution which is explained in a greater interaction with the cellular environment and in the regulation of gene expression (Klinge *et al.*, 2012). Based on these considerations, the different stability of EIF2A revealed by DARTS in 2D and 3D cell models could depend on a different assembly status of the eukaryotic translation complex in the two conditions. According to this hypothesis, in 3D U87MG cells EIF2A could be present mainly as a member of that complex, whereas in the 2D-cultured cells it possibly exists primary as an isolated protein. Starting from these different conditions, the effect of CBDA could appear to be opposite in the two systems: indeed, interacting with the isolated EIF2A the cannabinoid induces a stiffening of the protein structure, resulting in a partial stabilization of some protein-protein interactions. Conversely, when the same interaction with CBDA occurs on EIF2A involved in the eukaryotic translation complex, it interferes with the oligomeric structure thus exposing EIF2A to proteolytic digestion.

These results, on the one hand suggests that culture conditions affect not only the proteome, but also many others biochemical aspects of the cells, which could significantly impact on the results of drug discovery and development studies. This finding unequivocally confirms the urgency of moving from the classic monolayer cell culture to more complex models that represent in more detail the complexity of the *in vivo* conditions, in the aim of perform effective preclinical studies. On the other

hand, the differences that occur in the two *in vitro* models studied for the binding between EIF2A and its partners suggest that this protein may also play an important role in the processes that regulate the ability of the cells to adapt to the surrounding environment.



## **Chapter 4 – Conclusions**



## Conclusions

The purpose of this research project was to study the biological effect of CBDA on glioblastoma. In addition to allowing to shed light on the mechanism of action of this compound, this study also contributed to confirm the emerging role of mass spectrometry-based proteomic approaches in the drug discovery process.

As a first result, in the present work the use of multiple and orthogonal approaches (DARTS, CETSA, LiP, MD) led to the identification of EIF2A as a protein target of CBDA in the cancer cells, to the definition of the protein region 460-480 as that directly involved in the cannabinoid binding and to the description of the conformational changes occurring in the protein structure after this interaction. The effect of CBDA/EIF2A interaction also involved other component of the multi-protein complex to which this protein belongs. Indeed, CBDA appeared to induce an anomalous stabilization of the entire translation mechanism complex, as demonstrated by the CBDA-induced resistance to proteolysis and thermal stabilization of the translation factor EEF1G, albeit slightly compared to EIF2A. Subsequently, a functional investigation of this interaction allowed us to define summarily the mechanism of action of CBDA. Indeed, the analysis of nascent proteome provided an instant capture of pathways modulation as a response to CBDA treatment. Precisely, the up- and down-regulated proteins involved in oxidative phosphorylation were representative of the dual effect produced by glioblastoma cells incubation with CBDA consisting in a balance between the ER stress response and the attempt to restore cellular homeostasis.

To investigate the binding between CBDA and EIF2A in a cell model closer to *in vivo* tumor, a 3D cellular model was set up. Therefore, a comparison of CBDA-EIF2A interaction between 2D- and 3D- cell model was carried out, by comparing the results obtained performing DARTS on 2D and 3D-cultured cells. EIF2A-CBDA interaction was confirmed in both the models, but some interesting insights about EIF2A interactome emerged (Figure 60).

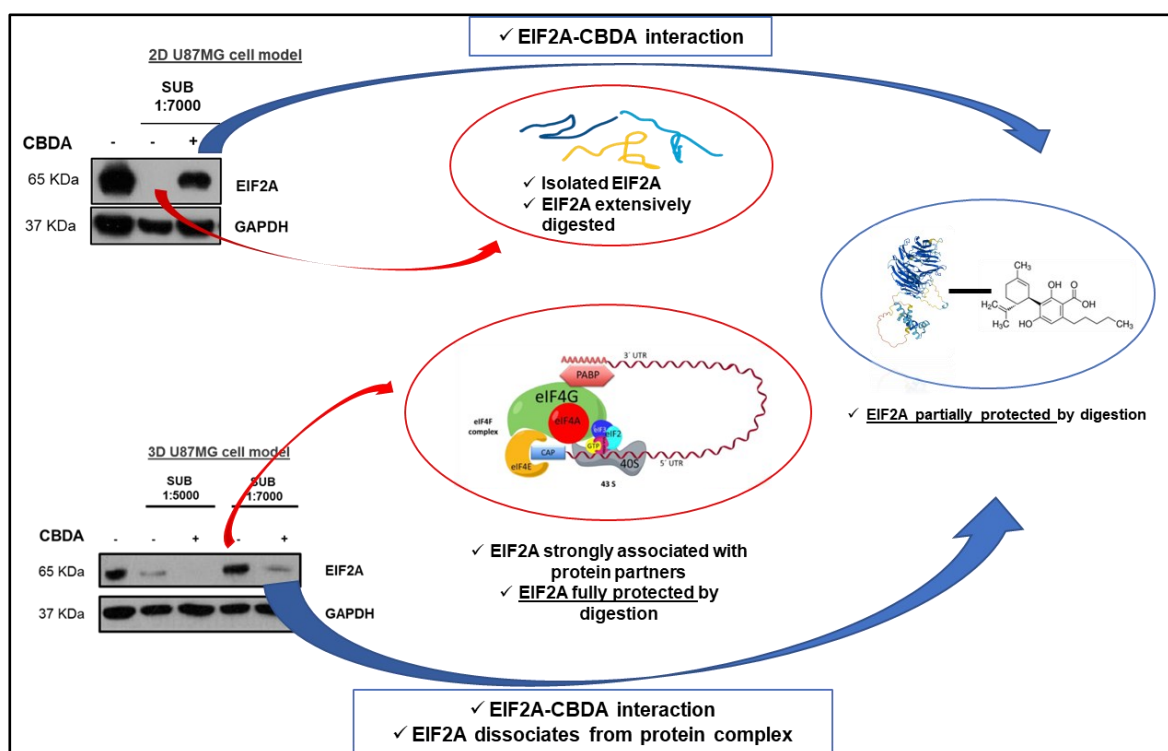


**Figure 60** DARTS performed on U87MG cells cultured in 2D or in 3D suggested a different assembly status of the eukaryotic translation complex in the two models

In particular, in the 2D cell model DARTS revealed that in the untreated cells EIF2A was very prone to enzymatic-catalyzed proteolysis, suggesting that under these conditions the protein was mainly dissociated from its partners. Conversely, in the 3D cultured cells the protein appeared to be strongly associated with the other

components of the eukaryotic translation complex in physiological condition, as inferred by its almost complete resistance to hydrolysis. Accordingly, the effect of CBDA binding was opposite in the two models. Indeed, it increased the stability of EIF2A in the 2D-cultured cells, inducing the protein to establish protein-protein interactions, while it destabilized EIF2A in the 3D model by leading the protein to dissociate from the pre-existing complex. These findings underlined the importance of using three-dimensional culture in drug discovery process. The hypothesis of the different interactome should necessarily be included in the context of a different global proteomic profile of 2D- and 3D-U87MG cells. Indeed, U87MG cells cultured in a three-dimensional space establish cell-cell and cell-ECM interactions, as revealed by the increased expression of proteins related to the invasion process in the 3D cell model.

Moreover, it is noteworthy to highlight the critical role of FBS in performing cannabinoid bioactivity investigation. Indeed, as shown from the 2D cytotoxicity assessment to the 3D cellular model setup, FBS could determine an alteration of the efficacy of CBDA, thus inducing an altered assessment of the potential biological effect of this, as well as of other cannabinoids. Since the present work aimed to conduct a target investigation, all results are representative of a treatment with CBDA in classical conditions of 10% FBS-DMEM, thus avoiding overestimating outcomes provided by pre-existing ER stress depending on FBS deprivation.

In closing of this study, the identification of EIF2A as potential target of CBDA allowed to elucidate better the role of this neglected protein as potential therapeutic target. Indeed, Chen and collaborators highlighted the role of EIF2A essential for tumor cell survival after paclitaxel-mediated ISR *in vitro* and *in vivo* thus suggesting

the importance of targeting EIF2A in parallel with ISR agonist use, thereby overcoming drug resistance in breast cancer (Chen *et al.*, 2019). In summary, the present work allows to identify CBDA as a potential therapeutic candidate for the treatment of cancer by targeting the eukaryotic translation machinery and with the consequent remodeling of the nascent proteome.

## **Chapter 5 - Material and Methods**



## Material and methods

### 5.1 Reagents and materials

Cannabidiolic acid was kindly provided by the group of Professor Giovanni Appendino (University of Piemonte Orientale). The purity of CBDA was 99.9% as proved by HPLC and NMR analyses. For NHA cell culture, ABMTM BulletKit™ was purchased from Lonza Biosciences (Morrisville, United State). Cell Counting Kit-8 was purchased from Dojindo EU GmbH (München, Germany). ON-TARGETplus Human EIF2A (83939) siRNA-SMARTpool was purchased from Dharmacon (Lafayette, Colorado, United States). Lipofectamine™ RNAiMAX, Click-IT Protein Enrichment Kit, Dulbecco Eagles's medium (DMEM), Dulbecco's Phosphate Buffered Saline (PBS), 0.5 % Trypsin-EDTA, dialyzed FBS, BCA Protein Assay Kit and Corning Matrigel were purchased from ThermoFischer (Waltham, Massachusetts, United States). DMEM-High Glucose for the preparation of SILAC medium was purchased from Athena Enzyme Systems (Baltimore, United States). EIF2A primary antibody for immunoprecipitation and immunoblotting were purchased from Proteintech (Rosemont, Illinois). Protein A / G PLUS Agarose and EEF1G primary antibody were purchased from SantaCruz Biotechnology (Dallas, Texas, United States). Secondary antibodies were purchased from Jackson ImmunoResearch Laboratories (West Grove, Pennsylvania). Corning For pulsed-SILAC, Labelling amino acids,  $^{13}\text{C}_6^{14}\text{N}_4$ -L-arginine (Arg6), 4,4,5,5-D<sub>4</sub>-L-lysine (Lys4),  $^{13}\text{C}_6^{15}\text{N}_4$ -L-arginine (Arg10) and  $^{13}\text{C}_6^{15}\text{N}_2$ -L-Lysine (Lys8) were purchased from Silantes (Gollierstraße, München, Germany). For the peptide clean-up, Oasis

plates were purchased from Waters Corporation (Milford, Massachusetts, United States).

## **5.2 Cell culture**

Human glioma cells (U87MG) (ECACC No: 89081402) were grown in DMEM supplemented with 1% penicillin/streptomycin, 1 % L-glutamine, 1 % sodium pyruvate, 1 % non-essential amino acids and 10 % fetal bovine serum (FBS, Thermo). Normal human astrocytes cells (NHA) were kindly provided by Professor Patrizia Gazerro (Department of Pharmacy, University of Salerno). These were grown in ABMTM BulletKit™. Both of cell lines were maintained under a humidified atmosphere of 5 % CO<sub>2</sub> at 37°C.

## **5.3 Cellular Viability Assay**

Cell viability was measured by the 3-[4,5-dimethylthiazole-2-yl]-2,5-diphenyltetrazolium bromide (MTT) assay (Sigma). U87MG and NHA cells were seeded at  $7 \times 10^3$  per well into 96-well plates. The day after, cells were treated with CBDA and DMSO as vehicle, tested at the concentrations of 12.5-25-50  $\mu$ M. To properly assess the cytotoxic effect, CBDA was incubated for 48h at different concentrations of FBS: 10%, 5% and 0%. Subsequently, the cells were incubated with MTT solution at the final concentration of 1 mg/mL and incubated for 4h. Then, the MTT-formazan crystals were solubilized in dimethyl sulfoxide (DMSO) and absorbance was read at 550 and 620 nm using Multiskan GO (Thermo Scientific). Experiments were performed in technical triplicates and repeated two times with similar results. The experiments were performed two times with similar results.

#### 5.4 Drug Affinity Target Stability Assay (DARTS)

DARTS assay was performed on U87MG intact cells and on cell lysate. The cells were seeded  $2 \times 10^5$  per well into 6-well plates in 10 % FBS-DMEM. The day after, the cells were treated with CBDA and DMSO as vehicle at the concentration of 50  $\mu\text{M}$  for 4h. The cells were lysed in RIPA buffer (20 mM Tris HCl pH 7.5, 150mM NaCl, 1 mM EDTA, 1 % NP-40, 1 % sodium deoxycholate, 2.5mM sodium pyrophosphate, 1mM  $\text{Na}_3\text{VO}_4$ ), centrifugated at 14000 rpm for 20 min. Then, 50  $\mu\text{g}$  of protein lysate were subjected to a limited digestion with subtilisin (enzyme:protein 1:3500 and 1:7000 w/w) for 30 min at 37°C.

Differently, DARTS on cell lysate was performed first by lysing the untreated U87MG in RIPA buffer as described above. Then, 100  $\mu\text{g}$  of cell lysate were treated with 50  $\mu\text{M}$  CBDA and DMSO as vehicle, for 1 hour on ice. The protein lysates were subjected to a limited digestion with subtilisin (enzyme:protein 1:7000 w/w) for 30 min at 37°C.

The reactions of both DARTS approaches were stopped by adding Laemmli buffer 4x and incubating the mixture at 95°C for 5 min. The samples were separated into 12% SDS-PAGE. Firstly, to perform protein identification, SDS-PAGE was treated with fixing solution for 30 minutes, stained with GelCode solution. Then it was divided into 10 pieces and digested as reported in gel digestion protocol described by (Shevchenko *et al.*, 2006). The mass spectrometry analysis was performed using Q-Exactive Orbitrap mass spectrometer (Thermo Fisher Scientific), coupled with a nanoUltimate3000 UHPLC system (Thermo Fisher Scientific). Peptide separation was performed on a capillary EASY-Spray PepMap column (0.075 mm  $\times$  50 mm, 2  $\mu\text{m}$ , Thermo Fisher Scientific) using aqueous 0.1% formic acid (A) and  $\text{CH}_3\text{CN}$

containing 0.1% formic acid (B) as mobile phases and a linear gradient from 3% to 40% of B in 45 min and a 300 nL/min flow rate. Mass spectra were acquired over an m/z range from 375 to 1500. MS and MS/MS data underwent Mascot software (v2.5, Matrix Science, Boston, MA, USA) analysis using the nonredundant data bank UniprotKB/Swiss-Prot. Parameters were set as follows: trypsin cleavage; carbamidomethylation of cysteine as a fixed modification and methionine oxidation as a variable modification; a maximum of two missed cleavages; false discovery rate (FDR), calculated by searching the decoy database, 0.05. The data analysis of protein was performed using the gene ontology tool in the UniProt Knowledgebase (UniProtKB; <http://www.uniprot.org>). Once the putative target protein was identified, western blot was performed under the same experimental condition as before. The experiments were performed two times with similar results.

### **5.5 Cellular Thermal Shift Assay**

CETSA assay was performed on U87MG cell line. The cells were seeded  $1 \times 10^5$  per well into 12-well plates in 10 % FBS-DMEM. The day after, the cells were treated with CBDA and DMSO as vehicle, both at the concentration of 50  $\mu$ M for 4h. After washing, the cells were collected, dissolved in PBS 1X and each sample was divided in 12 aliquots and subjected to a 5 min incubation at the different temperatures in the range 53-60 °C. Subsequently, the cells were lysed by freeze/thaw cycles and centrifugated. The soluble proteins were loaded onto 12% SDS-PAGE and western blot analysis was carried out at 100 V for 1h. The experiments were performed two times with similar results.

## **5.6 EIF2A silencing siRNA treatment**

U87MG were transfected using EIF2A siRNA. The cells were seeded at  $2 \times 10^6$  cells / 150mm-dish according to the manufacturer's specifications for forward transfection. EIF2A siRNA (Dharmacon) was transfected at the final concentration of 10 nM for 24h and 48h, considering 4h of washout as required by pSILAC protocol. For immunoblot analysis the whole cell lysates were harvested in RIPA buffer. Protein concentration was determined by a BCA Protein Assay Kit using BSA as a standard. Proteins fractionated by 4-20% SDS-PAGE followed by electrotransfer to a PVDF membrane (Trans-Blot Turbo Transfer, Bio-Rad) and immunoblotted with the appropriate primary antibody. After incubation with secondary antibody, the signals were visualized with the appropriate horseradish peroxidase-conjugated secondary antibody and enhanced chemiluminescence (GE Healthcare). Densitometric analyses were carried out using the ImageJ software.

## **5.7 Pulsed-Stable Isotope Labeling by amino acids in cell culture (pSILAC)**

To perform pSILAC, EIF2A silencing siRNA treatment was used as positive control. U87MG were seeded  $2 \times 10^6$  / 150 mm-dish in DMEM with and without antibiotics for compound treatment and for transfection, respectively. As reported in the figure (Figure 36), initially only silencing treatment was performed by incubating EIF2A siRNA for 24h. The day after, to perform p-SILAC experiments, the cells were washed twice with PBS and then incubated in depletion media (reduced component DMEM) for 30 minutes. The cells were treated with Heavy (Lys8-Arg10) or Intermediate (Lys4-Arg6) medium in the presence of 0.1mM AHA and the specific compounds (CBDA, CBCA or DMSO as vehicle) at 50  $\mu$ M for 4h. Then, the cells were harvested in cold PBS 1X and pelleted. Then, the cell lysate was obtained by

resuspending the cells in Urea lysis buffer and sonicated with a probe sonicator. Finally, the cyclo-addition enrichment was performed according to the instructions of the manufacturer. Proteins were eluted from the beads and subjected to trypsin digestion. The peptides were cleaned up using an Oasis PRiME HKB  $\mu$ Elution Plate, dissolved in 0.1% trifluoroacetic acid and analyzed by LC-MS/MS. The mass spectrometry analysis was performed using Tri-Hybrid Orbitrap Fusion mass spectrometer (Thermo Fisher Scientific), coupled with a Easy nLC 1200 nanospray source (Thermo Fisher Scientific). Peptides were loaded on a trap column (PepMap100 C18 Nano-Trap 100 $\mu$ m  $\times$  20mm) and separated over a 25cm analytical column (Waters nanoEase BEH, 75 $\mu$ m  $\times$  250mm, C18, 1.7 $\mu$ m, 130Å) using aqueous 0.1% formic acid (A) and 80% CH<sub>3</sub>CN containing 0.1% formic acid (B) as mobile phases and a linear gradient from 3% to 100% of B in 105 min and a 300 nL/min flow rate. Mass spectra were acquired over an m/z range from 375 to 1500. MS and MS/MS data underwent MaxQuant software (v2.5, Matrix Science, Boston, MA, USA) analysis using the nonredundant data bank UniprotKB/Swiss-Prot. Parameters were set as described above. The data analysis of protein was carried out using the gene ontology tool in the UniProt Knowledgebase (UniProtKB; <http://www.uniprot.org>). Perseus software was used for data analysis. The plots were generated on R studio (<https://rstudio.com>) and Perseus. The experiments were performed five times with similar results.

## **5.8 Limited Proteolysis**

The cells were seeded and treated with subtilisin as previously described for DARTS analysis. Subtilisin was inactivated boiling for 5 min at 95°C. Then, the cysteine residues were reduced by adding 10 mM Dithiothreitol (DTT) for 30 min at 37°C and

subsequently alkylated by adding 30 mM iodoacetamide (IAA) for 45 min at room temperature. Once reestablished pH 7.5-8.5, proteins were subjected to trypsin/LysC digestion 1:100 enzyme/substrate ratio (wt/wt) and incubated overnight at 37°C. Sodium deoxycholate was precipitated by adding formic acid to a final concentration of 2% (vol/vol). Once verified that the final pH of the sample was less than 3, the peptide cleanup was carried out using OasisPlate. The chromatography columns were washed and activated using 1% formic acid (buffer A) and 60% methanol with 1% formic acid (buffer B). Peptide cleaning was performed using both buffers and elution in buffer B. Samples were dried in speedvac, dissolved in 0.1% trifluoroacetic acid (TFA) and injected to the mass spectrometer. The samples were run to mass spectrometer as described in pulsed-SILAC paragraph. MaxQuant analysis was performed setting number of maximum missed cleavage site to 4 for single-limited digestion. In contrast, for double-limited digestion the number of maximum missed cleavage site was restored to 2 and the minimum peptide length was reduced to 2. The experiment was performed two times with similar results.

## **5.9 Computational Methods**

The three-dimensional model of the full EIF2A was retrieved from AlphaFold Protein Structure Database (<https://alphafold.ebi.ac.uk>). The protein model was then energy minimized (EM) and underwent molecular dynamics (MD) simulations with Amber20 pmemd.cuda module using ff14SB version of Amber force field (Case Ross C Walker and Roitberg Kenneth Merz Pengfei Li, no date). To perform MD simulations in solvent, the protein was confined in a TIP3P water periodic box exhibiting a minimum distance between solute atoms and box surfaces of 10 Å, using the tleap module of the AmberTools20 package. The systems were then neutralized by

addition of counterions (Cl<sup>-</sup>) and subjected to 1000 steps of EM with solute atoms harmonically restrained to their starting positions ( $K_r = 10 \text{ kcal.mol}^{-1}.\text{\AA}^{-1}$ ). Then, a 500 ps restrained MD simulation ( $K_r = 5 \text{ kcal kcal.mol}^{-1}.\text{\AA}^{-1}$ ) at constant pressure (1 atm) was run on the solvated protein, gradually heating the system to 300 K, followed by a 500 ps restrained MD simulation ( $K_r = 5 \text{ kcal.mol}^{-1}.\text{\AA}^{-1}$ ) at constant temperature (300 K) and pressure (1 atm) to adjust system density. Production MD simulations were carried out at constant temperature (300 K) and pressure (1 atm) for 400 ns, with a time step of 2 fs. Bonds involving hydrogens were constrained using the SHAKE algorithm. Starting ligands geometry were built with UCSF Chimera program, followed by initial energy minimization (EM) at the AM1 semi-empirical level. The molecules were then fully optimized using the GAMESS program at the Hartree–Fock level with the STO-3G basis set and subjected to HF/6-31G\*/STO-3G single-point calculations to derive the partial atomic charges using the RESP procedure (Pettersen *et al.*, 2004), (Schmidt *et al.*, 1993) (Fox and Kollman, 1998). Docking studies were performed with AutoDock 4.2 (Morris *et al.*, 2009). Both proteins and ligands were processed with AutoDock Tools (ADT) package version 1.5.6rc1 to merge non-polar hydrogens and calculate Gasteiger charges. Grids for docking evaluation with a spacing of 0.375 Å and 50 x 50 x70 points, centered on the protein region 460-480, were generated using the program AutoGrid 4.2 included in Autodock 4.2 distribution. The Lamarckian genetic algorithm (LGA) was adopted to perform 100 docking runs with the following parameters: 100 individuals in a population with a maximum of 15 million energy evaluations and a maximum of 37,000 generations, followed by 300 iterations of Solis and Wets local search. The complexes, selected on the basis of binding energy and cluster population, were completed by addition of all hydrogen atoms,

and they underwent energy minimization (EM) and then molecular dynamics (MD) simulations with Amber20 pmemd.cuda module, using the 14SB version of the AMBER force field for the protein and gaff parameters for the ligand. The protocol was the same used for the protein alone. Production MD simulations were carried out at constant temperature (300 K) and pressure (1 atm) for 200 ns, with a time step of 2 fs. The cpptraj module of AmberTools20 and program UCSF Chimera 1.10.1 were used to perform MD analysis and to draw the figures, respectively. Cluster analysis was carried out with the cpptraj module using the dbscan clustering algorithm. The representative frames were taken from the most populated clusters of each MD simulation.

### **5.10 Immunoprecipitation of EIF2A**

Immunoprecipitation assay was performed on U87MG intact cells. The cells were seeded  $2 \times 10^5$  per well into 6-well plates in 10 % FBS-DMEM. The day after, the cells were treated with CBDA and DMSO as vehicle at the concentration of 50  $\mu$ M for 4h. The cells were lysed in RIPA buffer and centrifugated. Then, the proteins were incubated with primary antibody anti-EIF2A for 2h on rotator (antibody:protein ratio 1:100). Then, Protein A / G PLUS Agarose beads were incubated on rotator overnight according to the manufacturer's instructions. The samples underwent to washing and elution as follows: the beads were gently washed with wash buffer, centrifugated at 2000g for 3 minutes at 4°C and the supernatants were discarded. After repeating the washing phase twice, the beads were eluted by heating the pellet in 2 x SDS loading buffer without DTT for 10 min at 50°C, centrifgated and supernatants harvested. Then, a second step of elution was carried out by heating the remaining pellet in 2 x SDS buffer with DTT 100mM. Then, the samples were

loaded on 12% SDS- PAGE that was treated with fixing solution for 30 minutes, stained with GelCode solution. Then each lane was divided into 10 pieces. In-gel digestion and MS analysis was performed as described in DARTS protocol. Finally, the characterization and quantification of proteins was carried out on Proteome Discoverer software by setting the abundance ratio CBDA sample with respect to the DMSO control. The proteins having abundance ratio greater than 2 were considered. The experiment was performed in two replicates.

### **5.11 3D cell model**

For 3D cell model, a classic sandwich system was generated using Matrigel mixture at 50% and 25% concentration. In 96-well plates, bottom wells were filled with 50% Matrigel and left to polymerize at 37°C, 5% CO<sub>2</sub> for 1h. Then, the wells were filled with U87MG cells ( $8 \times 10^3$  cells/well) in 25% Matrigel and polymerized for 3h at the same culturing conditions thus creating the upper-gel. Finally, the cells were culturing adding complete culture medium.

#### **5.11.1 Cell viability on 3D U87MG cells**

For cell viability, three different cell models were generated using different concentration of FBS. The experimental model were the following: 1° model: Bottom/Upper Gel: 0%FBS. Culture medium: 1,5%FBS-DMEM; 2° model: Bottom/Upper Gel: 1,5%FBS. Culture medium: 1,5%FBS; 3° model: Bottom/Upper Gel: 0%FBS. Culture medium: 10%FBS. U87MG cells were seeded as described above and cultured for 5 days. Then, they were treated with CBDA and DMSO as vehicle at the concentration of 50 µM for 72h in DMEM at different concentrations of FBS: 10%, 5% and 0%. Subsequently, the cell viability was measured using Cell Counting Kit-8 solution according to the manufacturer's instructions. The

experiments were performed in technical triplicates and repeated two times with similar results.

#### **5.11.2 Global proteome analysis on 2D and 3D U87MG cells**

For global proteome analysis, U87MG were normally cultured in monolayer and in 3D cell model, as described above. As for the 3D cell model, the Matrigel was removed by incubating the cellular pellet in 5mM EDTA. Then, the cell pellets of both 2D- and 3D- cells were lysed in RIPA buffer and 30 µg of proteins were fractionated on SDS-PAGE and immunoblotted. The experiments were performed in three replicates.

#### **5.11.3 DARTS assay on 3D U87MG cells**

In contrast, for DARTS analysis, the 3D cell model was generated using two different cell models: 1°model: Matrigel of bottom/upper gel at 0% FBS and cell culture medium at 10% FBS; 2°model: Matrigel of bottom/upper gel at 1.5% FBS and cell culture medium at 1.5% FBS After 5 days, the cells were incubated with CBDA or DMSO as vehicle at the concentration of 50 µM. Then, the cell pellet was obtained after removing of Matrigel, lysed in RIPA buffer and fractionated on SDS-PAGE and immunoblotted. 50 µg of protein lysate were subjected to a limited digestion with subtilisin (enzyme:protein 1:5000 and 1:7000 w/w) for 30 min at 37°, loaded on SDS-PAGE and immunoblotted. The experiment was performed two times with similar results.

## References

Alcaraz, J. *et al.* (2018) 'Bidirectional mechanobiology between cells and their local extracellular matrix probed by atomic force microscopy', *Seminars in cell & developmental biology*, 73, pp. 71–81. doi:10.1016/J.SEMCDB.2017.07.020.

Altelaar, A.F.M., Munoz, J. and Heck, A.J.R. (2013) 'Next-generation proteomics: towards an integrative view of proteome dynamics', *Nature reviews. Genetics*, 14(1), pp. 35–48. doi:10.1038/NRG3356.

Amantini, C. *et al.* (2007) 'Capsaicin-induced apoptosis of glioma cells is mediated by TRPV1 vanilloid receptor and requires p38 MAPK activation', *Journal of neurochemistry*, 102(3), pp. 977–990. doi:10.1111/J.1471-4159.2007.04582.X.

Andre, C.M., Hausman, J.F. and Guerriero, G. (2016) 'Cannabis sativa: The Plant of the Thousand and One Molecules', *Frontiers in plant science*, 7(FEB2016). doi:10.3389/FPLS.2016.00019.

Artero-Castro, A. *et al.* (2015) 'Disruption of the ribosomal P complex leads to stress-induced autophagy', *Autophagy*, 11(9), pp. 1499–1519. doi:10.1080/15548627.2015.1063764.

Atanasov, A.G. *et al.* (2021) 'Natural products in drug discovery: advances and opportunities', *Nature reviews. Drug discovery*, 20(3), pp. 200–216. doi:10.1038/S41573-020-00114-Z.

Atzrodt, J. *et al.* (2018) 'Deuterium- and Tritium-Labelled Compounds: Applications in the Life Sciences', *Angewandte Chemie (International ed. in English)*, 57(7), pp.

1758–1784. doi:10.1002/ANIE.201704146.

Baghban, R. *et al.* (2020) 'Tumor microenvironment complexity and therapeutic implications at a glance', *Cell communication and signaling: CCS*, 18(1). doi:10.1186/S12964-020-0530-4.

Barnes, J.M., Przybyla, L. and Weaver, V.M. (2017) 'Tissue mechanics regulate brain development, homeostasis and disease', *Journal of cell science*, 130(1), pp. 71–82. doi:10.1242/JCS.191742.

Benedetti, R. *et al.* (2022) 'ATF6 prevents DNA damage and cell death in colon cancer cells undergoing ER stress', *Cell death discovery*, 8(1). doi:10.1038/S41420-022-01085-3.

Carracedo, A. *et al.* (2006) 'The stress-regulated protein p8 mediates cannabinoid-induced apoptosis of tumor cells', *Cancer cell*, 9(4), pp. 301–312. doi:10.1016/J.CCR.2006.03.005.

Case Ross C Walker, D.A. and Roitberg Kenneth Merz Pengfei Li, A.M. (no date) 'Amber 2020 Reference Manual Principal contributors to the current codes'. Available at: <http://ambermd.org/contributors.html> (Accessed: 26 January 2023).

Chaicharoenaudomrung, N., Kunhorm, P. and Noisa, P. (2019) 'Three-dimensional cell culture systems as an in vitro platform for cancer and stem cell modeling', *World journal of stem cells*, 11(12), pp. 1065–1083. doi:10.4252/WJSC.V11.I12.1065.

Chen, J. *et al.* (2020) 'Upregulation of oxidative stress-responsive 1(OXSR1) predicts poor prognosis and promotes hepatocellular carcinoma progression', *Bioengineered*, 11(1), pp. 958–971. doi:10.1080/21655979.2020.1814659.

Chen, L. *et al.* (2019) 'EIF2A promotes cell survival during paclitaxel treatment in

vitro and in vivo', *Journal of cellular and molecular medicine*, 23(9), pp. 6060–6071. doi:10.1111/JCMM.14469.

Chen, X. *et al.* (2015) 'Quantitative proteomics using SILAC: Principles, applications, and developments', *Proteomics*, 15(18), pp. 3175–3192. doi:10.1002/PMIC.201500108.

Cui, J. *et al.* (2020) 'GSTP1 and cancer: Expression, methylation, polymorphisms and signaling (Review)', *International journal of oncology*, 56(4), pp. 867–878. doi:10.3892/IJO.2020.4979.

Dolgacheva, L.P. *et al.* (2019) 'Role of DJ-1 in the mechanism of pathogenesis of Parkinson's disease', *Journal of bioenergetics and biomembranes*, 51(3), pp. 175–188. doi:10.1007/S10863-019-09798-4.

Eastman, A. (2017) 'Improving anticancer drug development begins with cell culture: misinformation perpetrated by the misuse of cytotoxicity assays', *Oncotarget*, 8(5), pp. 8854–8866. doi:10.18632/ONCOTARGET.12673.

Eichelbaum, K. *et al.* (2012) 'Selective enrichment of newly synthesized proteins for quantitative secretome analysis', *Nature Biotechnology*, 30(10), pp. 984–990. doi:10.1038/nbt.2356.

Eichelbaum, K. and Krijgsveld, J. (2014) 'Combining pulsed SILAC labeling and click-chemistry for quantitative secretome analysis', *Methods in Molecular Biology*, 1174, pp. 101–114. doi:10.1007/978-1-4939-0944-5\_7/COVER.

Feng, Y. *et al.* (2014) 'Global analysis of protein structural changes in complex proteomes', *Nature biotechnology*, 32(10), pp. 1036–1044. doi:10.1038/NBT.2999.

Fierro-Monti, I. *et al.* (2013) 'A novel pulse-chase SILAC strategy measures changes

in protein decay and synthesis rates induced by perturbation of proteostasis with an Hsp90 inhibitor', *PloS one*, 8(11). doi:10.1371/JOURNAL.PONE.0080423.

Formato, M. *et al.* (2020) '(–)-Cannabidiolic Acid, a Still Overlooked Bioactive Compound: An Introductory Review and Preliminary Research', *Molecules (Basel, Switzerland)*, 25(11). doi:10.3390/MOLECULES25112638.

Fox, T. and Kollman, P.A. (1998) 'Application of the RESP Methodology in the Parametrization of Organic Solvents', *Journal of Physical Chemistry B*, 102(41), pp. 8070–8079. doi:10.1021/JP9717655.

Grantham, J. (2020) 'The Molecular Chaperone CCT/TRiC: An Essential Component of Proteostasis and a Potential Modulator of Protein Aggregation', *Frontiers in genetics*, 11. doi:10.3389/FGENE.2020.00172.

Guo, C. *et al.* (2013) 'Potential role of annexin A7 in cancers', *Clinica chimica acta; international journal of clinical chemistry*, 423, pp. 83–89. doi:10.1016/J.CCA.2013.04.018.

Hanuš, L.O. *et al.* (2016) 'Phytocannabinoids: a unified critical inventory', *Natural product reports*, 33(12), pp. 1357–1392. doi:10.1039/C6NP00074F.

Härmä, V. *et al.* (2010) 'A comprehensive panel of three-dimensional models for studies of prostate cancer growth, invasion and drug responses', *PloS one*, 5(5). doi:10.1371/JOURNAL.PONE.0010431.

Haustrate, A., Prevarskaya, N. and Lehen'kyi, V. (2020) 'Role of the TRPV Channels in the Endoplasmic Reticulum Calcium Homeostasis', *Cells*, 9(2). doi:10.3390/CELLS9020317.

Heider, C.G. *et al.* (2022) 'Mechanisms of Cannabidiol (CBD) in Cancer Treatment:

A Review', *Biology*, 11(6). doi:10.3390/BIOLOGY11060817.

Henderson, M.J. *et al.* (2020) 'High-Throughput Cellular Thermal Shift Assays in Research and Drug Discovery', *SLAS discovery: advancing life sciences R & D*, 25(2), pp. 137–147. doi:10.1177/2472555219877183.

Henrich, C.J. and Beutler, J.A. (2013) 'Matching the power of high throughput screening to the chemical diversity of natural products', *Natural product reports*, 30(10), pp. 1284–1298. doi:10.1039/C3NP70052F.

Huang, L., Wang, D. and Zhang, C. (2021) 'Drug Affinity Responsive Target Stability (DARTS ) Assay to Detect Interaction Between a Purified Protein and a Small Molecule', *Methods in molecular biology (Clifton, N.J.)*, 2213, pp. 175–182. doi:10.1007/978-1-0716-0954-5\_15.

Huang, T. *et al.* (2021) 'Cannabidiol inhibits human glioma by induction of lethal mitophagy through activating TRPV4', *Autophagy*, 17(11), pp. 3592–3606. doi:10.1080/15548627.2021.1885203.

Ibarrola, N. *et al.* (2003) 'A proteomic approach for quantitation of phosphorylation using stable isotope labeling in cell culture', *Analytical chemistry*, 75(22), pp. 6043–6049. doi:10.1021/AC034931F.

Jacobsson, S.O.P. *et al.* (2000) 'Serum-dependent effects of tamoxifen and cannabinoids upon C6 glioma cell viability', *Biochemical Pharmacology*, 60(12), pp. 1807–1813. doi:10.1016/S0006-2952(00)00492-5.

Jafari, R. *et al.* (2014) 'The cellular thermal shift assay for evaluating drug target interactions in cells', *Nature protocols*, 9(9), pp. 2100–2122. doi:10.1038/NPROT.2014.138.

Jensen, C. and Teng, Y. (2020) 'Is It Time to Start Transitioning From 2D to 3D Cell Culture?', *Frontiers in molecular biosciences*, 7. doi:10.3389/FMOLB.2020.00033.

Joseph, J.S., Malindisa, S.T. and Ntwasa, M. (2018) 'Two-Dimensional (2D) and Three-Dimensional (3D) Cell Culturing in Drug Discovery', in Mehanna, R.A. (ed.) *Cell Culture*. Rijeka: IntechOpen. doi:10.5772/intechopen.81552.

Kim, E. *et al.* (2018) 'eIF2A, an initiator tRNA carrier refractory to eIF2 $\alpha$  kinases, functions synergistically with eIF5B', *Cellular and molecular life sciences: CMLS*, 75(23), pp. 4287–4300. doi:10.1007/S00018-018-2870-4.

Klinge, S. *et al.* (2012) 'Atomic structures of the eukaryotic ribosome', *Trends in biochemical sciences*, 37(5), pp. 189–198. doi:10.1016/J.TIBS.2012.02.007.

Komar, A.A. and Merrick, W.C. (2020) 'A Retrospective on eIF2A-and Not the Alpha Subunit of eIF2', *International journal of molecular sciences*, 21(6). doi:10.3390/IJMS21062054.

Kubota, K., Funabashi, M. and Ogura, Y. (2019) 'Target deconvolution from phenotype-based drug discovery by using chemical proteomics approaches', *Biochimica et biophysica acta. Proteins and proteomics*, 1867(1), pp. 22–27. doi:10.1016/J.BBAPAP.2018.08.002.

Kwon, O.S. *et al.* (2017) 'An mRNA-specific tRNAi carrier eIF2A plays a pivotal role in cell proliferation under stress conditions: stress-resistant translation of c-Src mRNA is mediated by eIF2A', *Nucleic acids research*, 45(1), pp. 296–310. doi:10.1093/NAR/GKW1117.

de la Harpe, A., Beukes, N. and Frost, C.L. (2022) 'CBD activation of TRPV1 induces oxidative signaling and subsequent ER stress in breast cancer cell lines',

*Biotechnology and applied biochemistry*, 69(2), pp. 420–430.  
doi:10.1002/BAB.2119.

Ligresti, A. *et al.* (2006) 'Antitumor activity of plant cannabinoids with emphasis on the effect of cannabidiol on human breast carcinoma', *The Journal of pharmacology and experimental therapeutics*, 318(3), pp. 1375–1387.  
doi:10.1124/JPET.106.105247.

Lim, M.P., Devi, L.A. and Rozenfeld, R. (2011) 'Cannabidiol causes activated hepatic stellate cell death through a mechanism of endoplasmic reticulum stress-induced apoptosis', *Cell death & disease*, 2(6). doi:10.1038/CDDIS.2011.52.

Liu, R. *et al.* (2009) 'Enzymatically inactive adenylate kinase 4 interacts with mitochondrial ADP/ATP translocase', *The international journal of biochemistry & cell biology*, 41(6), pp. 1371–1380. doi:10.1016/J.BIOCEL.2008.12.002.

Liu, Y. (2004) 'Epithelial to mesenchymal transition in renal fibrogenesis: pathologic significance, molecular mechanism, and therapeutic intervention', *Journal of the American Society of Nephrology: JASN*, 15(1), pp. 1–12.  
doi:10.1097/01.ASN.0000106015.29070.E7.

Lomenick, B. *et al.* (2009) 'Target identification using drug affinity responsive target stability (DARTS)', *Proceedings of the National Academy of Sciences of the United States of America*, 106(51), pp. 21984–21989. doi:10.1073/PNAS.0910040106.

López-Valero, I. *et al.* (2018) 'Targeting Glioma Initiating Cells with A combined therapy of cannabinoids and temozolomide', *Biochemical pharmacology*, 157, pp. 266–274. doi:10.1016/J.BCP.2018.09.007.

Lundgren, S. (2019) 'Focusing on Relevance: CETSA-Guided Medicinal Chemistry

and Lead Generation', *ACS Medicinal Chemistry Letters*, 10(5), pp. 690–693. doi:10.1021/ACSMEDCHEMLETT.9B00112/ASSET/IMAGES/LARGE/ML-2019-001127\_0003.JPEG.

Mangal, N. *et al.* (2021) 'Cannabinoids in the landscape of cancer', *Journal of cancer research and clinical oncology*, 147(9), pp. 2507–2534. doi:10.1007/S00432-021-03710-7.

Mann, M. (2006) 'Functional and quantitative proteomics using SILAC', *Nature reviews. Molecular cell biology*, 7(12), pp. 952–958. doi:10.1038/NRM2067.

Massi, P. *et al.* (2004) 'Antitumor effects of cannabidiol, a nonpsychoactive cannabinoid, on human glioma cell lines', *The Journal of pharmacology and experimental therapeutics*, 308(3), pp. 838–845. doi:10.1124/JPET.103.061002.

Mateus, A. *et al.* (2020) 'Thermal proteome profiling for interrogating protein interactions', *Molecular systems biology*, 16(3). doi:10.15252/MSB.20199232.

Matsumoto, T. *et al.* (2015) 'Small Heat Shock Protein Beta-1 (HSPB1) Is Upregulated and Regulates Autophagy and Apoptosis of Renal Tubular Cells in Acute Kidney Injury', *PloS one*, 10(5). doi:10.1371/JOURNAL.PONE.0126229.

Meissner, F. *et al.* (2022) 'The emerging role of mass spectrometry-based proteomics in drug discovery', *Nature reviews. Drug discovery*, 21(9), pp. 637–654. doi:10.1038/S41573-022-00409-3.

Mirsaeidi, M. *et al.* (2016) 'Annexins family: insights into their functions and potential role in pathogenesis of sarcoidosis', *Journal of translational medicine*, 14(1). doi:10.1186/S12967-016-0843-7.

Mitchell, D.A. *et al.* (2007) 'Thioredoxin is required for S-nitrosation of procaspase-

3 and the inhibition of apoptosis in Jurkat cells', *Proceedings of the National Academy of Sciences of the United States of America*, 104(28), pp. 11609–11614. doi:10.1073/PNAS.0704898104.

Moon, S.Y. *et al.* (2014) 'Endoplasmic reticulum stress induces epithelial-mesenchymal transition through autophagy via activation of c-Src kinase', *Nephron. Experimental nephrology*, 126(3), pp. 127–140. doi:10.1159/000362457.

Morales, P., Hurst, D.P. and Reggio, P.H. (2017) 'Molecular Targets of the Phytocannabinoids: A Complex Picture', *Progress in the chemistry of organic natural products*, 103, pp. 103–131. doi:10.1007/978-3-319-45541-9\_4.

Morris, G.M. *et al.* (2009) 'AutoDock4 and AutoDockTools4: Automated docking with selective receptor flexibility', *Journal of computational chemistry*, 30(16), pp. 2785–2791. doi:10.1002/JCC.21256.

Navarro, G. *et al.* (2020) 'Pharmacological data of cannabidiol- and cannabigerol-type phytocannabinoids acting on cannabinoid CB1, CB2 and CB1/CB2 heteromer receptors', *Pharmacological research*, 159. doi:10.1016/J.PHRS.2020.104940.

Ong, S.E. *et al.* (2002) 'Stable isotope labeling by amino acids in cell culture, SILAC, as a simple and accurate approach to expression proteomics', *Molecular & cellular proteomics : MCP*, 1(5), pp. 376–386. doi:10.1074/MCP.M200025-MCP200.

Ong, S.E. and Mann, M. (2006) 'A practical recipe for stable isotope labeling by amino acids in cell culture (SILAC)', *Nature protocols*, 1(6), pp. 2650–2660. doi:10.1038/NPROT.2006.427.

Ortiz, Y.T., McMahon, L.R. and Wilkerson, J.L. (2022) 'Medicinal Cannabis and Central Nervous System Disorders', *Frontiers in pharmacology*, 13.

doi:10.3389/FPHAR.2022.881810.

Pagliarini, V. *et al.* (2015) 'Downregulation of E2F1 during ER stress is required to induce apoptosis', *Journal of cell science*, 128(6), pp. 1166–1179. doi:10.1242/JCS.164103.

Pattnaik, F. *et al.* (2022) 'Cannabis: Chemistry, extraction and therapeutic applications', *Chemosphere*, 289. doi:10.1016/J.CHEMOSPHERE.2021.133012.

Pavez, M. *et al.* (2019) 'STIM1 Is Required for Remodeling of the Endoplasmic Reticulum and Microtubule Cytoskeleton in Steering Growth Cones', *The Journal of neuroscience : the official journal of the Society for Neuroscience*, 39(26), pp. 5095–5114. doi:10.1523/JNEUROSCI.2496-18.2019.

Pellegatta, S. *et al.* (2018) 'Constitutive and TNF $\alpha$ -inducible expression of chondroitin sulfate proteoglycan 4 in glioblastoma and neurospheres: Implications for CAR-T cell therapy', *Science translational medicine*, 10(430). doi:10.1126/SCITRANSLMED.AAO2731.

Pepelnjak, M., de Souza, N. and Picotti, P. (2020) 'Detecting Protein-Small Molecule Interactions Using Limited Proteolysis-Mass Spectrometry (LiP-MS)', *Trends in biochemical sciences*, 45(10), pp. 919–920. doi:10.1016/J.TIBS.2020.05.006.

Pérez-Gómez, E. *et al.* (2015) 'Role of cannabinoid receptor CB2 in HER2 pro-oncogenic signaling in breast cancer', *Journal of the National Cancer Institute*, 107(6). doi:10.1093/JNCI/DJV077.

Perner, C. and Krüger, E. (2022) 'Endoplasmic Reticulum Stress and Its Role in Homeostasis and Immunity of Central and Peripheral Neurons', *Frontiers in immunology*, 13. doi:10.3389/FIMMU.2022.859703.

Pettersen, E.F. *et al.* (2004) 'UCSF Chimera--a visualization system for exploratory research and analysis', *Journal of computational chemistry*, 25(13), pp. 1605–1612. doi:10.1002/JCC.20084.

Qamri, Z. *et al.* (2009) 'Synthetic cannabinoid receptor agonists inhibit tumor growth and metastasis of breast cancer', *Molecular cancer therapeutics*, 8(11), pp. 3117–3129. doi:10.1158/1535-7163.MCT-09-0448.

Rebelo, A.P. *et al.* (2021) 'Biallelic loss-of-function variations in PRDX3 cause cerebellar ataxia', *Brain: a journal of neurology*, 144(5), pp. 1467–1481. doi:10.1093/BRAIN/AWAB071.

Reineke, L.C. *et al.* (2011) 'Insights into the role of yeast eIF2A in IRES-mediated translation', *PloS one*, 6(9). doi:10.1371/JOURNAL.PONE.0024492.

Ren, Y.S. *et al.* (2021) 'Drug affinity responsive target stability (DARTS) accelerated small molecules target discovery: Principles and application', *Biochemical pharmacology*, 194. doi:10.1016/J.BCP.2021.114798.

Roche, J. (2018) 'The Epithelial-to-Mesenchymal Transition in Cancer', *Cancers*, 10(2). doi:10.3390/CANCERS10020052.

Sahin Umut, U. *et al.* (2014) 'Oxidative stress-induced assembly of PML nuclear bodies controls sumoylation of partner proteins', *The Journal of cell biology*, 204(6), pp. 931–945. doi:10.1083/JCB.201305148.

Sainz-Cort, A., Müller-Sánchez, C. and Espel, E. (2020) 'Anti-proliferative and cytotoxic effect of cannabidiol on human cancer cell lines in presence of serum', *BMC research notes*, 13(1). doi:10.1186/S13104-020-05229-5.

Schilling, S., Melzer, R. and McCabe, P.F. (2020) 'Cannabis sativa', *Current*

*biology: CB*, 30(1), pp. R8–R9. doi:10.1016/J.CUB.2019.10.039.

Schmidt, M.W. *et al.* (1993) 'General atomic and molecular electronic structure system', *Journal of Computational Chemistry*, 14(11), pp. 1347–1363. doi:10.1002/JCC.540141112.

Schopper, S. *et al.* (2017) 'Measuring protein structural changes on a proteome-wide scale using limited proteolysis-coupled mass spectrometry', *Nature protocols*, 12(11), pp. 2391–2410. doi:10.1038/NPROT.2017.100.

Schulze, A. *et al.* (2020) 'MYC Targets Scores Are Associated with Cancer Aggressiveness and Poor Survival in ER-Positive Primary and Metastatic Breast Cancer', *International journal of molecular sciences*, 21(21), pp. 1–13. doi:10.3390/IJMS21218127.

Schurman, L.D. *et al.* (2020) 'Molecular Mechanism and Cannabinoid Pharmacology', *Handbook of experimental pharmacology*, 258, pp. 323–353. doi:10.1007/164\_2019\_298.

Scott, K.A., Dalgleish, A.G. and Liu, W.M. (2017) 'Anticancer effects of phytocannabinoids used with chemotherapy in leukaemia cells can be improved by altering the sequence of their administration', *International journal of oncology*, 51(1), pp. 369–377. doi:10.3892/IJO.2017.4022.

Seltzer, E.S. *et al.* (2020) 'Cannabidiol (CBD) as a Promising Anti-Cancer Drug', *Cancers*, 12(11), pp. 1–26. doi:10.3390/CANCERS12113203.

Sendoel, A. *et al.* (2017) 'Translation from unconventional 5' start sites drives tumour initiation', *Nature*, 541(7638), pp. 494–499. doi:10.1038/NATURE21036.

Shevchenko, A. *et al.* (2006) 'In-gel digestion for mass spectrometric

characterization of proteins and proteomes', *Nature protocols*, 1(6), pp. 2856–2860. doi:10.1038/NPROT.2006.468.

Singer, E. *et al.* (2015) 'Reactive oxygen species-mediated therapeutic response and resistance in glioblastoma', *Cell death & disease*, 6(1). doi:10.1038/CDDIS.2014.566.

Solinas, M. *et al.* (2013) 'Cannabidiol, a non-psychoactive cannabinoid compound, inhibits proliferation and invasion in U87-MG and T98G glioma cells through a multitarget effect', *PloS one*, 8(10). doi:10.1371/JOURNAL.PONE.0076918.

Sonenberg, N. and Hinnebusch, A.G. (2009) 'Regulation of translation initiation in eukaryotes: mechanisms and biological targets', *Cell*, 136(4), pp. 731–745. doi:10.1016/J.CELL.2009.01.042.

Starck, S.R. *et al.* (2016) 'Translation from the 5' untranslated region shapes the integrated stress response', *Science (New York, N.Y.)*, 351(6272). doi:10.1126/SCIENCE.AAD3867.

Stauffer, S. *et al.* (2014) 'Stepwise priming by acidic pH and a high K<sup>+</sup> concentration is required for efficient uncoating of influenza A virus cores after penetration', *Journal of virology*, 88(22), pp. 13029–13046. doi:10.1128/JVI.01430-14.

Stone, N.L. *et al.* (2020) 'A systematic review of minor phytocannabinoids with promising neuroprotective potential', *British journal of pharmacology*, 177(19), pp. 4330–4352. doi:10.1111/BPH.15185.

Tanjore, H. *et al.* (2011) 'Alveolar epithelial cells undergo epithelial-to-mesenchymal transition in response to endoplasmic reticulum stress', *The Journal of biological chemistry*, 286(35), pp. 30972–30980. doi:10.1074/JBC.M110.181164.

Terstappen, G.C. *et al.* (2007) 'Target deconvolution strategies in drug discovery', *Nature reviews. Drug discovery*, 6(11), pp. 891–903. doi:10.1038/NRD2410.

Torres, S. *et al.* (2011) 'A combined preclinical therapy of cannabinoids and temozolomide against glioma', *Molecular cancer therapeutics*, 10(1), pp. 90–103. doi:10.1158/1535-7163.MCT-10-0688.

Ulianich, L. *et al.* (2008) 'ER stress is associated with dedifferentiation and an epithelial-to-mesenchymal transition-like phenotype in PC C13 thyroid cells', *Journal of cell science*, 121(Pt 4), pp. 477–486. doi:10.1242/JCS.017202.

Velasco, G., Sánchez, C. and Guzmán, M. (2016) 'Anticancer mechanisms of cannabinoids', *Current oncology (Toronto, Ont.)*, 23(2), pp. S23–S32. doi:10.3747/CO.23.3080.

Vickery, A.W. and Finch, P.M. (2020) 'Cannabis: are there any benefits?', *Internal medicine journal*, 50(11), pp. 1326–1332. doi:10.1111/IMJ.15052.

Wang, D. *et al.* (2008) 'Loss of cannabinoid receptor 1 accelerates intestinal tumor growth', *Cancer research*, 68(15), pp. 6468–6476. doi:10.1158/0008-5472.CAN-08-0896.

Wu, C. *et al.* (2012) 'A protease for "middle-down" proteomics', *Nature methods*, 9(8), pp. 822–824. doi:10.1038/NMETH.2074.

Xu, H. *et al.* (2021) 'The role of EEF1D in disease pathogenesis: a narrative review', *Annals of translational medicine*, 9(20), pp. 1600–1600. doi:10.21037/ATM-21-5025.

Yang, L. *et al.* (2005) 'Multiple signals induce endoplasmic reticulum stress in both primary and immortalized chondrocytes resulting in loss of differentiation, impaired

cell growth, and apoptosis', *The Journal of biological chemistry*, 280(35), pp. 31156–31165. doi:10.1074/JBC.M501069200.

Zhang, J. and Veeramachaneni, N. (2022) 'Targeting interleukin-1 $\beta$  and inflammation in lung cancer', *Biomarker research*, 10(1). doi:10.1186/S40364-021-00341-5.

Zhang, Y. *et al.* (2013) 'Protein analysis by shotgun/bottom-up proteomics', *Chemical reviews*, 113(4), pp. 2343–2394. doi:10.1021/CR3003533.

Zhou, Y. *et al.* (2017) 'NID1, a new regulator of EMT required for metastasis and chemoresistance of ovarian cancer cells', *Oncotarget*, 8(20), pp. 33110–33121. doi:10.18632/ONCOTARGET.16145.

Zou, S. and Kumar, U. (2018) 'Cannabinoid Receptors and the Endocannabinoid System: Signaling and Function in the Central Nervous System', *International journal of molecular sciences*, 19(3). doi:10.3390/IJMS19030833.

